

Influence of Trotterization error on single-particle tunneling

Anton V. Khvalyuk*

LPMMC, University Grenoble-Alpes, France

Kostyantyn Kechedzhi, Vadim S. Smelyansky, and Lev. B. Ioffe

Google Research, Mountain View, CA, USA

(Dated: February 19, 2024)

Simulation of the single-particle tunneling problem by means of the Suzuki-Trotter approximation (STA) is analyzed. The target system describes a particle hopping across a chain of sites with position-dependent potential profile. The latter is assumed to be smooth and possess several local minima separated by a potential barrier, arranging a tunneling problem between the localized states in different minima. The STA error is found to manifest itself in three ways: *i*) perturbative energy shifts, *ii*) nonperturbative renormalization of the tunneling rates, and *iii*) perturbative leakage of total probability to other states. In the general case, the first type of error is the most essential, as the emerging detuning of the tunneling resonance has to be compared with exponentially small tunneling rates. In absence of detuning (e.g. if the resonance is protected by symmetry), STA is found to cause exponential enhancement of the tunneling rates. The last type of error classifies the overall defect in the wave function and thus delineates the region of sufficiently weak distortion of the wave function due to STA. The conducted analysis confirms the naive criteria of applicability $\max\{T, P\} \ll \delta t^{-1}$ (with T, P being the typical scales of kinetic and potential terms, respectively), while also revealing the structure of error and its actual behavior with system parameters. Analysis of the case of large Trotter step is also performed, with the main result being the reconstruction of the low-energy spectrum due to coupling between states with energy difference close to $2\pi/\delta t$. The connection of the obtained results with the rigorous upper error bounds on the STA error is discussed, with particular emphasis on the reasons for the fact that these rigorous bounds are not always saturated. We also point out that the proposed problem can be directly implemented on existing quantum devices [1]. In particular, we give a detailed description of an experimental design that demonstrates the described physics.

I. INTRODUCTION

Simulating many-body quantum systems is a notoriously difficult problem that is often beyond the capabilities of even the most powerful classical supercomputers. In addressing this challenge, developing well-controlled quantum system that can further be used to simulate a wide range of other quantum systems has been a promising approach [2]. One example of such devices is given by superconducting systems [3, 4] that realize a 2D grid of two-level systems (qubits) with the possibility to apply any unitary operation involving one or two spatially adjacent qubits. These unitary operations (so-called gates) can be applied simultaneously for nonintersecting sets of qubits, which in the main idea behind all applications. In particular, such devices are a natural platform for simulating 1D and 2D spin-1/2 systems, as several prominent examples demonstrate [1, 5], but other computationally expensive tasks can also be executed [3]. However, several main obstacles stand in the way of practical applications of these devices [1]: *i*) dephasing and decoherence of many-body state caused by noise from coupling to external devices, *ii*) errors in unitary gates and in readout of the final state, and *iii*) representation of Hamiltonian evolution in terms of local unitary gates, with the latter being the topic of the present paper.

The primary challenge in simulating the evolution of a system with Hamiltonian H is that the evolution operator $\hat{U} = e^{-itH}$ is generally truly nonlocal unitary operator, whereas any unitary gate available on existing platforms is

local, so the exact evolution can only be restored with infinite number of gates. However, numerous algorithms [6] have been proposed to tackle this problem. All such algorithms essentially represent a cleverly designed sequence of local one- and two-qubit gates whose combined action U_{appr} approaches that of the target evolution operator \hat{U} as the number of elementary steps in the sequence M is increased. The convergence towards \hat{U} with the increase M is established by deriving a rigorous upper bound on the error measured, e.g., as the spectral norm distance $\|U - U_{\text{appr}}\|$. These schemes can also be viewed as quantum-mechanical analogs of Hamiltonian-blind symplectic integrators of Hamiltonian equations of motion that guarantees an upper bound on the error of the result. Ref [6] provides a concise review of existing approaches and the associated expressions for the upper bounds. Although it can be proved that any single algorithm cannot perform accurate simulation of *all* Hamiltonians with number of gates that grows slower than linearly with the required simulation time and/or system size [7, 8], the available algorithms are capable of coming arbitrarily close to the optimal linear scaling [6].

It is often the case, however, that the analytical upper bounds are not saturated by the actual evolution [6, 9, 10], so the natural question of the true value of the error emerges. Moreover, the total error in the wave function (measured e.g. as the square norm distance) does not necessarily translate to a comparable error in physical observables, as those might be largely insensitive to the sectors of the Hilbert space that host the largest part of the error. On the other hand, the idea of quantum simulations is beneficial for analysis of behavior of the systems that are not amenable for classical simulation, in which case it is also crucial to gain qualitative understanding of the errors

* anton.khvalyuk@lpmmc.cnrs.fr

brought in by the simulation routine. Detailed error analysis thus also serves the purpose of reducing of the required number of operations by accurately reproducing only the evolution of the part of the Hilbert space that plays the most important role in the target physical observables.

The present paper is focused on the detailed analysis of the error induced by the Suzuki-Trotter algorithm [11], also known as the product formula approach [6] or Trotterization. This algorithm has two practical advantages: *i*) it requires no qubits in excess of those directly storing the configuration of the target spin system, and *ii*) it approximately conserves the locality of the underlying Hamiltonian, which is also to the benefit of its theoretical analysis. The particular emphasis is made on the distortion of the tunneling processes, as those appear to play a role in quantum algorithms for combinatorial problems [12–14], although here we only focus on a single-particle model with sufficiently simple dynamics.

One particularly important question about the Suzuki-Trotter algorithm is the interpretation of the distortion brought in by this algorithm. The latter reproduces the evolution by performing a sequence of discrete steps, thus introducing a time scale of the Trotter step duration δt . As a result, it is tempting to regard the distortion of the evolution as perturbation at high frequencies $\sim 2\pi n/\delta t$, $n \in \mathbb{N}$, so one expects heating, assisted tunneling, and other irradiation-induced effects to occur. On the other hand, for a time-independent target Hamiltonian, the Suzuki-Trotter evolution is exactly periodic with period δt , so the Floquet theorem actually guarantees the existence of the effective time-independent Hamiltonian H_{eff} that exactly corresponds to evolution during a single Trotter step. H_{eff} is thus conserved during the Suzuki-Trotter evolution, which at first glance is in contradiction with heating. For a general setting, this issue has already been addressed in the literature [15], but in this work we intentionally avoid the problem altogether by restricting ourselves to a simple model that does not feature many-body physics.

The paper is organized as follows: the following Section II describes the model Hamiltonian and the associated Suzuki-Trotter algorithm. It then formulates more precisely two flavors of the tunneling problem to be discussed and provides a concise review in the semiclassical picture of the system's dynamics. Section III then exposes the detailed description of the error introduced by the simulation algorithm. It describes the three most important effects: resonance detuning due to the energy shift (Subsection III D), enhancement of the tunneling rate (Subsections III E and III F), and probability defect due to leak from the target initial state (Subsection III G). It also contains description of certain effects of sufficiently large Trotter steps (Subsection III H). Finally, Section IV summarizes the key qualitative findings of the work (Subsection IV A), conducts an instructive comparison with the rigorous upper bounds known from the literature (Subsection IV B), provides a conceptual description of the experimental setup that demonstrates the aforementioned effects (Subsection IV C), and outlines certain directions of further research (Subsection IV D). The paper is supplemented by three Appendices describing the technical details of the calculations and the design of the experiment.

II. SOLVABLE MODEL OF TROTTERIZED EVOLUTION

A. Hamiltonian

We consider the Hamiltonian of inhomogeneous chain of spins $1/2$ with XY nearest-neighbor interaction:

$$H = \sum_{i=1}^L h_i S_i^z - \sum_{i=1}^{L-1} J (S_i^x S_{i+1}^x + S_i^y S_{i+1}^y), \quad (1)$$

where h_i is position-dependent, $J > 0$ is a constant. The spatial profile of h_i is assumed to be smooth, as explained below in more detail. The Hamiltonian (1) conserves the z -projection of the total spin $S_{\text{total}}^z = \sum_i S_i^z$.

Crucially, the spin Hamiltonian (1) can be mapped onto a system of non-interacting fermions by means of the Jordan-Wigner transformation [16]:

$$S_i^z = a_i^\dagger a_i - \frac{1}{2}, \quad S_i^x S_{i+1}^x + S_i^y S_{i+1}^y = \frac{a_i^\dagger a_{i+1} + a_{i+1}^\dagger a_i}{2}, \quad (2)$$

where a_i^\dagger, a_i are fermionic creation and annihilation operators for site i . The vacuum state with no fermions corresponds to the state with all spins down $|\Omega\rangle = \otimes_i |\downarrow_i\rangle$, and, more generally, the subspace with N fermions reproduces the subspace with total z -projection $S_{\text{total}}^z = N - L/2$.

B. Approximate evolution by Suzuki-Trotter algorithm

The problem of simulating the unitary evolution under Hamiltonian (1) during time t amounts to approximating the unitary $U = \exp\{-itH\}$ with sufficient accuracy by a product of local one- and two-qubit gates available on the quantum hardware. This is a nontrivial task due to the noncommutativity of various local terms in the Hamiltonian (1). Indeed, Eq. (1) can be rewritten as

$$H = K_{\text{even}} + K_{\text{odd}} + P, \quad (3)$$

$$K_{\text{even(odd)}} = \sum_{k:\text{even(odd)}} H_{k,k+1}, \quad P = \sum_{k=1}^L H_k, \quad (4)$$

$$H_{k,k+1} = -J (S_k^x S_{k+1}^x + S_k^y S_{k+1}^y), \quad H_k = h_k S_k^z. \quad (5)$$

The operators within each term in Eq. (4) commute with each other, but the three terms $K_{\text{even}}, K_{\text{odd}}, P$ are mutually non-commuting. As a result, on quantum hardware one can apply only the evolution operators corresponding to $aK_{\text{even}}, bK_{\text{odd}}$ and cP with some real coefficients a, b, c . The operators of the form $aK_{\text{even}} + bP$ and $cK_{\text{odd}} + dP$ with real a, b, c, d can be further represented as a collection of unitaries acting on nonintersecting pairs of qubits. Although at the hardware level each such unitary is typically implemented as a combination of one- and two-qubit gates, such grouping allows one to remove part of the error from noncommutativity of $K_{\text{even(odd)}}$ and P .

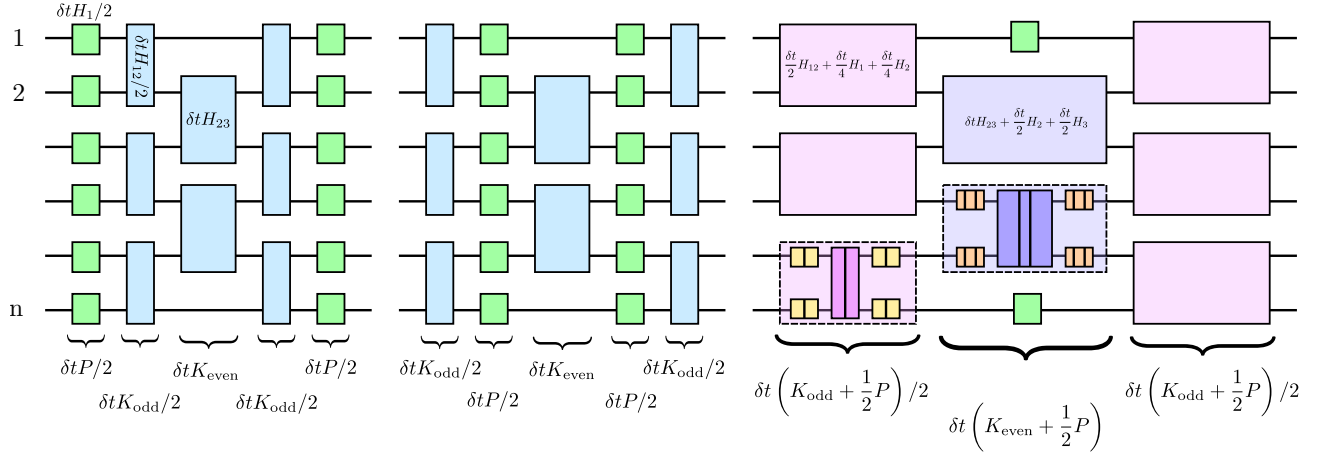


Figure 1. Circuits for the three possible orderings of non-commuting operators in Suzuki-Trotter formula. Horizontal black lines correspond to qubits, and rectangular blocks represent gates executed on the corresponding qubits at a given time step (horizontal axis). Each circuit represents one step of Suzuki-Trotter algorithm according to Eq. (7): *left*: $\{P, K_{\text{odd}}, K_{\text{even}}\}$, *center*: $\{K_{\text{odd}}, P, K_{\text{even}}\}$, *right*: $\{K_{\text{odd}} + (1 - \alpha)P, K_{\text{even}} + \alpha P\}$ for $\alpha = 1/2$. Written inside or near a block are the operators whose exponent is being applied within this block. Below each vertical cross-section of the circuits written are the parts of the Hamiltonian applied by the corresponding layer of the circuit. For all three circuits, the central parts of the Suzuki-Trotter formula (7) have been coalesced as $e^{-i\delta t A_n/2} e^{-i\delta t A_n/2} = e^{-i\delta t A_n}$. In all three circuits, obvious optimizations are possible for multiple Trotter steps (such as, e.g. merging the two adjacent single-qubit gates into a single one, and so on). For the right circuit, the scheme inside the block indicates that to reproduce the target two-qubit operator a sequence of several one- and two-qubit gates is applied to the hardware. Note also the $\delta t P/2$ gates (green) applied at both end qubits on the left circuit – a consequence of open boundary conditions.

On the other hand, such grouping might potentially increase the share number of gates depending on the compilation algorithm, so we will consider both cases: with and without such grouping.

The second order Suzuki-Trotter formula [7, 11] provides the approximation for the evolution operator $U = e^{-itH}$ for $H = A_1 + \dots + A_n$, where each of A_k can be exponentiated exactly. The whole evolution is partitioned into identical steps of length δt (assuming that $t/\delta t$ is an integer):

$$U_{\text{appr}}(t) = \{U_{\text{appr}}(\delta t)\}^{t/\delta t}, \quad (6)$$

with each step performed according to the approximate evolution operator

$$U_{\text{appr}}(\delta t) = e^{-iA_n \delta t/2} \dots e^{-iA_1 \delta t/2} \times e^{-iA_1 \delta t/2} \dots e^{-iA_n \delta t/2}, \quad (7)$$

where $A_k, k = 1, \dots, n$ correspond to the set of applicable operators in any fixed order, and the second term in Eq. (7) features product of operators in reverse direction relative to that of the first term. In the limit $\delta t \rightarrow 0$, the approximate evolution operator $U_{\text{appr}}(t)$ approaches the target one e^{-itH} , while finite δt causes a distortion of the evolution, which can be characterized by the effective Hamiltonian:

$$U_{\text{appr}}(t) = e^{-itH_{\text{eff}}}, \quad H_{\text{eff}} = -\frac{1}{i\delta t} \text{Ln} U_{\text{appr}}(\delta t), \quad (8)$$

so the actual evolution after $t/\delta t$ steps is described by $U_{\text{appr}}(t) = \exp\{-iH_{\text{eff}}t\}$. The result of Ref. [11] is that

$$H_{\text{eff}} - H = O(\delta t^2). \quad (9)$$

The Suzuki-Trotter algorithm can be viewed as the quantum-mechanical counterpart of the symplectic Runge-Kutta method [17] for classical Hamiltonian equations of motion, thus also sharing certain features, such as naturally occurring energy conservation (i.e., symplecticity), locality and the existence of an effective semiclassical Hamiltonian.

The appropriate values of δt are determined from the naive comparison of the characteristic energy scales:

$$|J\delta t|, |P\delta t| \ll 1, \quad (10)$$

where $P = \max_i h_i - \min_i h_i$ is the magnitude of the potential term, and J is the order of magnitude of the kinetic term. However, if the problem contains other relevant energy scales, one should also require these scales to be small compared to δt^{-1} , which might lead to a much stronger requirement on the step size δt , as it is shown below.

Eq. (7) admits different splittings of the total Hamiltonian (3) into allowed operators, with three conceptually distinct options: $\{K_{\text{even}}, K_{\text{odd}}, P\}$, $\{K_{\text{even}}, P, K_{\text{odd}}\}$, and $\{K_{\text{even}} + \alpha P, K_{\text{odd}} + (1 - \alpha)P\}$ for some $\alpha \in [0, 1]$. All other groupings differ from these three either by redefining the “beginning” of each Trotter step to be at a different gate, or by interchanging K_{even} and K_{odd} . Moreover, the structure of and the effect from the resulting error term is similar for both cases, as it will be shown below, so the choice of the particular design boils down to hardware considerations. The visualization of the three different versions of algorithm is shown on Figure 1.

Because the original problem is non-interacting, the problem of calculating H_{eff} can be reduced to a similar problem for just a single fermion. Indeed, at each phase of an individual Trotter step (7), the fermionic system evolves according to a

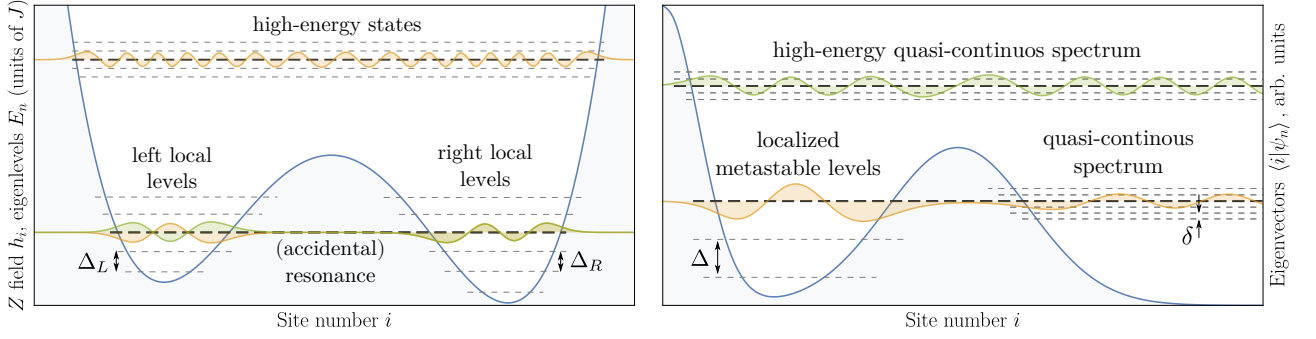


Figure 2. Sketch of the potential profile (filled blue curve), the resulting eigenlevels (horizontal dashed lines) and wave functions (filled curves) for the two tunneling problems in question. For a given energy, the potential defines a set of classically allowed and forbidden regions. If the allowed region is bounded, it hosts a series of discrete levels with energy-dependent level spacing Δ that is determined by the particular geometry of the allowed region, typically being inversely proportional to the size of the allowed region at a given energy. *Left*: double-well potential with two sets of discrete energy levels. Due to finite height of the potential barrier, the resonant states in the two wells are hybridized with small energy splitting η . The resonance between left and right metastable state can be either accidental (and thus characterized by finite detuning $\varepsilon \sim \eta$) or protected by symmetry of the potential. *Right*: a potential with a single metastable minimum separated from large region with dense quasi-continuous spectrum. Each bound state inside the local minimum is coupled to the quasi-continuous spectrum outside the well is small level spacing $\delta \ll \Delta$. This induces a small level width $\Gamma \ll \Delta$ of the local states, which is assumed to also satisfy $\Gamma \gg \delta$.

Hamiltonian that is quadratic in fermionic operators:

$$A_k = \sum_{ij} a_i^\dagger A_k^{ij} a_j \quad (11)$$

where the sum goes over all sites i, j , and the matrix elements A_k^{ij} are obtained from Eqs. (4)-5 by substitution (2). Due to the Wick's theorem, the composition (7) is still generated by a quadratic Hamiltonian:

$$U_{\text{appr}}(\delta t) = \exp \left\{ -i\delta t \sum_{ij} a_i^\dagger \mathcal{H}_{\text{eff}}^{ij} a_j \right\} \quad (12)$$

where the effective single-particle Hamiltonian \mathcal{H}_{eff} is defined via its evolution operator $\mathcal{U} = e^{-i\delta t \mathcal{H}_{\text{eff}}}$ by the same Suzuki-Trotter formula (7), but with each A_k replaced by a single-particle matrix according to the correspondence

$$H_{k,k+1} \mapsto \mathcal{H}_{k,k+1}^{ij} = -\frac{J}{2} (\delta_{ik} \delta_{j,k+1} + \delta_{i+1,k} \delta_{jk}), \quad (13)$$

$$H_k \mapsto \mathcal{H}_k^{ij} = \left(h_k - \frac{1}{2} \right) \delta_{ik} \delta_{jk}. \quad (14)$$

The behavior of a given spin state under the evolution with the approximate unitary is thus entirely described by the single-particles effects and the Fermi statistics of the Jordan-Wigner fermions.

C. Single-particle tunneling problem

In what follows, we are interested in the single spin flip subspace corresponding to just a single fermion, which means

that our problem is described by a single-particle Hamiltonian of fermions:

$$\mathcal{H} = \sum_{k=1}^L h_k |k\rangle \langle k| - \sum_{k=1}^{L-1} \frac{J}{2} (|k\rangle \langle k+1| + |k+1\rangle \langle k|) \quad (15)$$

where we have dropped the additional $1/2$ after h_k as it produces a constant energy shift. Unless stated otherwise, we consider smooth potential profiles of the form $h_n = h(an)$, where $h(x)$ is a smooth function, and $a \ll 1$ plays the role of small lattice constant. We are then interested in describing the problem of tunneling outside the local minimum of the potential. In terms of the original spins, this corresponds to creating a single-spin excitation with spin density localized in a local minimum of $h(x)$ and observing how the spin density tunnels through the potential barrier. The two potential profiles of particular interest are sketched on Figure 2 and discussed below. In both cases, we assume that the initial state $|\psi_{\text{init}}\rangle$ of the excitation is close to a certain localized metastable state $|\psi_N\rangle$ of a local minimum of the potential.

1. Rabi oscillations. Consider the double-well potential on Figure 2, left. If the barrier is infinite, each well hosts a series of discrete energy levels characterized by typical level spacing Δ (energy-dependent for an anharmonic well). Suppose that a pair of those levels from different wells has a small energy difference $\varepsilon = E_{\text{right}} - E_{\text{left}} \ll \Delta$, either due to reflection symmetry of the potential (in which case $\varepsilon = 0$) or by accident. Finite transparency of the potential barrier then leads to hybridization of those levels according to the following Hamiltonian of the resonant subspace:

$$H_{\text{res.}} = \begin{pmatrix} -\varepsilon/2 & \eta \\ \eta & \varepsilon/2 \end{pmatrix} \quad (16)$$

where $\eta \ll \Delta$ is the tunneling amplitude between the two resonant states, exponentially small for a large barrier.

This problem is readily implementable on existing quantum devices [1]. However, the approximate evolution operator (7) distorts the evolution in two ways: *i*) the energies of the discrete states in each of the wells and the tunneling amplitude are distorted, leading to a change in the resonant subspace Hamiltonian (16), and *ii*) the wave functions of the discrete states are distorted as well, so an arbitrary initial state $|\psi\rangle$ localized in either of the wells now has a different overlap with the target resonance subspace. Our task is to describe these effects.

2. Decay into continuous spectrum. Consider now a local minimum separated from a large region of small potential by a potential barrier, Figure 2, right. The well still hosts a set of discrete metastable states with typical level spacing Δ , and the region beyond the barrier is characterized by a nearly continuous spectrum with level spacing $\delta \ll \Delta$. Finite width of the barrier arranges a coupling of the two regions by a finite transmission amplitude η , which we assume to be much smaller than the discrete level spacing Δ . While $\delta \gg \eta$ would correspond to the previously considered case of discrete resonance, the opposite situation $\delta \ll \eta$ causes the decay of the metastable state due to coupling with the continuous spectrum. As a result, each discrete metastable state in the well is now characterized by an exponential decay of probability $|\psi_N(t)|^2 \propto \exp\{-\Gamma_N t\}$ with small characteristic decay rate $\Gamma_N \sim \eta^2/\Delta \ll \Delta$, and after $t \sim \Gamma_N^{-1}$ such state decays into states of continuous spectrum with energies close to E_N according to a Lorentzian profile of width $\sim \Gamma_N$.

Attempting to simulate this process using the Suzuki-Trotter approach distorts this evolution by *i*) introducing corrections to the values of E_N, Γ_N and *ii*) by altering the wave functions inside the well, which changes the distribution of energies in the initial state. We are interested in describing these changes. Although this problem is not practical for existing hardware, as one needs exponentially large system sizes to render the continuous part of the spectrum sufficiently dense to satisfy $\delta \ll \Gamma$, it still presents interest from the physics point of view.

D. Semiclassical approximation for single-particle tunneling

In this section, we review some of the well-known results of the semiclassical approximation in application to the problems of Subsection II C, with the intention to refer to these results in what follows. The semiclassical approach is a conventional tool for describing the events of tunneling through a large barrier. It consists of two parts [18]: *i*) constructing semiclassical wave functions in the region where the semiclassical approximation is applicable and *ii*) asymptotic matching of two regions of applicability with a transfer matrix obtained from exact solution of the neighborhood of the problematic region. In our problem, there is a complication in the form of discretized spatial dimension, but this does not reduce the power of the semiclassical approach [19]. A detailed overview of the procedure for the particular system in question is given in Appendix A.

The WKB approximation amounts to the following asymptotic series w.r.t the small lattice constant $a \ll 1$ (being a closed analog of the Planck's constant) for the stationary wave

function:

$$\psi_n = \frac{e^{iS(an)/a}}{\sqrt{v(an)}} [1 + O(a)], \quad (17)$$

where v, S are assumed to be smooth functions of x . The classical action $S(x)$ obeys the classical Hamilton-Jacobi equation:

$$\mathcal{H}(x, p) = E, \quad p = S'(x), \quad (18)$$

which also defines the classical momentum $p(x)$. Here, the classical counterpart of the Hamiltonian is defined through the Wigner transform:

$$\mathcal{H}(x = an, p) = \sum_m \mathcal{H}^{nm} e^{ip(m-n)} = -J \cos p + h(x) \quad (19)$$

where the sum in the r.h.s of the middle expression goes over all sites, and the last expression corresponds to the particular case of Hamiltonian (15). Finally, $v(x)$ in Eq. (17) is the classical group velocity:

$$v(x) = \left. \frac{\partial \mathcal{H}}{\partial p} \right|_{p=p(x)} = J \sin p(x) \quad (20)$$

The approximation (17) is only applicable in the region where the relative change of the de Broglie wave length at the spatial scale of the wave length itself is small, i.e., the wave length is well defined locally:

$$\frac{a h'(x)}{p^2(x) v(x)} \ll 1. \quad (21)$$

This condition is violated if the potential is not smooth (i.e., $h'(x) \sim 1/a \gg 1$) or when either the classical momentum p or the group velocity v vanishes. Such points are called the classical turning points. In addition to the standard turning points $p, v = 0$, there are also anomalous turning points corresponding to $v = 0, p = \pm\pi$, which is the consequence of the discreteness of the problem. The existence of this points is the semiclassical explanation of the Bloch's oscillations [20].

In the regions where the semiclassical approximation breaks down, the corresponding stationary Schrodinger equation has to be solved exactly. The asymptotic behavior of the result is then matched to the semiclassical expressions (17), and the latter are required to be applicable in a sufficiently large region, i.e. $\Delta x \gg \lambda(x)$, which also implies $S/a \sim \Delta x/\lambda \gg 1$. The procedure yields a connection between the coefficients of two linearly independent semiclassical solutions on either side of the non-classical region. The example of this procedure for a simple turning point is presented in Appendix Subsection A.2.

The semiclassical procedure allows one to compute the answers to the two problems described in Subsection II C, as explained in Appendix Subsection A.2 or otherwise known from the literature [18, 19, 21]. The discrete energy levels in a potential well are described by the celebrated Bohr quantization rule:

$$\frac{S_{12}}{a} = \frac{1}{a} \int_{x_1}^{x_2} p(E_N; x) dx = \pi \left(N + \frac{1}{2} \right) + \theta_2 - \theta_1, \quad (22)$$

where $N \in \mathbb{N} \cup \{0\}$ is the level quantum number, $p(E, x)$ is the classical momentum at energy E found from Eq. (18), $x_{1,2}$ are the positions of the classical turning points defined by vanishing group velocity $v(x_i) = 0$, and $\theta_{1,2}$ are the additional phases introduced by the anomalous turning points [19]:

$$\theta_i = \begin{cases} 0, & p(x_i) = 0, \\ -\frac{\pi}{2} + \pi x_i/a, & p(x_i) = \pm\pi. \end{cases} \quad (23)$$

The phases θ_i in Eqs. (22) and (23) actually depend on the exact position $n = x/a \in \mathbb{R}$ of the anomalous turning point *between* the two sites, which is essential for correctly reproducing the quantization conditions in problems with discrete coordinate, as pointed out in Ref [19] and explained in Appendix Subsection A 2.

Eq. (22) also produces the well-known expression for the single-particle level spacing $\Delta = E_{N+1} - E_N$:

$$T_{12}(E) \Delta(E) = 2\pi a \quad (24)$$

where $T_{12} = 2 \partial S_{12} / \partial E$ is the period of classical motion at energy E .

Eqs. (22-24) are applicable if the region of applicability of the semiclassical approximation inside the well is sufficiently large, i.e. $S_{12}/a \gg 1$. This condition is typically violated for the lowest energy levels of the well, so one is required to solve the eigenproblem exactly in this case. However, even for such cases the parametric dependence of the semiclassical result is correct up to a numeric coefficient of the order of unity, and it turns out to be exact if the potential minimum is described by a quadratic approximation.

The tunnel splitting of two semiclassical levels with close energies is described by

$$\eta = \frac{\sqrt{\Delta_L \Delta_R}}{2\pi} \exp \left\{ -\frac{1}{a} S_B \left(\frac{E_L + E_R}{2} \right) \right\} \quad (25)$$

where $\Delta_{L,R}$ are the local level spacings at energies $E_{L,R}$ in the corresponding wells, and

$$S_B(E) = \int_{x_L}^{x_R} |p(E; x)| dx \quad (26)$$

is the under-barrier action calculated from the imaginary momentum of the forbidden region between the classical turning points x_L, x_R such that $v(x_{L,R}) = 0$. Finally, the same method gives the celebrated Gamow's formula [21, par. 50] for the decay rate:

$$\Gamma_N = \frac{\Delta_N}{2\pi} \exp \left\{ -\frac{2}{a} S_B(E_N) \right\} \quad (27)$$

with Δ_N being the level spacing of the metastable states inside the well, and S_B given by the same Eq. (26) at the energy E_N of the corresponding metastable state. If the states inside the well are not described by the semiclassical approximation (e.g., several first low-energy states of the potential minimum), both expressions (25) and (27) typically remain valid up to a numerical factor of the order unity, with the case of a quadratic minimum of the potential described exactly.

III. INFLUENCE OF TROTTERIZATION ON SINGLE-PARTICLE TUNNELING

A. Matrix elements of the effective Hamiltonian

By construction, each operator applied within one Suzuki-Trotter step (7) has nonzero matrix elements only at distances at most two, i.e., $\langle i | \exp \{-iA_k \delta t/2\} | j \rangle = 0$ for $|i - j| > 2$, as it is composed of commuting two-qubit gates. Moreover, due to the smallness of the Trotter step δt , nondiagonal matrix elements ought to be small as $O(J\delta t)$, with J being the characteristic scale of the kinetic energy. For our case, the single-particle evolution operator $\mathcal{U} = e^{-i\delta t \mathcal{H}_{\text{eff}}}$ is composed either of 5 such operators, two of which are diagonal (as they represent the potential term), or just of 3 operators. As a result, it can only have nonzero matrix elements at distances not exceeding 3, and these matrix elements bear the corresponding order of smallness in powers of $J\delta t$:

$$\mathcal{U}^{ij} \sim \begin{cases} (J\delta t/4)^{|i-j|}, & |i-j| \leq 3, \\ 0, & |i-j| > 3. \end{cases} \quad (28)$$

It then follows from direct expansion of Eq. (8) in powers of δt that large-distance matrix elements of the effective Hamiltonian \mathcal{H}_{eff} decay exponentially with distance:

$$\mathcal{H}_{\text{eff}}^{ij} \sim J \cdot (J\delta t/4)^{|i-j|-1}, \quad |i-j| > 3. \quad (29)$$

Evidently, it is crucial that

$$J\delta t/4 < 1, \quad (30)$$

in order for the resulting Hamiltonian to be truly local, which is but one of the applicability criteria (10).

Small-distance matrix elements of \mathcal{H}_{eff} can be computed in the leading order in powers of δt by directly expanding Eqs. (7) and (8). The exact expression are presented in Appendix Subsection B 1, while here we present a simple recursive formula for the leading order defect $\delta t^2 \cdot \mathcal{D} = \mathcal{H}_{\text{eff}} - \mathcal{H}$ for the Hamiltonian of the form $\mathcal{H} = A_1 + \dots + A_n$:

$$\begin{aligned} \delta \mathcal{D}_{k+1} - \delta \mathcal{D}_k = \\ -\frac{1}{12} \left\{ [\mathcal{H}_k, [\mathcal{H}_k, A_{k+1}]] - \frac{1}{2} [A_{k+1}, [A_{k+1}, \mathcal{H}_k]] \right\} \end{aligned} \quad (31)$$

where A_k are applied according to Eq. (7), $\mathcal{H}_k = \sum_{j=1}^k A_j$ is the target Hamiltonian after adding k operators, and the recursion starts from $\mathcal{D}_1 = 0$.

Straightforward application of the semiclassical description of Subsection II D is hindered by the oscillating terms in the effective Hamiltonian. Indeed, applying the semiclassical description requires that the Wigner's transform (19) of the Hamiltonian is a smooth function of $x = an$. However, the correction $\delta t^2 \mathcal{D} = \mathcal{H}_{\text{eff}} - \mathcal{H}$ has the following spatial structure of the matrix elements:

$$\mathcal{D}^{ij} = U^{ij} + (-1)^i W^{ij} + (-1)^j \overline{W^{ij}}, \quad (32)$$

with both operators U, W having smooth Wigner's transforms (19). The Trotterization procedure thus introduces an oscillating term with matrix elements proportional to $(-1)^n$ that seemingly renders the semiclassical approximation inapplicable. Upon closer look, the problematic term causes weak scattering of waves with momentum p to those with momentum $p \pm \pi$, thus requiring a change of energy by $\sim 2J$. Therefore, all such processes are virtual and amount to an additive correction to the Hamiltonian \mathcal{H}_{eff} with a quantity of the order $\delta t^4 W^2/J^2$. The Wigner's transform of this correction is yet another smooth function and constitutes $O(\delta t^4)$ contribution, which is beyond the precision of the analysis. As a result, we can safely discard this term in our analysis, as far as semiclassical quantization condition is concerned. A more detailed version of this argument is presented in Appendix Subsection B 3.

There is additional simplification due to the same assumption of smoothness that validates the semiclassical approximation. Consider, for instance, the $\{K_{\text{even}}, K_{\text{odd}}, P\}$ ordering of the operators in the Suzuki-Trotter approximation (7). Eq. (31) then suggests that the corrections contains terms from noncommutativity of K_{even} and K_{odd} as well as terms from noncommutativity of the full kinetic energy $K = K_{\text{even}} + K_{\text{odd}}$ with the potential term P . However, if the potential is homogeneous, it certainly commutes with K , so the second contribution vanishes. Inhomogeneity of the potential then produces contributions that are proportional to $a^2 (\nabla h)^2$, $a^2 \Delta h$, so they can safely be neglected as subleading w.r.t the main semiclassical approximation. A more rigorous analysis for all possible groupings of operators is presented in Appendix Subsection B 3.

B. Trotterization as a periodic perturbation at large frequency $\Omega = 2\pi/\delta t$ and prethermalization

The Suzuki-Trotter algorithm (7) is described by the following piecewise-constant time-dependent Hamiltonian:

$$H_{\text{appr.}}(t) = n \times \begin{cases} A_n, & \frac{1}{2n} < t/\delta t \leq \frac{1}{n}, \\ \dots, \\ A_k, & \frac{n-k}{2n} < t/\delta t \leq \frac{n-k+1}{2n}, \\ \dots, \\ A_1, & \frac{n-1}{2n} < t/\delta t \leq \frac{n+1}{2n}, \\ \dots, \\ A_n, & \frac{2n-1}{2n} < t/\delta t \leq 1, \end{cases} \quad (33)$$

which is periodically repeated every Trotter step of length δt , with the overall factor of n needed simply to identify the "system time" t describing the evolution of the target model (1) with the actual physical time on the device. Being averaged over one Trotter step, it produces the target Hamiltonian, i.e.

$$\int_0^{\delta t} dt H_{\text{appr.}}(t) = \delta t H. \quad (34)$$

The difference $H_{\text{appr.}}(t) - H$ can be regarded as high-frequency perturbation, as it can be expanded in cosine series with the

main frequency $\Omega = 2\pi/\delta t$ (due to symmetry $t \leftrightarrow \delta t - t$ in $H_{\text{appr.}}(t)$, sine components are absent).

Because $H_{\text{appr.}}(t)$ is periodic with period δt , the Floquet theorem guarantees the existence of the effective time-independent Hamiltonian H_{eff} that describes the evolution of the system at stroboscopic times $t_n = n\delta t$, $n \in \mathbb{N}$: $\psi(t_n) = \exp\{-it_n H_{\text{eff}}\} \psi(0)$. One can then develop perturbative expansion [22, Sec. 3] to express the effective Hamiltonian H_{eff} via a series in powers of $1/\Omega$. In particular, Eq. (31) describes the leading term of this expansion of order Ω^{-2} (with Ω^{-1} term vanishing due to symmetry $t \leftrightarrow \delta t - t$ of the circuit).

The question then arises whether the high-frequency expansion is applicable in the thermodynamic limit. Indeed, one expects a system under periodic drive to absorb energy, unless the latter is in many-body localized phase. However, heating is clearly inconsistent with the exact conservation of any quasi-local Hamiltonian H_{eff} with finite energy density at stroboscopic times. This implies that the power series of H_{eff} must be asymptotic, i.e. diverge beyond certain order n_* . However, as it was shown in Ref. [15], truncating the power series at the optimally chosen order n_* allows to correctly describe stroboscopic evolution up to time τ_* that is exponentially large in frequency, viz., $\ln \tau_* \sim \Omega/\Lambda$, where Λ is the typical energy scale of the matrix elements of the Hamiltonian, e.g. $\Lambda = \max\{J, h\}$ for Hamiltonian (1). We therefore expect our analysis to be qualitatively valid for sufficiently small Trotter step δt if the simulation is carried out for times T shorter than the prethermalization time τ_* . In particular, the latter has to be longer than the characteristic tunneling times of interest.

However, for the system considered in the present work the issue of heating is absent to begin with. The Hamiltonian (1) is mapped to noninteracting fermions, so the exact dynamics of the many-body wave function is fully determined by the single-particle evolution operator \mathcal{U} , see Eq. (12). Because \mathcal{U} now describes just one particle with bounded spectrum, no heating is present, and the associated high-frequency expansion of the effective single-particle Hamiltonian \mathcal{H}_{eff} is thus convergent, allowing one to infer its properties from the perturbation theory in powers of Ω^{-1} . As a result, our analysis is quantitatively correct for arbitrary long times for the system (1) in question.

C. Correction to the semiclassical description and discrete energy levels

Due to the smoothness of the potential, the procedure of calculating the correction to the semiclassical description of the problem thus looks as follows: one applies Eq. (31) only once to compute the contribution to H_{eff} arising from noncommutativity of the components $K_{\text{even}}, K_{\text{odd}}$ of the kinetic energy. In the resulting operator, only the part that has smooth dependence on the coordinate is preserved, and the associated correction to the Wigner's transform (19) of the effective Hamiltonian is computed. The result reads:

$$\delta \mathcal{H}_{\text{eff}}(x, p) = J \frac{(J\delta t)^2}{24} \cos p \sin^2 p. \quad (35)$$

Crucially, this function vanishes at $p = 0, \pm\pi$, so the positions of all classical turning points according to Eq. (18) remain intact. Note also that this correction is not sensitive to the ordering of the operators in Eq. (7) (see also Figure 1), as illustrated in detail in Appendix Subsection B 3.

We are now in position to describe the correction to the semiclassical treatment arising from the presence of perturbation. Similarly to the semiclassical approach itself, it consists of three parts: *i*) the change of the action in the semiclassical regions, both allowed and forbidden ones, *ii*) the modification of the matching conditions for the regions where the semiclassical approximation is not applicable, and *iii*) the shift in the energy value induced by the perturbation. The first effect is found from the perturbed version of the classical equation of motion (18) and reads

$$\delta S(E; x) = - \int^x dx' \frac{\delta \mathcal{H}_{\text{eff}}(x', p(E; x'))}{v(p(E; x'))}, \quad (36)$$

where $p(E; x')$ is computed from the unperturbed equation of motion (18). The deformation of the matching conditions at the classical turning points is actually absent because it only relies on the fact that the turning point is isolated and produced by a potential with small but finite gradient, as discussed in Appendix B in more detail. The energy shift of a semiclassical bound state is described by a deformed version of the quantization condition (22):

$$S_{12}(E + \delta E) - S_{12}(E) + \delta S_{12}(E) = 0. \quad (37)$$

where δS_{12} is computed as the integral (36) between the two turning points, similarly to S_{12} in Eq. (22). While the correction $\delta S_{12}/a$ can be much larger than π if the allowed region is large enough, both S_{12} and its energy derivative are always large in the classically allowed region, hence the equation admits perturbative solution:

$$\delta E = - \frac{2 \delta S_{12}(E)}{T_{12}(E)}, \quad (38)$$

where $T_{12}(E) = 2 \partial S_{12} / \partial E$ is the classical period of motion in the allowed region. Remarkably, the answer remains correct up to a numerical prefactor of order unity even for the states that are not described by the semiclassical expression [21, par. 48]. Using Eq. (35), this energy shift can be estimated as

$$|\delta E| \lesssim \frac{(J\delta t)^2}{24} \frac{4S_{12}}{T_{12}} \leq \frac{(J\delta t)^2}{24} \frac{2n_{\text{cl}}}{\pi} \Delta(E) \quad (39)$$

with Δ being the semiclassical level spacing according to Eq. (24), S_{12} being the unperturbed classical action of the corresponding energy level, and $n_{\text{cl}} = |x_2 - x_1|/a$ is the total number of sites in the classically allowed region, which serves as an upper bound for S_{12}/a , as evident from Eq. (26).

D. Dynamics of Rabi oscillations are detuned in general case

The key distortion of the Rabi oscillations comes from the shift of the energy levels within each of the wells. Within the

semiclassical approximation, the detuning parameter ε in the resonant subspace Hamiltonian (16) is found as

$$\varepsilon_{\text{eff}} = \varepsilon + \left(-\frac{\delta S_L}{T_L} + \frac{\delta S_R}{T_R} \right), \quad (40)$$

where the index L, R describes the characteristics of left and right well, respectively, according to Eq.(38). If the two energy shifts are different, the additional detuning in ε_{eff} can be estimated as $(J\delta t)^2 n_{\text{cl}} \Delta$ according to Eq. (39), with n_{cl} being the total number of sites in the allowed region. On the other hand, if ε_{eff} becomes significantly larger than the tunneling amplitude η , the hybridization of the two levels disappears and no tunneling is observed. Thus, another applicability condition of the Suzuki-Trotter approach emerges in the form

$$(J\delta t)^2 \lesssim \eta n_{\text{cl}} / \Delta, \quad (41)$$

where η is the tunneling amplitude, Eq. (16). Given that the latter is itself an exponentially small quantity, the simple detuning of the resonant levels turns out to be the main limitation on the size of Trotter step δt (e.g., it is much more restrictive than the naive criteria (10)). In particular, it allows one to completely neglect all other effects described below as long as one is tasked with observing the tunneling in the first place, as those other effects are rendered exponentially small if Eq. (41) is satisfied. The criterion (41) can be viewed as comparison of the energy scale of Trotterization δt^{-1} to the ones defined by tunneling, with the latter being exponentially smaller than the energy scales P, J of kinetic and potential terms of the Hamiltonian.

E. Rabi oscillations with no detuning: enhancement of tunneling

The change in the tunneling amplitude η ought to be addressed as well. As it follows from Eq. (25), the correction to the tunnel splitting of the resonance subspace η_N consists of two effects: direct change of the the underbarrier action S according to (36) and the energy shift (38) of the resonance subspace. The new value of the tunneling amplitude is given by

$$\frac{\eta_{N,\text{eff}}}{\eta_N} \approx \exp \left\{ -\frac{1}{a} \left(\delta S_B(E_N) + \frac{\partial S_B(E_N)}{\partial E} \delta E_N \right) \right\}, \quad (42)$$

where the change of the subexponential prefactor of Eq. (25) was neglected in comparison to the change of the exponent due to the smoothness of the potential expressed as $a \ll 1$, as explained in Appendix Subsection B 5. The first term in the exponent of Eq. (42) reflects the change in the underbarrier action due to perturbation, Eqs. (35)-(36):

$$\delta S_B = - \frac{(J\delta t)^2}{24} \int_{x_L}^{x_R} dx \frac{\sinh 2|p(x)|}{2}, \quad (43)$$

with the purely imaginary momentum $p(x)$ found from the equation of motion (18) in the forbidden region. The second term of Eq. (42) stands for the change of the underbarrier action (26) due to the induced shift in the energy of the resonance subspace:

$$\delta E_N = -\frac{\delta S_L}{T_L} - \frac{\delta S_R}{T_R} \quad (44)$$

with the same notations as in Eq. (40).

It is now evident that in the presence of detuning of an accidental resonance the criterion (41) puts a strong limitation on δt , rendering the change of η negligible. The situation changes drastically if the effects of detuning are irrelevant, so the main distortion of the evolution is due to the change in the tunneling amplitude η , which can then constitute multiple orders of magnitude, as it will be shown below. Consider the case of two *symmetric* wells (Figure 2, left), in which case each discrete state in one of the wells is weakly coupled to its counterpart in the other well. The introduced perturbation then causes symmetric shifts in the wells, provided the symmetry of the potential is respected by the perturbation. As a result, all of the perturbed discrete states remain perfectly hybridized ($\varepsilon \equiv 0$) with the corresponding partner in the other well, but the tunneling amplitude η of each resonant subspace is distorted by perturbation according to Eq. (42).

Importantly, the corrected value η_{eff} is always larger than original η because the correction to the tunneling action is negative for the majority of states. Indeed, the first term in the exponent of Eq. (42) is always negative, as evident from Eq. (43), while the second term is negative for states with absolute value of classical momentum either always above or always below $\pi/2$, as can be verified from Eqs. (38) and (26) for δE_N and $S_B(E_N)$, respectively. This fact expresses the suppression of the potential barrier by the Trotterization due to next-to-nearest neighbor hopping.

Furthermore, if δt is not limited by the condition (41) due to detuning, large values of the exponent in Eq. (42) become possible, implying the change of η_{eff} by several orders of magnitude, as the effect of next-to-nearest hopping accumulates along the length of the barrier. Indeed, the first term in the exponent of Eq. (42) can roughly be estimated as

$$\frac{\delta S_B}{a} \sim -(J\delta t)^2 n_{\text{barr}} \times \begin{cases} \sqrt{P/J}, & P/J \ll 1, \\ (P/J)^2, & P/J \gg 1, \end{cases} \quad (45)$$

where n_{barr} is the number of sites in the forbidden region corresponding to the barrier, $P = \max_{x \in \text{barr}} |h(x) - E| - J$ is the energy scale of the potential barrier. While it is difficult to provide a similar estimation for the second term in the exponent of Eq. (42), it only enhances the suppression of the potential barrier as it is also negative in most cases. As a result, if $|\delta S_B|/a \gtrsim 1$, which might happen even if $J\delta t \ll 1$ for sufficiently large heights P/J and lengths n_{barr} of the barrier, the effective tunneling amplitude η_{eff} might become exponentially larger than that of the unperturbed Hamiltonian.

Of course, the resulting value of η_{eff} still has to be small compared to all other energy scales of the problem in order for the semiclassical approximation to be applicable. In the spirit

of Eq. (45), the underbarrier action S_B without perturbation can be estimated as

$$\frac{S_B}{a} \sim n_{\text{barr}} \times \begin{cases} \sqrt{P/J}, & P/J \ll 1, \\ P/J, & P/J \gg 1. \end{cases} \quad (46)$$

Requiring now that $\eta_{\text{eff}} \ll J, P, \Delta, \dots$ while still assuming that the barrier is semiclassical, i.e., $n_{\text{barr}} \gg 1$ and $S_B/a \gg 1$, thus leads to the following condition on δt :

$$\frac{S_B + \delta S_B}{a} \gg 1 \Rightarrow (J\delta t)^2 < \begin{cases} 1, & P/J \ll 1, \\ (P/J)^{-1}, & P/J \gg 1, \end{cases} \quad (47)$$

which is literally equivalent to the naive criteria (10). As a result, within its entire range of applicability, the Suzuki-Trotter approximation is capable of strongly enhancing tunneling as compared to the unperturbed evolution provided that the detuning effects described in Subsection III D are irrelevant.

The case of high barriers $P/J \gg 1$ is additionally interesting in the following regard: the estimations (45) and (46) show that the additional tunneling action (43) due to the Suzuki-Trotter approximation grows faster with the height P/J of the potential barrier than the unperturbed tunneling action (26), while the ensuing criteria of applicability Eq. (47) shows that the true parameter of the perturbation theory is $J\delta t \cdot P\delta t$. Should it be large, the perturbation $\delta\mathcal{H}$ actually governs the motion of the particle under the barrier, as evident from Eq. (47), implying that higher orders in δt corresponding to large-distance hopping also become important. In certain cases, these terms can be analyzed analytically, as explained in Subsection III H.

F. Enhancement of the decay rate

The case of the decay of a metastable state is governed by the same physics as the Rabi oscillations, safe for the different structure of single-particle levels at either side of the potential barrier (see Figure 2, right). According to Eq. (27), the decay rate of a given metastable state $|N\rangle$ inside the well changes to

$$\frac{\Gamma_{N,\text{eff}}}{\Gamma_N} \approx \exp \left\{ -\frac{2}{a} \left(\delta S_B(E_N) + \frac{\partial S_B(E_N)}{\partial E} \delta E_N \right) \right\}, \quad (48)$$

with the only difference with Eq. (42) being the extra factor of 2 in the exponent. Similarly to the previous case, the change of prefactor of Eq. (27) is neglected as a subleading correction, although it can trivially be taken into account, see Appendix Subsection B 5.

What is different with the case of Rabi oscillations is the effect of detuning: because all states inside the well are metastable, detuning does not prevent the decay process because it cannot detune the resonance with the dense spectrum on the other side of the well. In other words, the situation is similar to that of the previous Subsection III E: *i*) in most cases, trotterization enhances tunneling because the exponent of Eq. (48) is negative, and *ii*) this enhancement can constitute several orders of magnitude, but *iii*) for sufficiently high

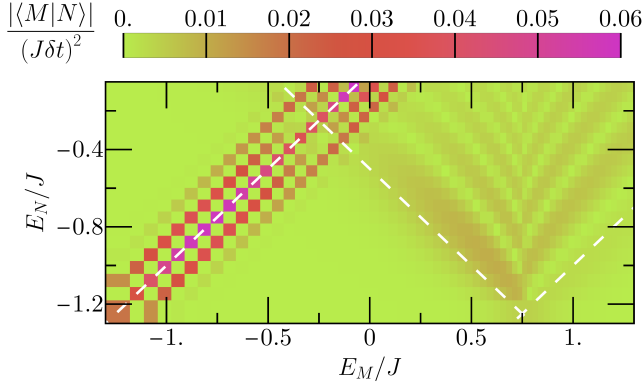


Figure 3. Color plot of the absolute value of the overlap $|\langle M|N\rangle|$ between a given local level $|N\rangle$ in local well of the exact Hamiltonian and the local level $|M\rangle$ of the effective Hamiltonian with $\delta t J = 0.2$ for the circuit on Figure 1, left. The potential profile is given by $h_n = P \cos\{4\pi(n-1)/(L-1)\}$, $P = 1.25J$ and the picture corresponds to the states in the left local well. For $N = M$ the quantity $\sqrt{1 - |\langle N|N_{\text{eff}}\rangle|^2}$ is plotted. All overlaps are normalized by $(J\delta t)^2$. All energies are shifted by J to simplify comparison with the potential profile. Diagonal white dashed lines correspond to (from left to right): *i*) $E_M = E_N$, *ii*) $E_M = 2J - 2P - E_N$, *iii*) $E_M = 2J + E_N$, so significant overlap close to these lines corresponds to *i*) smearing of the target state over close-lying states, *ii*) overlap with states that have typical momenta $\pi - p$, where p is the typical momentum of the original state, and *iii*) overlap with states with energy difference $2J$, corresponding to a different band. Computing the same quantity by 1st order perturbation theory $\langle N|M\rangle \approx \langle N|\delta\mathcal{H}|M\rangle / (E_N - E_M)$ and Eq. (49) for $N = M$ gives indistinguishable results.

barriers the perturbative treatment of Subsection III C is inapplicable, necessitating a more accurate description of the underbarrier motion with large-distance jumps taken into account.

G. Probability defect

Suppose the particle was originally prepared with the wave function $|N\rangle$ of a resonant state inside either of the wells. The perturbation due to Suzuki-Trotter approximation changes the stationary wave function in the well to $|N_{\text{eff}}\rangle$, so the latter acquires a finite overlap with other localized states $|M\rangle$, $M \neq N$ inside the well. As far as tunneling processes are concerned, of particular interest is the overlap with high-energy states, as the latter have much smaller tunneling exponents or even no tunnel barriers at all, thus introducing completely different character of evolution to the system. Motivated by this, we estimate the total probability defect $\delta P = 1 - |\langle N_{\text{eff}}|N\rangle|^2$ due to the distortion of the semiclassical wave function in the allowed region. The detailed calculation is presented in Appendix Subsection B 6, and the result reads

$$\delta P_N \approx \sum_{N' \neq N} \frac{|\langle N'|\delta\mathcal{H}|N\rangle|^2}{(E_N - E_{N'})^2} \approx C_N (J\delta t)^4, \quad (49)$$

where C_N is a positive constant bounded from above by n_{cl}^2 (with n_{cl} being the number of sites in the classically allowed region at energy E_N) but typically of the order of 1, as shown in Appendix Subsection B 6. The resulting probability defect is guaranteed to be small if

$$(J\delta t)^2 n_{\text{cl}} \ll 1. \quad (50)$$

This result can be understood from energy conservation. Indeed, the typical energy shift of a given state inside the well is given by Eq. (38), and if this shift approaches the typical level spacing Δ (which happens exactly when the criterion (50) is violated) then the initial state has no choice but to get distributed across $\delta N \sim \delta E_N / \Delta \sim (J\delta t)^2 n_{\text{cl}} \sim 1$ neighboring eigenstates of the distorted system.

It is important, however, that the distribution of the overlaps $\langle N'|N_{\text{eff}}\rangle$ might be quite different from the one expected from naive energy conservation law. In fact, two additional effects arrange a significant overlap with higher-energy states: *i*) the perturbation arranges overlap with states at energy difference $\approx J$ if those are present, as both have comparable classical momenta and *ii*) the presence of oscillating term, Eq. (32), in the effective Hamiltonian (neglected up until this point) arranges a finite overlap between states with momenta $\sim p$ and $\sim \pm\pi + p$. Those two phenomena are present on Fig. 3. While not directly relevant to the single-particle problem, this phenomena might turn out to be important for many-body problem by means of so-called orthogonality catastrophe [23].

H. Large Trotter steps within the semiclassical picture

We now discuss the effect of large-distance matrix elements of the full effective Hamiltonian \mathcal{H}_{eff} , which become important if $J\delta t$ is not very small, with special emphasis on the forbidden region, as hinted by the estimations of Subsection III E. The peculiarity of this region can be seen in the Wigner's transform (19) of the effective Hamiltonian given the estimation (29) of the large-distance matrix elements. Indeed, the Wigner's transform of the full Hamiltonian can be represented as

$$\delta\mathcal{H}(x = an, p) = \langle n|\delta\mathcal{H}|n\rangle + \sum_{|k|=1}^3 [\langle n|\delta\mathcal{H}|n+k\rangle e^{ipk}] + \sum_{|k|>3} \langle n|\delta\mathcal{H}|n+k\rangle e^{ipk}, \quad (51)$$

where the summation over k includes both positive and negative values. According to Subsection III A, the first two terms are of the order of $(J\delta t)^2$ and are discussed in detail in Sections III A-III F, while the last one is $O([J\delta t]^3)$ and the sum terms decay with k exponentially as $(J\delta t/4)^k$, according to Eq. (29). It then follows that the latter term is not important as far as the motion with real momentum is concerned. However, the higher-order term diverges at a imaginary momentum corresponding to

$$p_c \approx \pm i \ln \frac{4}{J\delta t}. \quad (52)$$

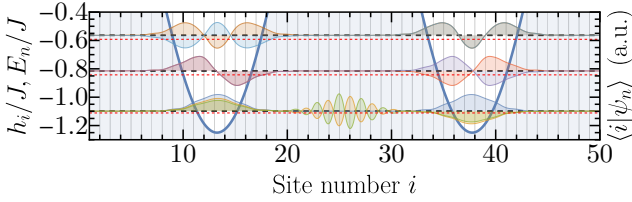


Figure 4. Visualization of the portion of the eigenlevels (horizontal black dashed lines) and eigenfunctions (curves with colored filling) for the Suzuki-Trotter simulation of the problem with the left circuit of Figure 1 and trotter step $J\delta t = 1.49707035$, $L = 50$ sites and potential profile $h_n/J = 5/4 \cos 4\pi(n-1)/(L-1)$ (thick blue line) realizing the double-well experiment (Figure 2, left). The horizontal red dashed lines represent the position of the energy levels of the original Hamiltonian (15). The tunnel splitting between symmetric and antisymmetric combination of the two wells is too small to be visible. All energies are shifted by J to simplify comparison with the potential profile. The precise choice of δt is required to tune the mode inside the forbidden region into resonance with one of the two states in the two wells, so two instances (green and orange) of hybridization of the antisymmetric state with the bound state inside the barrier state are observed. The energy splitting between symmetric (blue) and any of the the lowest antisymmetric states (green, orange) is $\sim 10^9$ bigger than the one in the unperturbed case, while for higher pairs of states (the first one on the plot is purple and red) the amplification of splitting is given by 9.3×10^4 , 4.1×10^3 . Note that the bound state deep inside the potential barrier corresponds to momenta close to π as its wave function demonstrates oscillations of the form $\psi_n \propto (-1)^n$.

Clearly, the presence of this singularity has important implications for the tunneling processes, as those are represented by the motion with imaginary momenta. If the latter approach the threshold value (58), one expects the semiclassical behavior to be significantly altered. Estimating the maximum momentum in the forbidden region by its unperturbed dynamics, Eqs. (18-19), we obtain that the tunneling trajectory does not approach this singularity if

$$(h(x) - E) \delta t \ll 1. \quad (53)$$

In this way, the second part of the criteria of applicability (10) of the Suzuki-Trotter approximation is reinstated. If condition (53) is violated, large-distance hopping becomes more favorable than tunneling through the barrier. Moreover, as evident from Eq. (53), the low-energy subspace is the first to be affected, with the most prominent effect occurring exactly at the point with the highest potential barrier. This also elucidates the observed difference in the scaling of the underbarrier action (46) and the correction (45) with the potential height P : Suzuki-Trotter error is dominant in the regions with sufficiently high potential barriers.

1. Floquet theorem and practical implications

As explained above, when either $J\delta t$ or $P\delta t$ is of order unity one expects certain qualitative differences between the evolution under the original Hamiltonian (15) and that under

the corresponding Suzuki-Trotter approximation. Indeed, as the total bandwidth of the original Hamiltonian $\Lambda \approx 2J + P$ approaches the value of $\Omega = 2\pi/\delta t$, inelastic processes involving changes of energy by a multiple of Ω cease to be purely virtual, thus causing a complete reconstruction of the eigenstates of the evolution. Mathematically, this is expressed by the Floquet theorem: because the energy spectrum of a system evolving under periodic drive with period δt is defined modulo $\Omega = 2\pi/\delta t$, high-energy states of the original Hamiltonian get mixed with low-energy ones due to the emerging periodicity in energy. The latter effect causes a strong distortion of the evolution in the low-energy subspace of interest.

One particular example of such distortion is shown on Figure 4: the system is fine-tuned close to $J\delta t \sim h\delta t \sim \pi/2$ to bring the high-energy states localized *inside* the barrier into resonance with bound states of the potential well. The resulting tunneling amplitude is exponentially enhanced due to the presence of an intermediate state.

2. Semiclassical description

The situation of large Trotter steps $(2J + P) \delta t \sim 1$ can be understood semiclassically. Indeed, the semiclassical approximation essentially relies on the fact that the classical momentum p changes slowly with spatial coordinate due to smoothness of the potential profile. On the other hand, the latter also manifests itself in the smallness of corrections (31) to the effective Hamiltonian due to the noncommutativity of the kinetic and potential terms. The main correction thus originates from noncommutativity of the kinetic terms on even and odd sites *in all orders* of $J\delta t$, as the latter is not small anymore. However, the procedure of collecting all those corrections exactly corresponds to computing the Suzuki-Trotter evolution operator (7) in absence of the potential term, which is straightforward in the momentum space. The semiclassical description of the Suzuki-Trotter evolution in a smooth potential thus amounts to diagonalizing the effective Hamiltonian in absence of the potential term and using the resulting wave functions to perform the semiclassical ansatz. The detailed procedure is presented in Appendix Subsection B 7, and here we just quote the result.

The semiclassical Hamiltonian is given by

$$\mathcal{H}_{\text{eff}}(x, p) = -\frac{2}{\delta t} \arcsin \left\{ \sin \frac{J\delta t}{2} \cos p \right\} + h(x), \quad (54)$$

where we assume that $J\delta t < 2\pi$. Naturally, expanding this expression in powers of δt restores the unperturbed Hamiltonian (19) and the correction (35). On the other hand, the form of the kinetic energy coincides with that of Ref [1] for $J\delta t = \pi/2$. The corresponding semiclassical wave function reads

$$\psi(x = na) = \frac{e^{iS(x)/a}}{\sqrt{v_p}} \left(\cos \theta_p - i e^{i\pi x/a} \sin \theta_p \right), \quad (55)$$

where $p = S'(x)$, the angle $\theta_p \in [0, \pi]$ is determined by the

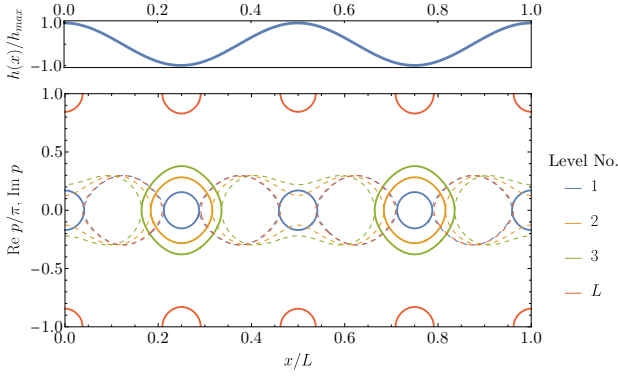


Figure 5. Phase portraits of the effective classical Hamiltonian (54) with the same parameters as on Figure 4 for three lowest and one highest eigenenergies of the unperturbed problem. Solid (dashed) lines denote real (imaginary) part of the momentum. Above the main figure presented is the corresponding potential profile. The hybridization observed on Figure 4 appears due to the exact resonance between the energies of the bound states inside the three regions around $x/L = 1/4, 1/2, 3/4$ (expressed as a match in the areas enclosed by the corresponding classical trajectories, in accordance with the quantization condition). This also explains the huge amplification of the tunnel splitting quoted on Figure 4.

problem without potential:

$$\sin 2\theta_p = \frac{\sin^2 \frac{J\delta t}{4} \sin 2p}{\sqrt{1 - (\cos p \sin \frac{J\delta t}{2})^2}}, \quad (56)$$

and the normalization v is the group velocity given by

$$v_p = \frac{\partial T}{\partial p} \cos 4\theta_p + \frac{1}{2} T \frac{\partial \cos 4\theta_p}{\partial p}, \quad (57)$$

with $T(p)$ being the kinetic energy of the semiclassical Hamiltonian 54.

Crucially, the amplitude of wave function (55) now contains both a smooth contribution and strongly oscillating contribution proportional to $(-1)^n$, which is the manifestation of the fact that the true translation period of the system under the Suzuki-Trotter evolution operator is doubled. It is for the same reason that the group velocity (57) differs from its original value $J \sin p$. For small $J\delta t$, the difference of the new wave function (55) and its counterpart (17) in the original system is $O((J\delta t)^2)$, in agreement with considerations of Subsection III A, while the correction to the group velocity v is $O((J\delta t)^4)$, which is beyond the precision of the previous subsections and hence also absent therein. On the contrary, for $J\delta t \sim \pi/2$ the magnitudes of the two terms in the prefactor of the wave function become comparable even for small momenta $|p| \gtrsim |\pi/2 - J\delta t|$, indicating the presence of strong oscillations even in the wave functions at low energies. At $J\delta t \sim \pi$, θ_p approaches $\pi/2$, rendering the oscillating component the dominant one.

Turning now to the motion with imaginary momenta corresponding to tunneling, the kinetic term of (54) has singularity

at imaginary momenta

$$p_c = \pm i \operatorname{arccosh} \frac{1}{\sin J\delta t/2} \quad (58)$$

which reduces to Eq. (52) in the limit of small δt . The associated equation of motion corresponding to the classical Hamiltonian (54) reads

$$\sin \frac{J\delta t}{2} \cos p = -\sin \frac{(E - h(x)) \delta t}{2}. \quad (59)$$

The violation of condition (53) by approaching to the singularity (58) in the momentum space then corresponds to the appearance of an allowed region inside the barrier, as shown on Figure 5. This region hosts bound states, which are the same states that would otherwise be observed at high energies $E \sim 2h + J$. In particular, this implies that at certain configurations a resonance is possible between such states and the states inside the well. If, in addition, $J\delta t \sim \pi/2$, both wave functions exhibit noticeable oscillations and thus have little overlap with the original bound state inside the well, as also hinted by the perturbative estimation (49) for the total probability defect.

IV. DISCUSSION

A. Main qualitative results

We constructed an analytical description of the distortion introduced by the Suzuki-Trotter algorithm (7) to the unitary evolution under the Hamiltonian (1) of XY chain with position-dependent z field, with emphasis on tunneling through potential barriers. Because the Hamiltonian (1) can be mapped to a system of noninteracting fermions by the Jordan-Wigner transformation [16], our analysis was focused on the distortion of the evolution under the corresponding single-particle Hamiltonian (15). We further restricted our analysis to the states with total z projection of spin equal to $-L/2 + 1$ (with L being the length of the spin chain), which translates to the single-particle subspace in terms of fermions.

Our approach is based on constructing an approximation to the effective time-independent Hamiltonian H_{eff} that governs the evolution of the system between discrete moments of time $t_n = n\delta t$, with δt being the Trotter step. We do so by examining formal expansion of H_{eff} in powers of δt . While in general this procedure is hindered by heating due to the periodic drive, we specifically consider the problem that is noninteracting in terms of fermions, which eliminates the issue of heating, as explained in Subsection III C. As a result, the evolution under the Suzuki-Trotter algorithm is fully characterized by an effective time-independent single-particle Hamiltonian \mathcal{H}_{eff} that can further be found as a series in powers of δt . Due to discrete nature of the evolution, the eigenenergies of this effective Hamiltonian are defined up to a multiple of $\Omega = 2\pi/\delta t$. That is why the criteria of applicability based on naive comparison of energy scales of the target Hamiltonian with Ω accurately capture the magnitude of the evolution distortion. Indeed, the

fact that Ω is the largest energy scale in the problem simply implies that all transitions induced by the Suzuki-Trotter error are virtual.

The situation of time-independent Hamiltonian and the emergent periodic evolution is to be contrasted to the case of aperiodic time-dependent Hamiltonian, for which low-frequency tails in the continuous spectrum of the perturbation might lead to significant modification of the tunneling dynamics by cascades of inelastic transitions [24].

Under the assumption of smooth potential profile, we employed the semiclassical approximation and showed that the main contribution to the error comes from noncommutativity of kinetic terms at neighboring pairs of sites. This contribution produces an additional term to the semiclassical Hamiltonian:

$$\delta\mathcal{H}_{\text{eff}}(x, p) = J \frac{(J\delta t)^2}{24} \cos p \sin^2 p, \quad (60)$$

which, in turn, leads to quantitative changes in certain tunneling processes.

One of the main effects of Trotterization is the shift of energies caused by the perturbation in the classically allowed region. The magnitude of this shift is given by (38) and can roughly be estimated as

$$|\delta E| \lesssim \frac{(J\delta t)^2}{24} \frac{2n_{\text{cl}}}{\pi} \Delta, \quad (61)$$

where J is the characteristic kinetic energy scale, Δ is the relevant local level spacing, n_{cl} is the size of the classically allowed region (that is, the region of localization of the metastable state of interest). This shift has the potential to detune the resonance and thus render the tunneling impossible in the first place. This effect puts a limitation on the Trotter size δt :

$$\eta \leq \delta E \Leftrightarrow (J\delta t)^2 \lesssim \eta n_{\text{cl}} / \Delta, \quad (62)$$

where η is the tunneling amplitude, an exponentially small quantity, which makes Eq. (62) the most essential limitation on the size of the Trotter step δt .

Hand in hand with the detuning goes the defect in the overlap between the initial state and the target subspace. If the initial state is prepared to exactly match the wave function corresponding to a metastable state that experiences tunneling, the perturbation of the classically allowed region deforms this target state. The corresponding overlap defect can be estimated as

$$\delta P_N = 1 - |\langle \psi_{\text{init}} | \psi_N \rangle|^2 \sim C_N (J\delta t)^4, \quad (63)$$

where $C_N \leq n_{\text{cl}}^2$ is state-dependent constant that can be expressed semiclassically, and n_{cl} is the size of the allowed region for the N -th level. Notably, this probability defect gets distributed across all kinds of states, including high-energy states, as demonstrated on Figure 3, although the majority of the probability defect is still localized around the target energy level.

The situation changes significantly if the resonance is not spoiled, e.g., due to the symmetry of the wells (in which cases it has to be preserved by the simulation protocol), or continuous

spectrum with level spacing $\delta \ll \eta$ outside the well. In this case, the main effect of the perturbation is to alter the tunneling amplitude, and the decay rate, respectively:

$$\frac{\eta_{N,\text{eff}}}{\eta_N} = \sqrt{\frac{\Gamma_{N,\text{eff}}}{\Gamma_N}} \approx \exp \left\{ -\frac{1}{a} \left(\delta S_B + \frac{\partial S_B}{\partial E} \delta E \right) \right\}, \quad (64)$$

where δS_B is the correction to the underbarrier action given by Eq. (43), S_B is the original tunneling action given by Eq. (26), and $\delta E \sim (J\delta t)^2 n_{\text{cl}} \Delta$ is the energy shift induced by the perturbation. In most cases, the exponent of Eq. (64) is positive, and the resulting effect can thus represent and exponentially large *increase* in the tunneling rate, even for small values of δt .

An increase in performance due to discretization has been reported for Quantum Annealing Algorithms [25, 26] that supposedly rely on tunneling. While the systems used to study quantum optimization algorithms typically feature strongly disordered potential landscapes, rendering our approach inapplicable even in principle, one might still expect that the discussed large-distance hops induced by the Suzuki-Trotter approximation do increase tunneling rates.

We also demonstrated that for sufficiently large values of δt the unitary evolution under the Suzuki-Trotter approximation is starkly different from the original Hamiltonian evolution. As it is shown in Subsection III H, large-distance hops dominate the behavior of the system, with the most prominent effect observed for the states with the largest potential barriers $P\delta t \sim 1$, where $P \sim \max_x h(x) - E$ is the height of the barrier. This also provides an evidence against the use of large-step Suzuki-Trotter approximation for examining low-energy physics. The values of δt that do not cause such behavior are given by the naive comparison of energy scales:

$$J\delta t, P\delta t \ll 1, \quad (65)$$

where J, P is the typical magnitude of the kinetic and potential terms, respectively.

B. Relation with the rigorous error bounds

It is instructive to compare our results with the available rigorous bounds and see whether they are saturated. The rigorous upper bound on the spectral norm distance $\|O\| = \sqrt{\frac{1}{2^n} \text{Tr} O^\dagger O}$ (with n being the number of qubits) between the exact U and approximate U_{appr} evolution operators during one Trotter step is given by [6, Sec. F.2.1, Eq. (86)]:

$$\|U(\delta t) - U_{\text{appr}}(\delta t)\| \leq C \frac{x^3}{n} + \frac{x^4}{12} e^x \quad (66)$$

where $x = 3n\Lambda\delta t$, $C < 1/4$ is a certain numerical constant, $\Lambda = \max\{h, J/2\}$ is the maximum magnitude of local terms in the Hamiltonian, and n is the system size. This implies a rigorous upper bound on eigenvalue difference:

$$|E_N - E_{N,\text{eff}}| \leq 3C\Lambda (3n\Lambda\delta t)^2, \quad (67)$$

where we neglected the subleading second term in Eq. (66), which is justified for small δt . In comparison to the estimate

of Eq. (39), the upper bound is tight as a function of δt and $\Lambda = \max\{P, J/2\}$, while the overall energy scale $n_{\text{cl}}\Delta$ is replaced by its model-blind upper bound $n\Lambda$ up to an overall numerical coefficient. We also note that, while bound (66) applies to arbitrary initial state of a chain of qubits, reducing the problem to the single-particle subspace only changes the overall prefactor and thus does not alter the qualitative behavior.

However, the rigorous bound (66) predictably fails to accurately reflect the structure of error at large times. After $r = t/\delta t$ Trotter steps, the upper bound on the error in the evolution operator reads [6, Sec. F.2.1, Eq. (86)]

$$\left\| U(t) - [U_{\text{appr}}(\delta t)]^{t/\delta t} \right\| \leq \frac{t}{\delta t} \left(C \frac{x^3}{n} + \frac{x^4}{12} e^x \right), \quad (68)$$

which implies that at time scales of the order of the inverse detuning (67)

$$\Lambda t_{\text{bound}} \sim \frac{\Lambda}{\delta E} \sim (3n\Lambda\delta t)^{-2}, \quad (69)$$

the difference between the exact and approximate evolution operators can be expected to attain order of unity, implying a noticeable divergence of the simulation from the target. However, this statement is strongly dependent on the physical observable in question and the required precision. As an example, consider the expectation value of the number of particles in the left well $\mathcal{N}_{\text{left}} = 2 \sum_{i=1}^{L/2} S_i^z + L$ for the double-well experiment described in Subsection II C and a measurement precision $\epsilon \leq 1$ that is still larger than the total probability defect, Eq (63). Each pair of resonant states in the two wells is then characterized by its respective effective Hamiltonian (16). The initial state is prepared as one of the exact left states $|\psi_{N,\text{left}}\rangle$. In the simulation by means of Suzuki-Trotter algorithm, the time dynamics of the expectation value $\langle \mathcal{N}_{\text{left}} \rangle$ is approximately described as

$$\langle \mathcal{N}_{\text{left}}(t) \rangle \approx \frac{\epsilon_{N,\text{eff}}^2/4}{\Omega_{N,\text{eff}}^2} + \left\{ 1 - \frac{\epsilon_{N,\text{eff}}^2/4}{\Omega_{N,\text{eff}}^2} \right\} \cos^2 \Omega_{N,\text{eff}} t, \quad (70)$$

where $\Omega_{N,\text{eff}} = \sqrt{\eta_{N,\text{eff}}^2 + \epsilon_{N,\text{eff}}^2/4}$, and both the exponentially small contribution of states in the right well to $\langle \mathcal{N}_{\text{left}} \rangle$ and the total probability defect, Eq. (63), were neglected, as the allowed error ϵ is assumed to be larger than those effects. The dynamics of $\langle \mathcal{N}_{\text{left}} \rangle$ is thus starkly different depending on whether the detuning effect due to Suzuki-Trotter error is present or not, although in both cases the dominant error reveals itself only at times much larger than t_{bound} . In the former case, the tunneling is destroyed as $\epsilon_{N,\text{eff}} \gg \eta_N$, but the difference between now nearly constant $\langle \mathcal{N}_{\text{left}} \rangle$ with its unperturbed counterpart exhibiting Rabi oscillations reaches ϵ at exponentially large times $t \sim \eta_N^{-1} \sqrt{\epsilon} \gg t_{\text{bound}}$. In the case of no detuning, Rabi oscillations are still observed in the perturbed evolution, but the frequency of oscillations is changed according to Eq (64), so the difference ϵ is reached at slightly smaller times $t \sim \sqrt{|\eta_{N,\text{eff}}^{-2} - \eta_N^{-2}|} \sqrt{\epsilon} \lesssim \eta_N^{-1} \sqrt{\epsilon}$, but this time is still

much larger than t_{bound} implied by the rigorous bound. Certainly, this analysis looses the short-time error occurring due to both detuning (if present) and probability defect δP_N , which is precisely the content of the rigorous bound (66). However, it clearly illustrates that rigorous upper bounds overstate the actual magnitude of error at large times for certain observables.

C. Immediate experimental realization

In this section, we propose a particular circuit that demonstrates the presented physics and its extensions with circuit depth of $1.2 \cdot 10^5$, with all the details presented in Appendix C. While Ref. [1] performed spectral analysis of noisy circuits with depths up to $1.4 \cdot 10^3$ for a similar experiment, we expect depths $\sim 10^5$ to be possible in the near future. The latter anticipation is motivated by two reasons: *i*) the problem is manifestly single-particle, which renders error mitigation by post-selection efficient [1], and *ii*) the coherent times of superconducting devices are already in the range of $3 \times 10^2 \mu\text{s}$ [4, 27], more than 10 times larger than that of the device in Ref. [1], and further improvement is likely to occur. Moreover, due to optimized design choices, the proposed experiment can tolerate relative static coherent error of order 5×10^{-3} , which is well within the capabilities of the device used in Ref. [1]. As a result, we expect this experiment to be feasible in the near future.

The idea behind the proposed design is to observe the Rabi oscillations in the double-well potential. One prepares the initial state in one of the wells, and then observes the occupation number in either of the wells. To better resolve the oscillations, one can analyze the Fourier transform of the occupation number, as done in Ref. [1]. Due to the limitations of the current devices, several optimizations have to be made: *i*) the energy of the initial state has to be close to the top of the potential barrier, to avoid too large tunneling times; *ii*) the typical momentum of the initial state has to be close to $\pi/2$, in order to reduce the perturbative energy shift (38) that may otherwise lift the target state above the barrier; *iii*) the initial state has to be close to one of the resonant states to maximize the visibility of the Rabi oscillations. The detailed discussion of these requirements and the resulting experimental design for a system of $L = 50$ qubits are presented in Appendix C.

The plot of the resulting period of the observed Rabi oscillations as a function of the Trotter step δt is presented on Figure 6 together with the corresponding semiclassical prediction. In particular, one can clearly see nearly fivefold acceleration of tunneling at large Trotter step (the value of $2\pi J/\omega$ drops from 5×10^3 to 1×10^3) while the energy shift of the corresponding state is practically absent (it becomes smaller than the tunnel splitting at large Trotter steps). The detailed procedure for the numerical simulation is presented in Appendix C.

D. Outlook

Recent literature demonstrates a revival of the debate on the exact interpretation of what happens in the classically forbid-

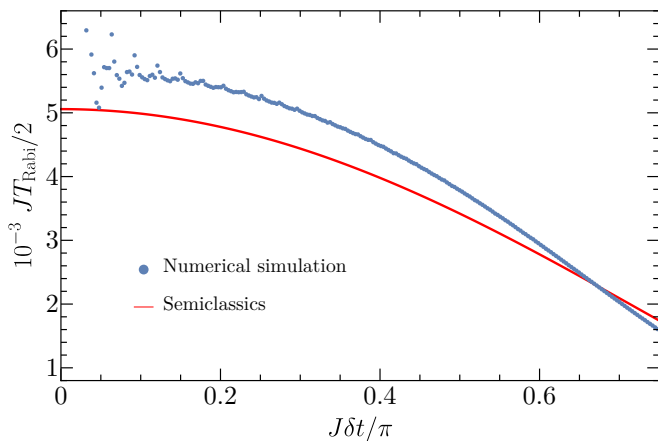


Figure 6. Dependence of the period of Rabi oscillations on the Trotter step δt for system described in Subsection C2. The blue dots are obtained by simulating the dynamics of the total occupation number in one of the potential wells. The observed noise at small δt is due to the fact that the maximum allowed number of Trotter steps allows to simulate only one full period of oscillations. The red curve corresponds to semiclassical description of the Rabi oscillations, as detailed in Appendix C. The remaining discrepancy between the semiclassical description and direct simulation is due to corrections beyond the semiclassical description (the potential is not sufficiently smooth).

den region during a tunneling event, with particular emphasize on the question of the tunneling time [28]. The discussion is complicated by nontrivial interpretation of the measurement outcomes in many experimental designs. Based on the result of our analysis, we believe that the existing superconducting qubit systems provide a promising platform for an in-depth study of the issue, especially given the unique opportunity to perform simultaneous measurements at every spatial point. However, a practical challenge of characterizing tunneling experimentally is to design a clock to measure the time spent under the barrier, with a notable implementation by a controlled periodic modulation of the barrier height [29]. The latter is straightforwardly realized in existing qubit platforms, hence the experiment described in the previous subsection can be tailored to contribute to the debate on the tunneling time. However, the structure of error due to the Suzuki-Trotter approximation applied to the resulting *time-dependent* Hamiltonian should also be carefully analyzed, as described below.

The present theoretical analysis can be generalized to higher-order product formulas that are expected to yield $O((J\delta t)^{2k})$ naive accuracy of $H_{\text{eff}} - H$ in powers of δt [11]. Those corrections are clearly more nonlocal and are thus more sensitive to the exact shape of the potential (expansion in gradients of the potential converges slower). However, we expect the qualitative content of the analysis to remain the same as that of $k = 1$: effects in the classically allowed region are perturbative, while the effects on tunneling can be described by the leading-order correction to the classical tunneling action, as long as the barrier is not too high. It also follows that the tunneling events still impose the limitation $P\delta t \ll 1$ regardless of the order k

of the product formula due to the Floquet theorem reasoning (in terms of Subsection III H, the singularities in the kinetic part of the effective semiclassical Hamiltonian are still located at $p \sim \pm i \ln \frac{1}{J\delta t}$).

There are many ways to extend the proposed model to more physically nontrivial situations. One particularly important question is the interplay between fermionic statistics and Trotterization, which appears as soon as many-body states are considered. One immediate example is the decay of large spin density (or, equivalently, fermionic particle density) confined to a local minimum of the potential such as on Figure 2, right.

Connected to the many-body physics is the question of interaction: our model enjoys a mapping to non-interacting fermions, whereas all known applications of the existing quantum hardware necessarily imply true many-body dynamics that is capable of taking advantage of large Hilbert space [12–14]. Analyzing the qualitative effects of Trotterization in this class of problems is thus of great practical significance. One particularly important effect completely absent in a single-particle setting is that generic many-body system subject to periodic perturbation (such as the one induced by the Suzuki-Trotter approximation) will heat up even at high frequencies of the perturbation [15].

An instance of non-integrable many-body evolution in *homogeneous* potential was studied numerically in Ref. [30]. In this work, considered is the Ising spin chain, with Z being the quantization direction, supplemented by a certain local interaction term, and subject to external homogeneous field along X and Z directions, with the Z component being small. By using a carefully crafted state containing a localized boundary between regions with opposite spin polarizations, the authors of Ref. [30] quantitatively analyzed *i*) the Bloch's oscillations of the boundary due to finite band width, and *ii*) excitation production due to collision of two such boundaries. The question of whether Trotterization has a qualitative effect on these results then becomes practically important as soon as one wishes to reproduce and extend these results using quantum hardware. However, addressing many-body physics of this type is not possible with existing noisy quantum devices [30] and requires instead implementing quantum error correction protocols [31, 32].

Several immediate developments of the proposed model concern the introduction of potential disorder to the single-particle Hamiltonian (15), as has been done in Ref. [1] for small systems. On the one hand, arbitrarily small disorder induces Anderson localization in one dimension at length scales comparable to the mean free path [33]. While our method is not straightforwardly applicable to local potential disorder, we still expect that the key effect of Suzuki-Trotter approximation for small disorder amounts to smearing the potential disorder, causing only a renormalization of the mean free path and, consequently, of the localization length. On the other hand, sufficiently strong disorder drives the system deep into the localized phase, which is obviously beyond the approximation of smooth potential employed in the present work, so we leave this for future studies.

Extending the presented analysis to the case of a time-dependent Hamiltonian represents another interesting chal-

lenge. While rigorous upper bounds on the Suzuki-Trotter error for time-dependent Hamiltonians are also available [9], the question of their saturation is much less trivial, as it depends on the exact dynamics arranged by the target time-dependent Hamiltonian. In particular, explicit time dependence renders the Floquet theorem inapplicable, enabling a wide range of additional physical effects. One particular example is the dynamic inelastic enhancement of tunneling due to a periodic drive of the Hamiltonian with frequencies much larger than the tunneling rate η but smaller than the height of the barrier potential barriers [24].

Finally, an important issue is that of external time-dependent noise, both as a part of the Hamiltonian and as an inescapable consequence of coupling between the physical device imple-

menting the qubit system and the environment. Among the most substantial effects for tunneling is the suppression of tunneling due to coupling to external bath [34, Sec. 3.5]. It is then of practical importance to find out whether sufficiently strong large-distance hopping or other effects induced by Trotterization are capable of influencing this effect.

ACKNOWLEDGMENTS

The authors would like to thank Mikhail V. Feigel'man for numerous fruitful discussions. A.V.K. is also grateful for the support by Laboratoire d'excellence LANEF in Grenoble (ANR-10-LABX-51-01).

-
- [1] C. Neill, T. McCourt, X. Mi, Z. Jiang, M. Y. Niu, W. Mroczkiewicz, I. Aleiner, F. Arute, K. Arya, J. Atalaya, *et al.*, *Nature* **594**, 508 (2021).
 - [2] I. M. Georgescu, S. Ashhab, and F. Nori, *Rev. Mod. Phys.* **86**, 153 (2014).
 - [3] F. Arute, K. Arya, R. Babbush, D. Bacon, J. C. Bardin, R. Barends, R. Biswas, S. Boixo, F. G. S. L. Brandao, D. A. Buell, *et al.*, *Nature* **574**, 505–510 (2019).
 - [4] A. P. M. Place, L. V. H. Rodgers, P. Mundada, B. M. Smitham, M. Fitzpatrick, Z. Leng, A. Premkumar, J. Bryon, A. Vrajitoarea, S. Sussman, *et al.*, *Nature communications* **12**, 1779 (2021).
 - [5] K. J. Satzinger, Y.-J. Liu, A. Smith, C. Knapp, M. Newman, C. Jones, Z. Chen, C. Quintana, X. Mi, A. Dunsworth, *et al.*, *Science* **374**, 1237–1241 (2021).
 - [6] A. Childs, D. Maslov, T. Nam, N. J. Ross, and Y. Su, *Proceedings of the National Academy of Sciences* **115**, 9456–9461 (2018).
 - [7] D. W. Berry, G. Ahokas, R. Cleve, and B. C. Sanders, *Communications in Mathematical Physics* **270**, 359–371 (2007).
 - [8] J. Haah, M. B. Hastings, R. Kothari, and G. H. Low, *SIAM Journal on Computing Special Section FOCS*, 250 (2018).
 - [9] A. M. Childs and Y. Su, *Physical review letters* **123**, 050503 (2019).
 - [10] A. M. Childs, A. Ostrander, and Y. Su, *Quantum* **3**, 182 (2019).
 - [11] M. Suzuki, *Journal of Mathematical Physics* **32**, 400–407 (1991).
 - [12] V. N. Smelyanskiy, K. Kechedzhi, S. Boixo, S. V. Isakov, H. Neven, and B. Altshuler, *Physical Review X* **10**, 011017 (2020).
 - [13] T. Albash and D. A. Lidar, *Rev. Mod. Phys.* **90**, 015002 (2018).
 - [14] K. Bharti, A. Cervera-Lierta, T. Kyaw, T. Haug, S. Alperin-Lea, A. Anand, M. Degroote, H. Heimonen, J. Kottmann, T. Menke, *et al.*, *Rev. Mod. Phys.* **94**, 015004 (2022).
 - [15] D. A. Abanin, W. De Roeck, W. W. Ho, and F. H. L. Heekeren, *Physical Review B* **95**, 014112 (2017).
 - [16] E. Lieb, T. Schultz, and D. Mattis, *Annals of Physics* **16**, 407–466 (1961).
 - [17] H. Yoshida, *Physics letters A* **150**, 262–268 (1990).
 - [18] M. V. Berry and K. E. Mount, *Reports on Progress in Physics* **35**, 315 (1972).
 - [19] P. A. Braun, *Reviews of modern physics* **65**, 115 (1993).
 - [20] F. Bloch, *Zeitschrift für physik* **52**, 555–600 (1929).
 - [21] L. D. Landau and E. M. Lifshitz, *Quantum mechanics: non-relativistic theory*, Vol. 3 (Elsevier, 2013).
 - [22] M. Bukov, L. D'Alessio, and A. Polkovnikov, *Advances in Physics* **64**, 139–226 (2015).
 - [23] P. W. Anderson, *Physical Review Letters* **18**, 1049 (1967).
 - [24] B. I. Ivlev and V. I. Melnikov, in *Quantum tunnelling in condensed media.*, edited by Y. Kagan and A. J. Leggett (Elsevier, 1992) Chap. 5, p. 265–312.
 - [25] B. Heim, T. F. Rønnow, S. V. Isakov, and M. Troyer, *Science* **348**, 215–217 (2015).
 - [26] D. S. Steiger, T. F. Rønnow, and M. Troyer, *Physical review letters* **115**, 230501 (2015).
 - [27] V. V. Sivak, A. Eickbusch, B. Royer, S. Singh, I. Tsioutsios, S. Ganjam, A. Miano, B. L. Brock, A. Z. Ding, L. Frunzio, *et al.*, *Nature* **616**, 50 (2023).
 - [28] U. S. Sainadh, R. T. Sang, and I. V. Litvinyuk, *Journal of Physics: Photonics* **2**, 042002 (2020).
 - [29] M. Büttiker, Traversal, Reflection and Dwell Time for Quantum Tunneling, in *Electronic Properties of Multilayers and Low-Dimensional Semiconductor Structures*, edited by J. M. Chamberlain, L. Eaves, and J.-C. Portal (Springer US, Boston, MA, 1990) pp. 297–315.
 - [30] A. Milsted, J. Liu, J. Preskill, and G. Vidal, *PRX Quantum* **3**, 020316 (2022).
 - [31] Google Quantum AI, *Nature* **614**, 676 (2023).
 - [32] A. Kitaev, *Annals of Physics* **303**, 2–30 (2003).
 - [33] E. Abrahams, P. W. Anderson, D. C. Licciardello, and T. V. Ramakrishnan, *Phys. Rev. Lett.* **42**, 673 (1979).
 - [34] A. Kamenev, *Field theory of non-equilibrium systems* (Cambridge University Press, 2023).
 - [35] V. P. Maslov and M. V. Fedoriuk, *Semi-classical approximation in quantum mechanics*, Vol. 7 (Springer Science & Business Media, 2001).

Appendix A: Discrete Semiclassical Approximation

In this Appendix, the semiclassical approximation for 1D systems is reviewed. The derivation of the semiclassical ansatz is in line with Ref. [35], and the matching procedure is done similarly to Ref. [18].

1. Semiclassical wave function

We start from the exact Shroedinger equation:

$$\sum_m \mathcal{H}_{nm} \psi_m = E \psi_n, \quad (\text{A1})$$

where \mathcal{H}_{nm} are matrix elements of the Hamiltonian in certain basis, such as the site position basis for the Hamiltonian (15) of the present paper. We assume that in this basis the matrix elements \mathcal{H}_{nm} obey two conditions: *i) locality*: \mathcal{H}_{nm} decay quickly (e.g., exponentially) with the difference $|n - m|$, and *ii) smoothness*: \mathcal{H}_{nm} depend smoothly on $a(n + m)$ with some characteristic scale $a \ll 1$. For the case of hopping Hamiltonians of the form (15) this implies only short-distance hopping, with both the hopping constants and the potential terms depending on site number n only via a combination an . We then search the wave function in the form of the following asymptotic series:

$$\psi_n = \exp \left\{ \frac{iS(x)}{a} \right\} [\varphi_0(x) + a \varphi_1(x) + \dots], \quad x = an \quad (\text{A2})$$

where $S(x)$ and $\varphi_i(x)$ are slow functions of their arguments. The action of the Hamiltonian on such wave functions can be expanded in powers of small a :

$$\begin{aligned} \sum_m \mathcal{H}_{nm} \psi_m &= \sum_m \mathcal{H}_{nm} \exp \left\{ \frac{iS(am)}{a} \right\} [\varphi_0(am) + a \varphi_1(am) + \dots] \\ &\approx \exp \left\{ \frac{iS(x)}{a} \right\} \mathcal{H}(x, p) [\varphi_0(x) + a \varphi_1(x) + \dots] \\ &+ (-ia) \exp \left\{ \frac{iS(x)}{a} \right\} \left\{ \partial_p \mathcal{H}(x, p) \varphi_0'(x) + \frac{1}{2} S''(x) \partial_p^2 \mathcal{H}(x, p) \varphi_0(x) \right\} + O(a^2), \end{aligned} \quad (\text{A3})$$

where $x = an$, $p = dS/dx$ is the semiclassical momentum, and $\mathcal{H}(n, p)$ is the Wigner's transform of the Hamiltonian:

$$\mathcal{H}(x = an, p) = \sum_m \mathcal{H}_{nm} \exp \{ ip(n - m) \}. \quad (\text{A4})$$

According to the locality and smoothness conditions, this function depends smoothly on both of its arguments, with n -dependence expressed via the combination an , $a \ll 1$. The two leading orders in powers of a of Eq. (A3) and the Schrodinger equation (A1) imply the classical equation of motion

$$\mathcal{H}(x, p) = E, \quad (\text{A5})$$

as well as an equation on φ_0 called the transport equations (as it ensures the conservation of probability density):

$$\left\{ \partial_p \mathcal{H}(x, p) \frac{d}{dx} + \frac{1}{2} S''(x) \partial_p^2 \mathcal{H}(x, p) \right\} \varphi_0(x) = 0, \quad (\text{A6})$$

with similar equations also available for higher orders φ_i , $i \geq 1$, if one were to retain higher orders in the expansion (A3). The transport equation can be solved explicitly, yielding

$$\varphi_0(x) = \frac{\text{const}}{\sqrt{\partial_p \mathcal{H}(x, p)}} \exp \left\{ \frac{1}{2} \int^x dx \frac{\partial_x \partial_p \mathcal{H}(x, p)}{\partial_p \mathcal{H}(x, p)} \right\} \quad (\text{A7})$$

where the position-dependent value of the classical wave length $p(x)$ found from Eq. (A5) is implied. In particular, if the Hamiltonian has the form $\mathcal{H}_{\text{kin}} + \mathcal{H}_{\text{pot}}$, with kinetic term being position-independent and H_{pot} being diagonal, the cross term $\partial_x \partial_p \mathcal{H}$ vanishes, and one arrives to the standard form of the WKB anstaz for the wave function:

$$\psi_n = \frac{\text{const}}{\sqrt{|v(x)|}} \exp \left\{ \frac{i}{a} \int^x p(x) dx \right\}, \quad x = an \quad (\text{A8})$$

where $v(x) = \partial_p \mathcal{H}(x, p(x))$ is the classical velocity, and $p(x)$ is the classical wave length found from the classical equation of motion, Eq. (A5), with the latter having solutions with two different signs of p , corresponding to particles propagating in different directions according to the sign of the semiclassical velocity.

The ansatz (A2) is an asymptotic series whose applicability is controlled by the two initial assumptions of locality and smoothness of the Hamiltonian. *A posteriori*, they are expressed in the requirement for the de Broglie wave length $\lambda(x) = 2\pi a/p(x)$ to change slowly with $x = an$ at the scale of the wave length itself:

$$\frac{d\lambda}{dx} \lambda \ll \lambda \Leftrightarrow a \frac{1}{p^2} \frac{\partial_x \mathcal{H}}{\partial_p \mathcal{H}} \ll 1, \quad (\text{A9})$$

While this condition is satisfied in general case due to smallness of a , it is clearly violated if either p or $v = \partial_p \mathcal{H}$ approach zero, which correspond to classical turning points. In this region, the semiclassical expansion (A2) is not applicable, and one has to employ the matching procedure.

2. Matching conditions and quantization rules for the cosine spectrum

For the particular case of Hamiltonian (15), the classical Hamiltonian is given by $-J \cos p + h(x)$, and the positions of the classical turning points are described by $\sin p = 0$, or $E - h(x) = \pm J$. If $dp/dx \neq 0$ at such point (where $p(x)$ is found from the classical equation of motion), the x axis is split by the turning point into classically allowed and classically forbidden region. At sufficiently large distances from the tuning point, the semiclassical solution becomes applicable, but one still has to connect the amplitudes of the semiclassical wave functions at either sides of the turning point. To do that, one needs to provide a solution for the vicinity of the tuning point, possibly exploiting. These two solutions are then matched together by their asymptotic forms. In order for this procedure to work, there has to be an overlap in the regions of applicability of the two approximations with spatial sizes that fit many de Broglie wave length, so the phase change $\frac{1}{a} \int^x p(x) dx \propto \int^x dx/\lambda(x)$ is large as one traverses the overlap region.

One particularly important case where the vicinity of the critical point can be analyzed is the case of smooth potential that can be expanded as $h(x) \approx h_0 + \alpha(x - x_0)$ in a sufficiently large neighborhood of the classical turning point x_0 . One then distinguishes two cases: standard turning point $p = 0$, corresponding to $h_0 = E + J$, and anomalous tuning point, for which one has $h_0 = E - J$. Both these cases are analyzed below in the respective subsections.

The existence of anomalous turning points leads to a different structure of the classically allowed region in comparison to the textbook case of quadratic dispersion law. In particular, if the potential $h(x)$ has a local minimum at $h(x_{\min}) = h_{\min}$, finite band width of the kinetic term implies that at energies higher than $J + h_{\min}$ one expects a forbidden zone to appear in the middle of the well. The quantization conditions involving anomalous turning points are then required to accurately describe the resulting eigenlevels.

a. Standard turning point

Let $\alpha > 0$ be the potential gradient, and E is such that $\alpha a \delta = E + J$ for some $\delta \in [0, 1]$ (one can always shift the numeration of sites in order to force the exact position of the tuning point to lie in the $[0, 1]$ section). The exact Shroedinger equation (A1) then reads

$$-\frac{J}{2} [\psi_{n+1} + \psi_{n-1}] + \alpha a n \psi_n = (\alpha a \delta - J) \psi_n. \quad (\text{A10})$$

Although this equation is exactly solvable in terms of Bessel functions, we will resort to an controllable approximation that exploits the smoothness of the potential and formally corresponds to asymptotic expansion of the exact solution in powers of the gradient of the potential $\alpha a \ll 1$. Near $n = 0$, we expect to find a solution that is a smooth function of $x = an$, as the relevant classical momenta are small due to the proximity to the standard turning point where $p(x_0 = a\delta) = 0$. One can then replace the discrete difference $\psi_{n+1} + \psi_{n-1} - 2\psi_n$ by its continuous approximation $a^2 d^2 \psi / dx^2 + O(a^4)$, which is equivalent to replacing the true p -dependence of the classical Hamiltonian (19) with its quadratic approximation near $p = 0$. The criterion of applicability for such a replacement is given by the smallness of the momentum that validates the quadratic expansion:

$$|p|^2 \approx \left| \frac{E + J - \alpha a x}{J} \right| \ll 1 \Leftrightarrow \frac{\alpha}{J} |x - a\delta| \ll 1, \quad (\text{A11})$$

where the momentum is estimated from the energy conservation. Performing the substitution, one obtains the following differential equation:

$$-\frac{J a^2}{2} \psi''(x) + \alpha x \psi(x) = \alpha a \delta \psi(x), \quad (\text{A12})$$

which is exactly solvable in terms of the Airy functions:

$$\psi(x) = C_1 \text{Ai}(K(x - a\delta)) + C_2 \text{Bi}(K(x - a\delta)), \quad K = \left(\frac{2\alpha}{Ja^2}\right)^{1/3} \gg 1. \quad (\text{A13})$$

Despite the condition (A11), $K(x - a\delta)$ can attain large values, so it is legitimate to use the asymptotic expansion of the Airy functions in the region $K^{-1} \ll |x - a\delta| \ll (\alpha/J)^{-1}$, rendering

$$\psi_n \approx \begin{cases} z > 0: & C_1 \frac{1}{2\sqrt{\pi}} \sqrt[4]{\frac{1}{z}} \exp\left(-\frac{2}{3}z^{3/2}\right) + C_2 \frac{1}{\sqrt{\pi}} \sqrt[4]{\frac{1}{z}} \exp\left(+\frac{2}{3}z^{3/2}\right), \\ z < 0: & C_1 \frac{1}{\sqrt{\pi}} \sqrt[4]{\frac{1}{|z|}} \cos\left(-\frac{2}{3}|z|^{3/2} + \frac{\pi}{4}\right) + C_2 \frac{1}{\sqrt{\pi}} \sqrt[4]{\frac{1}{|z|}} \cos\left(\frac{2}{3}|z|^{3/2} + \frac{\pi}{4}\right), \end{cases} \quad z = K(x - a\delta). \quad (\text{A14})$$

On the other hand, the semiclassical approximation can be applied in the region described by its applicability condition (A9), which amounts to $K|x - a\delta| \gg 1$. The semiclassical wave functions then reads:

$$\psi(x) \approx \begin{cases} \text{allowed region:} & \frac{1}{\sqrt{|v(x)|}} \exp\left\{\pm \frac{i}{a} \int_{a\delta}^x p(x) dx\right\}, \\ \text{forbiden region:} & \frac{1}{\sqrt{|v(x)|}} \exp\left\{\pm \frac{1}{a} \int_{a\delta}^x |p(x)| dx\right\}, \end{cases} \quad (\text{A15})$$

where $p(x) = \arccos(h(x) - E)/J$, and $v(x) = J \sin p(x)$. Given the condition (A11), one can replace $\arccos 1 - u \approx \sqrt{2u}$, which is equivalent to replacing the kinetic energy with its quadratic approximation, so the semiclassical approximation for the wave function is given by

$$\psi_n \approx \begin{cases} z > 0: & C_{\text{decaying}} \frac{1}{z^{1/4}} \exp\left\{-\frac{2}{3}z^{3/2}\right\} + C_{\text{growing}} \frac{1}{z^{1/4}} \exp\left\{+\frac{2}{3}z^{3/2}\right\}, \\ z < 0: & C_{\text{towards}} \frac{1}{|z|^{1/4}} \exp\left\{+\frac{2i}{3}|z|^{3/2}\right\} + C_{\text{away}} \frac{1}{|z|^{1/4}} \exp\left\{-\frac{2i}{3}|z|^{3/2}\right\}, \end{cases} \quad z = K(n - a\delta), \quad (\text{A16})$$

where the labeling of the C coefficients represents the direction of propagation w.r.t the turning point according to the sign of the group velocity $v = J \sin p \approx Jp$ for $z > 0$ and the behavior with the distance from the tuning point for $z < 0$. Both expressions (A14) and (A16) are applicable in the same region, which contains $\frac{2}{3}(Ka)^{-1}$ de Broglie wave lengths, so for the matching procedure to be valid it is necessary to have $Ka \ll 1 \Leftrightarrow \alpha a/J \ll 1$, which is yet another expression of the smoothness of the potential. Matching the two asymptotic expressions then yields

$$\begin{cases} n > \delta: & C_{\text{decaying}} = C_1 \frac{1}{2\sqrt{\pi}}, \quad C_{\text{growing}} = C_2 \frac{1}{\sqrt{\pi}}, \\ n < \delta: & C_{\text{towards}} = C_1 \frac{1}{\sqrt{\pi}} \frac{e^{i\pi/4}}{2} + C_2 \frac{1}{\sqrt{\pi}} \frac{e^{-i\pi/4}}{2}, \quad C_{\text{away}} = C_1 \frac{1}{\sqrt{\pi}} \frac{e^{-i\pi/4}}{2} + C_2 \frac{1}{\sqrt{\pi}} \frac{e^{i\pi/4}}{2}. \end{cases} \quad (\text{A17})$$

Excluding C_1, C_2 , one obtains the well-known [18] connection between the coefficients of the semiclassical expansion on either side of the standard turning point:

$$\begin{cases} C_{\text{towards}} = C_{\text{decaying}} e^{i\pi/4} + C_{\text{growing}} \frac{e^{-i\pi/4}}{2}, \\ C_{\text{away}} = C_{\text{decaying}} e^{-i\pi/4} + C_{\text{growing}} \frac{e^{i\pi/4}}{2}. \end{cases} \quad (\text{A18})$$

Although these relations are obtain for the case $\alpha > 0$, they remain identical for the case $\alpha < 0$ upon correctly identifying growing and decaying solutions in the forbidden region and left- and right-propagating waves in the allowed region.

b. Anomalous turning point

Let $\alpha > 0$ be the potential gradient, and E is such that $\alpha a\delta = E - J$ for some $\delta \in [0, 1]$. This corresponds to anomalous turning described by $p(x_0 = a\delta) = \pm\pi$, with $x > a\delta$ being the classically allowed region and $x < a\delta$ being the classically forbidden one. To solve the exact Schroedinger equation (A1) for this case, we first perform the substitution $\psi_n = \eta_n (-1)^n$, which maps the problem to the previous case, Eq. (A10), with reversed sign of α :

$$-\frac{J}{2} [\psi_{n+1} + \psi_{n-1}] + \alpha a n \psi_n = (\alpha a\delta + J) \psi_n \Leftrightarrow -\frac{J}{2} [\eta_{n+1} + \eta_{n-1}] - \alpha a n \eta_n = (-\alpha a\delta - J) \eta_n. \quad (\text{A19})$$

Similarly to the previous subsection, the latter equation is solved by Airy function, so in the region $K^{-1} \ll |x - a\delta| \ll (\alpha/J)^{-1}$ the asymptotic form of the solution is given by:

$$\eta_n = \psi_n (-1)^n = \begin{cases} z < 0: & C_1 \frac{1}{2\sqrt{\pi}} \sqrt[4]{\frac{1}{|z|}} \exp\left(-\frac{2}{3}|z|^{3/2}\right) + C_2 \frac{1}{\sqrt{\pi}} \sqrt[4]{\frac{1}{|z|}} \exp\left(\frac{2}{3}|z|^{3/2}\right), \\ z > 0: & C_1 \frac{1}{\sqrt{\pi}} \sqrt[4]{\frac{1}{z}} \cos\left(-\frac{2}{3}z^{3/2} + \frac{\pi}{4}\right) + C_2 \frac{1}{\sqrt{\pi}} \sqrt[4]{\frac{1}{z}} \cos\left(\frac{2}{3}z^{3/2} + \frac{\pi}{4}\right), \end{cases} \quad z = -K(x - a\delta), \quad (\text{A20})$$

where $K = (2\alpha/Ja^2)^{1/3}$. On the other hand, the semiclassical momentum is close to $\pm\pi$, so semiclassical wave function is described by

$$\psi(x) \approx \begin{cases} \text{allowed region :} & \frac{1}{\sqrt{|v(x)|}} \exp \left\{ \pm \frac{i}{a} \int_{a\delta}^x [\pi - \delta p(x)] dx \right\}, \\ \text{forbiden region :} & \frac{1}{\sqrt{|v(x)|}} \exp \left\{ \pm \frac{1}{a} \int_{a\delta}^x [i\pi + |\delta p(x)|] dx \right\}, \end{cases} \quad (\text{A21})$$

where $\delta p = \pi - \arccos \{ (h(x) - E + J) / J - 1 \} \approx \sqrt{2(E - J - h(x)) / J}$ (positive quantity in the allowed region), while the group velocity reads $v = J \sin(\pi - \delta p) \approx J\delta p$. The anomalous turning point is characterized by the fact that the real contribution to the phase $\pm i\pi(x - a\delta) / a = \pm i\pi(n - \delta)$ is present at both sides of the turning point and causes oscillatory behavior of the wave function. The semiclassical solution then reads

$$\psi_n \approx \begin{cases} z < 0 : & C_{\text{decaying}} \frac{1}{|z|^{1/4}} \exp \left\{ +i\pi \frac{x-a\delta}{a} - \frac{2}{3} |z|^{3/2} \right\} + C_{\text{growing}} \frac{1}{|z|^{1/4}} \exp \left\{ -i\pi \frac{x-a\delta}{a} + \frac{2}{3} |z|^{3/2} \right\}, \\ z > 0 : & C_{\text{towards}} \frac{1}{|z|^{1/4}} \exp \left\{ -i\pi \frac{x-a\delta}{a} + \frac{2i}{3} z^{3/2} \right\} + C_{\text{away}} \frac{1}{|z|^{1/4}} \exp \left\{ +i\pi \frac{x-a\delta}{a} - \frac{2i}{3} z^{3/2} \right\}, \end{cases} \quad z = -K(x - \delta), \quad (\text{A22})$$

where the labeling of the constants is again chosen to reflect the characteristic behavior of the wave functions (e.g., the group velocity is positive for right-propagating wave, which corresponds to moving away from the turning point). Performing the matching procedure in the region $K^{-1} \ll |x - a\delta| \ll (\alpha/J)^{-1}$ then yields

$$\begin{cases} C_{\text{towards}} = C_{\text{decaying}} \exp \{-2i\pi\delta\} e^{-i\frac{\pi}{4}} + C_{\text{growing}} \frac{1}{2} e^{i\frac{\pi}{4}}, \\ C_{\text{away}} = C_{\text{decaying}} e^{i\frac{\pi}{4}} + C_{\text{growing}} \exp \{+2i\pi\delta\} \frac{1}{2} e^{-i\frac{\pi}{4}}. \end{cases} \quad (\text{A23})$$

where we have taken into account that $\exp \{ \pm i\pi x / a \} = \exp \{ \pm i\pi n \} = (-1)^n$.

One important feature of this matching condition in comparison to the standard one, Eq. (A18), is that it includes an additional phase factor featuring the exact position $\delta \in [0, 1]$ of the turning point, which has been a point of controversy for many authors [19]. While one might argue that the potential is not even well-defined at non-integer coordinate values of $n = x/a$, it becomes well-defined after one requires it to be a smooth function of the coordinate. Due to the fact that the wave function has momentum $p = \pm\pi$ at the turning point, this exact coordinate becomes essential. It is important for accurate description of the quantization conditions.

c. Quantization conditions

For a given energy E , consider a potential that arranges a bounded classically allowed region $x_1 < x < x_2$, where $x_{1,2}$ are turning points. If one does not consider tunneling outside this region, the matching conditions allow one to derive the quantization rules for the bound states. The latter is defined as a purely decaying wave in the forbidden region close to both of the tuning points $x_i, i = 1, 2$:

$$C_{\text{grow}}^{(i)} = 0 \Rightarrow \frac{C_{\text{towards}}^{(i)}}{C_{\text{away}}^{(i)}} = \begin{cases} e^{i\pi/2}, & p(x_i) = 0, \\ e^{-i\pi/2} \exp \{-2i\pi\delta^{(i)}\}, & p(x_i) = \pm\pi. \end{cases} \quad (\text{A24})$$

where $\delta^{(i)} \in [0, 1]$ is the exact position of the anomalous turning point. Obviously, one has $|C_{\text{towards}}^{(i)} / C_{\text{away}}^{(i)}| = 1$, so the phase $\theta_i = \arg C_{\text{towards}}^{(i)} / C_{\text{away}}^{(i)}$ defines the shape of the semiclassical wave function in the allowed region up to an overall phase as seen defined by the corresponding turning point:

$$\psi^{(1)}(x) = \frac{C_{\text{away}}^{(1)}}{\sqrt{|v(x)|}} \exp \left\{ \frac{i}{a} \int_{x_1}^x p(x) dx \right\} + \frac{C_{\text{towards}}^{(1)}}{\sqrt{|v(x)|}} \exp \left\{ -\frac{i}{a} \int_{x_1}^x p(x) dx \right\} = \frac{2C_{\text{away}}^{(1)} e^{\theta_1/2}}{\sqrt{|v(x)|}} \cos \left\{ \frac{1}{a} \int_{x_1}^x p(x) dx - \frac{\theta_1}{2} \right\}, \quad (\text{A25})$$

$$\psi^{(2)}(x) = \frac{C_{\text{towards}}^{(2)}}{\sqrt{|v(x)|}} \exp \left\{ \frac{i}{a} \int_{x_2}^x p(x) dx \right\} + \frac{C_{\text{away}}^{(2)}}{\sqrt{|v(x)|}} \exp \left\{ -\frac{i}{a} \int_{x_2}^x p(x) dx \right\} = \frac{2C_{\text{away}}^{(2)} e^{i\theta_2/2}}{\sqrt{|v(x)|}} \cos \left\{ \frac{1}{a} \int_{x_2}^x p(x) dx + \frac{\theta_2}{2} \right\} \quad (\text{A26})$$

where we have taken into account $x_1 < x < x_2$, and p is chosen to be a positive root of the classical equation of motion (A5) in the vicinity of the tuning point x_i (so the corresponding group velocity is also positive). The two expressions for $i = 1, 2$ should

actually yield the same wave function (up to an overall sign), which is equivalent to requiring that the difference of phases of the cosines is πN , yielding

$$\frac{1}{a} \int_{x_1}^{x_2} p(x) dx - \frac{\theta_1}{2} - \frac{\theta_2}{2} = \pi N, \quad (\text{A27})$$

which is equivalent to Eqs. (22) and (23) upon substitution of $\theta_i = \arg C_{\text{towards}}^{(i)} / C_{\text{away}}^{(i)}$ from Eq. (A24).

Let us illustrate this result for an exactly solvable case of linear potential $h_n = \alpha a n$ with $a \ll 1$. The exact eigenvalues of the corresponding Schroedinger equation (A1) are given by $E_N = \frac{J}{\alpha} + \alpha a N$, $N \in \mathbb{Z}$, and the associated eigenfunctions read

$$\langle n|N \rangle = J_{n-N} \left(\frac{J}{\alpha} \right), \quad (\text{A28})$$

where $J_k(x)$ is the Bessel function of order k (which promptly reproduces the special cases of Eqs. (A14) and (A20) with $C_2 = 0$ near the corresponding tuning points for $a \ll 1$). From the semiclassical point of view, at energy E the classically allowed region of Hamiltonian $-J \cos p + \alpha x$ is given by $x_1 < x < x_2$ with $x_{1,2} = (E \mp J) / \alpha$, and x_1 is the anomalous turning point with $p(x_1) = \pm\pi$, while x_2 is the standard turning point with $p(x_2) = 0$. Applying Eqs. (A24) and (A27) then renders $\theta_2 = +\pi/2$, and $\theta_1 = -\pi/2 - 2\pi \{x_1/a\}$, with $\{n\}$ corresponding to the fractional part of n , so

$$\frac{1}{a} \int_{x_1}^{x_2} \arccos \left\{ \frac{\alpha x - E}{J} \right\} dx + \pi \{x_1/a\} = \pi N, \quad (\text{A29})$$

The integral of momentum is $\pi J/\alpha$, so one obtains an equation on the value of E :

$$\frac{J}{\alpha a} + \left\{ \frac{E}{\alpha a} - \frac{J}{\alpha a} \right\} \in \mathbb{Z}, \quad (\text{A30})$$

which is solved by the correct value $E = \alpha a N$. Crucially, the correct quantization condition can be traced down to the presence of the additional dependence of the matching conditions (A24) on δ .

Appendix B: Correction to the semiclassical description due to Trotterization

This Appendix covers several technical details of calculations leading to the results of (III) by using the framework of semiclassical approximation for the matrix Hamiltonians as presented in Ref. [35, Ch. 11]., with the latter naturally arising due to the different periodicity of the target Hamiltonian (15) and the Suzuki-Trotter approximation (7).

1. Expression for the 2nd-order correction

The matrix elements of the difference between the single-particle effective Hamiltonian (8) of the Suzuki-Trotter evolution and the target Hamiltonian (15) are presented on Figure B1. Clearly, they are dominated by the close-neighbor hopping, which corresponds to leading-order perturbation theory in powers of the Trotter step δt . The Suzuki-Trotter evolution operator composed of k terms is described by the following recursion relation:

$$\mathcal{U}_k(\delta t) = e^{-iA_k \delta t/2} \mathcal{U}_{k-1}(\delta t) e^{-iA_k \delta t/2}, \quad \mathcal{U}_1 = e^{-iA_1 t}. \quad (\text{B1})$$

The effective Hamiltonian at each step has the following expansion in powers of t :

$$\mathcal{H}_{\text{eff}}^{(k)} = -\frac{1}{i\delta t} \text{Ln} \mathcal{U}_k(\delta t) = \mathcal{H}^{(k)} + \delta t^2 \mathcal{D}^{(k)} + O(\delta t^4), \quad \mathcal{H}^{(k)} = \sum_{j=1}^k A_j, \quad (\text{B2})$$

and we are interested in the value of $\mathcal{D}^{(k)}$. To do this, we apply the second order of Baker–Campbell–Hausdorff formula:

$$\text{Ln} \{ e^{-itA} e^{-itB} \} = -it \left[A + B + \frac{t}{2i} [A, B] + \frac{t^2}{12} ([A, [A, B]] + [B, [B, A]]) + O(t^3) \right]. \quad (\text{B3})$$

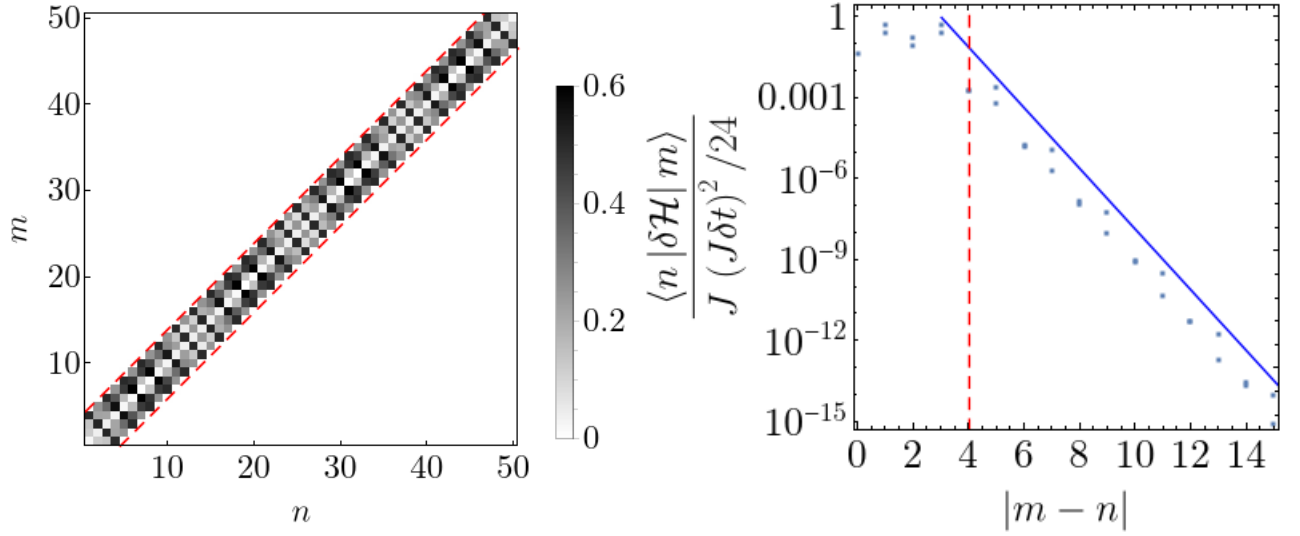


Figure B1. Visualization of the spatial matrix elements of the Suzuki-Trotter error $\langle n | \delta \mathcal{H} | m \rangle$ normalized by $J (J\delta t)^2 / 24$ with the same parameters as Figure 4 but $J\delta t = 0.3$. *Left*: color plot of the matrix elements. *Right*: matrix element as a function of distance between sites $|m - n|$ for fixed $n = L/2$, with the blue line corresponding to $(J\delta t/4)^{|m-n|-3}$, according to estimation (29). On both plots, red dashed line denotes $|m - n| = 4$.

Used twice on Eq. (B1) and then substituted in Eq. (B2), this yields Eq. (31) of the main text:

$$\mathcal{D}^{(k+1)} = \mathcal{D}^{(k)} - \frac{1}{12} \left\{ \left[\mathcal{H}^{(k)}, \left[\mathcal{H}^{(k)}, A_{k+1} \right] \right] - \frac{1}{2} \left[A_{k+1}, \left[A_{k+1}, \mathcal{H}^{(k)} \right] \right] \right\}. \quad (\text{B4})$$

If the target Hamiltonian can be decomposed as $\mathcal{H} = A_1 + A_2$, where both $A_{1,2}$ can be exponentiated exactly, the leading-order correction to the effective Hamiltonian simply reads

$$\mathcal{H}_{\text{eff}} = \mathcal{H} + \delta t^2 \mathcal{D}^{(2)} + O(\delta t^4), \quad \mathcal{D}^{(2)} = -\frac{1}{12} \left\{ \left[A_1, \left[A_1, A_2 \right] \right] - \frac{1}{2} \left[A_2, \left[A_2, A_1 \right] \right] \right\}. \quad (\text{B5})$$

Note that this expression is not symmetric to the order of A_i . Similarly, for the three-term decomposition $\mathcal{H} = A_1 + A_2 + A_3$ one has

$$\mathcal{H}_{\text{eff}} = \mathcal{H} + \delta t^2 \mathcal{D}^{(3)} + O(\delta t^4), \quad (\text{B6})$$

$$\mathcal{D}^{(3)} = -\frac{1}{12} \left\{ \left[A_1, \left[A_1, A_2 \right] \right] - \frac{1}{2} \left[A_2, \left[A_2, A_1 \right] \right] + \left[A_1 + A_2, \left[A_1 + A_2, A_3 \right] \right] - \frac{1}{2} \left[A_3, \left[A_3, A_1 + A_2 \right] \right] \right\}. \quad (\text{B7})$$

Clearly, the expression is not invariant w.r.t permutation of indices. We will later show, however, that the difference is inessential as far as the semiclassical approximation is concerned.

2. Treatment of alternating perturbation

As we can see from, e.g., Figure B1, even in the case of a smooth potential, the effective Hamiltonian \mathcal{H}_{eff} features a “staggered” structure:

$$\delta \mathcal{H}^{ij} := \mathcal{H}_{\text{eff}}^{ij} - \mathcal{H}^{ij} = U^{ij} + (-1)^i W^{ij} + (-1)^j \overline{W}^{ij}, \quad (\text{B8})$$

where both U and W depend smoothly on $m+n$ and decay quickly with $m-n$. In this case, the spatial dependence of the wave function is not smooth anymore. It essentially implies that even in the limit of homogeneous system the wave function has two components on even and odd sites respectively, thus reflecting the doubling of the translation period of the system. The corresponding Brillouin zone is halved to $p \in [-\pi/2, \pi/2]$.

Let's apply the operator of the form (B8) to a semiclassical wave function. A calculation identical to that of Subsection A 1 yields:

$$\begin{aligned} \sum_m \mathcal{H}_{\text{eff}}^{nm} \psi_m &\approx \exp \left\{ \frac{iS(x)}{a} \right\} \left[\mathcal{H}(x, p) \varphi - (ia) \left\{ \partial_p \mathcal{H}(x, p) \varphi' + \frac{1}{2} p' \partial_p^2 \mathcal{H}(x, p) \varphi \right\} + O(a^2) \right] \\ &\quad \exp \left\{ \frac{iS(x)}{a} \right\} \left[U(x, p) \varphi - (ia) \left\{ \partial_p U(x, p) \varphi' + \frac{1}{2} p' \partial_p^2 U(x, p) \varphi \right\} + O(a^2) \right] \\ &\quad + (-1)^n \exp \left\{ \frac{iS(x)}{a} \right\} \left[W(x, p) \varphi - (ia) \left\{ \partial_p W(x, p) \varphi' + \frac{1}{2} p' \partial_p^2 W(x, p) \varphi \right\} + O(a^2) \right], \end{aligned} \quad (\text{B9})$$

where $p = S'(x)$, $\mathcal{H}(x, p)$ is given by Eq. (B12), and

$$U(x = an, p) = \sum_m U^{nm} e^{ip(m-n)}, \quad W(x = an, p) = \sum_m \left[W^{nm} e^{ip(m-n)} + \overline{W^{mn}} e^{i(p+\pi)(m-n)} \right]. \quad (\text{B10})$$

We thus need to consider the two-component wave function:

$$\psi_n = \exp \left\{ \frac{iS(an)}{a} \right\} (\varphi(an) + (-1)^n \eta(an)). \quad (\text{B11})$$

Application of the full effective Hamiltonian \mathcal{H}_{eff} to the such wave function then yields

$$\sum_m \mathcal{H}_{\text{eff}}^{nm} \psi_m \approx \exp \left\{ \frac{iS(an)}{a} \right\} \left[\hat{\mathcal{H}}_{\text{eff}}(x, p) - (ia) \left\{ \partial_p \hat{\mathcal{H}}_{\text{eff}}(x, p) \frac{d}{dx} + \frac{1}{2} p' \partial_p^2 \hat{\mathcal{H}}_{\text{eff}}(x, p) + i \frac{\partial \hat{\mathcal{H}}_{\text{eff}}(x, p)}{\partial a} \right\} + O(a^2) \right] \vec{v}, \quad (\text{B12})$$

where $p(x) = S'(x)$, and the matrix $\hat{\mathcal{H}}_{\text{eff}}$ and vector \vec{v} are given by

$$\hat{\mathcal{H}}_{\text{eff}}(x, p) = \begin{pmatrix} \mathcal{H}(x, p) + U(x, p) & W(x, p + \pi) \\ W(x, p) & \mathcal{H}(x, p + \pi) + U(x, p + \pi) \end{pmatrix}, \quad \vec{v}(x) = \begin{pmatrix} \varphi(x) \\ \eta(x) \end{pmatrix}. \quad (\text{B13})$$

In Eq. (B12), we have also included the explicit dependence of $\hat{\mathcal{H}}$ on a , which will come in handy in the following sections.

Following Ref. [35], we then seek the solution to the Schroedinger equation expansion in powers of a :

$$\vec{v}(x) = \vec{v}_0(x) + a \vec{v}_1(x) + O(a^2), \quad (\text{B14})$$

with the the stationary Schroedinger equation (A1) producing

$$(E \hat{1} - \hat{\mathcal{H}}_{\text{eff}}(x, p)) \vec{v}_0 = 0, \quad (\text{B15})$$

$$(E \hat{1} - \hat{\mathcal{H}}_{\text{eff}}) \vec{v}_1 = \left\{ \partial_p \hat{\mathcal{H}}_{\text{eff}} \frac{d}{dx} + \frac{1}{2} p' \partial_p^2 \hat{\mathcal{H}}_{\text{eff}} + i \frac{\partial \hat{\mathcal{H}}_{\text{eff}}}{\partial a} \right\} \vec{v}_0. \quad (\text{B16})$$

In order for the system (B15) to possess nontrivial solution, it has to be degenerate, yielding a matrix generalization of the semiclassical equation of motion (A5):

$$\det \left\{ E \hat{1} - \hat{\mathcal{H}}_{\text{eff}}(x, p) \right\} = 0, \quad (\text{B17})$$

Eq. B16 then renders a condition that defines the spatial behavior of the *normalization* of \vec{v}_0 that solves Eq. (B15): since $E - \hat{\mathcal{H}}_{\text{eff}}$ is a degenerate matrix, the linear system (B16) has a solution for \vec{v}_1 only if the r.h.s of Eq. (B16) is orthogonal to the zero eigenvector:

$$\vec{v}_0^\dagger \left\{ \partial_p \hat{\mathcal{H}}_{\text{eff}} \frac{d}{dx} + \frac{1}{2} S'' \partial_p^2 \hat{\mathcal{H}}_{\text{eff}} + i \frac{\partial \hat{\mathcal{H}}_{\text{eff}}}{\partial a} \right\} \vec{v}_0 = 0, \quad (\text{B18})$$

where v_0^\dagger is the left eigenvector of $\hat{\mathcal{H}}_{\text{eff}}$ corresponding to eigenvalue E (not necessarily the conjugate of v_0 , since $\hat{\mathcal{H}}_{\text{eff}}$ is guaranteed to be hermitian). This is the generalization of the transport equation (A6).

From the equations above, we observe that action of a semiclassical operator O^{nm} on a semiclassical wave function (B11) is described the action of the corresponding 2×2 matrix $O(x, p)$ on a vector \vec{v} composed of components φ, η of the wave function. For the case of the Hamiltonian operator \mathcal{H}^{nm} , this results in the classical equation of motion (B17) expressed in terms of the semiclassical matrix Hamiltonian $\mathcal{H}(x, p)$ and the associated transport equation (B18), with the latter being structurally identical to that of the scalar case (A6) and expressible entirely in terms of $\mathcal{H}(x, p)$, $S(x)$, $\vec{v}(x)$ and their derivatives.

It is instructive to observe how this new description reduces to the scalar case of (A1). Without alternating perturbation, the matrix Hamiltonian (B13) is given by

$$\hat{\mathcal{H}}(x, p) = \begin{pmatrix} \mathcal{H}(x, p) & 0 \\ 0 & \mathcal{H}(x, p + \pi) \end{pmatrix} = -J \cos p \hat{\tau}_z + h(x) \hat{1}, \quad (\text{B19})$$

where the second equality represents the result for the target hopping Hamiltonian (15), with $\hat{\tau}_z$ being the Pauli matrix in the space of the wave function components. The classical equation of motion (B17) then reduces to

$$\begin{cases} \mathcal{H}(x, p) = E, & \vec{v}_0 = \begin{pmatrix} \varphi(x) \\ 0 \end{pmatrix}, & \vec{v}_0^\dagger = (\varphi^*(x), 0), \\ \mathcal{H}(x, p + \pi) = E, & \vec{v}_0 = \begin{pmatrix} 0 \\ \eta(x) \end{pmatrix}, & \vec{v}_0^\dagger = (0, \eta^*(x)), \end{cases} \quad (\text{B20})$$

and the semiclassical wave function (B11) is given by

$$\psi_n = \begin{cases} \mathcal{H}(x, p) = E : & e^{iS(x)/a} \varphi(x), \\ \mathcal{H}(x, p + \pi) = E : & e^{iS(x)/a} (-1)^n \eta(x) \end{cases} \equiv e^{iS(x)/a} \varphi(x), \quad \mathcal{H}(x, p) = E, \quad (\text{B21})$$

where we have used the fact that the second alternative reduces to the first one upon replacing $p \mapsto p + \pi$. The transport equation (B18) for both alternatives of Eq. (B20) coincides with the scalar one, Eq. (A6).

Just as the standard semiclassical treatment of Appendix A, this description is applicable for operators that can be represented in the form of Eq. (B8) with local and smooth U, W in the sense of Subsection A1. *A posteriori*, one should verify the smoothness of the de Broglie wave length $\lambda(x) = 2\pi a/p(x)$, which also indicates that semiclassical description still breaks down close to the classical turning points. The emerging matching conditions will be addressed later, after we examine the exact form of the perturbation we are interested in, as it has certain important properties.

3. Correction to the semiclassical Hamiltonian and transport equation

One now has to derive the semiclassical matrix Hamiltonian arising from the Suzuki-Trotter correction (B2). While we can directly compute the Wigner's transform of Eq. (B4), it is much more instructive and computationally transparent to derive the commutation formula that directly provides semiclassical matrix form for expressions involving commutators. While it is quite natural to expect that the leading $O(a^0)$ term of the commutation formula will just reflect the commutativity of the matrix structure of the semiclassical operators, it is less trivial to establish the correct form of the subleading $O(a)$ term responsible for the form of the transport equation (B18).

For two semiclassical matrix operators that obey the locality and smoothness conditions, their commutator acts on the semiclassical wave function (B11) as

$$\begin{aligned} e^{+iS(x)/a} \sum_m [A, B]^{nm} \psi_m &= [\hat{A}, \hat{B}] \vec{v} \\ &- (ia) \left[\left(\partial_p [\hat{A}, \hat{B}] \right) \frac{d}{dx} + \frac{1}{2} S''(x) \partial_p^2 [\hat{A}, \hat{B}] + i \frac{\partial [\hat{A}, \hat{B}]}{\partial a} \right] \vec{v} \\ &- (ia) \{ \hat{A}, \hat{B} \} \vec{v} + O(a^2) \end{aligned} \quad (\text{B22})$$

where $p = S'(x)$, \vec{v} is a two-component vector of slow variables φ, η , $[\hat{A}, \hat{B}] = \hat{A}(x, p) \hat{B}(x, p) - \hat{B}(x, p) \hat{A}(x, p)$ is the commutator of the semiclassical matrices w.r.t their 2×2 matrix structure, and the new term $\{ \hat{A}, \hat{B} \}$ is given by

$$\{ \hat{A}, B \} = \left(\partial_x \hat{A}(x, p) \right) \left(\partial_p \hat{B}(x, p) \right) - \left(\partial_p \hat{A}(x, p) \right) \left(\partial_x \hat{B}(x, p) \right), \quad (\text{B23})$$

and corresponds to the order-preserving Poisson bracket. This latter term is expected due to the quantum-classical correspondence $[A, B] \mapsto i\hbar \{A, B\}$ in the standard quantum mechanics.

Performing the same calculation for the double commutator renders the following action $\sum_m O^{nm} \psi_m \mapsto \hat{O}(x, p) \vec{v}$

$$\begin{aligned}
e^{+iS(x)/a} \sum_m [C, [A, B]]^{nm} \psi_m &= \left[\hat{C}, [\hat{A}, \hat{B}] \right] \vec{v} \\
&- (ia) \left(\partial_p [\hat{C}, [\hat{A}, \hat{B}]] \frac{d}{dx} + \frac{1}{2} S'' \partial_p^2 [\hat{C}, [\hat{A}, \hat{B}]] + i \frac{\partial [\hat{C}, [\hat{A}, \hat{B}]]}{\partial a} \right) \vec{v} \\
&- (ia) \left([\hat{C}, \{\hat{A}, \hat{B}\}] + \{\hat{C}, [\hat{A}, \hat{B}]\} \right) \vec{v}
\end{aligned} \tag{B24}$$

Yet again, the subleading term contains an extra contribution restoring the quantum-classical correspondence for scalar operators.

The results above allow us to avoid computing the matrix elements of the perturbation (B4) and instead simply deal with the semiclassical matrices. According to Subsection II B, the noncommuting operators of interest are the parts of the kinetic energy and the potential term:

$$\mathcal{K}_{\text{even(odd)}} = -\frac{J}{2} \sum_n \frac{1 \pm (-1)^n}{2} (|n\rangle \langle n+1| + |n+1\rangle \langle n|), \quad \mathcal{P} = \sum_n h(x=an) |n\rangle \langle n|. \tag{B25}$$

Eqs. (B10) and (B13) then produces the following semiclassical matrices:

$$\hat{\mathcal{K}}_{\text{even(odd)}}(p) = \frac{1}{2} (\mathcal{K}(p) \hat{\tau}_z \mp \hat{\tau}_y v(p)), \quad \mathcal{P}(x) = h(x) \cdot \hat{1}, \tag{B26}$$

where $\mathcal{K}(p) = -J \cos p$ is the full kinetic energy (in particular, $\hat{\mathcal{K}}_{\text{even}}(p) + \hat{\mathcal{K}}_{\text{odd}}(p) = -\mathcal{K}(p) \hat{\tau}_z$), $v(p) \equiv \partial_p \mathcal{K}(p)$ is the classical group velocity, and $\hat{\tau}_i$ are the Pauli matrices acting the space of components of the wave function.

Our task is now to compute the semiclassical operator $\hat{\mathcal{H}}_{\text{eff}}$ that describes the action of the effective Hamiltonian of the Suzuki-Trotter evolution on the semiclassical equation of motion as well as the corresponding transport equation. We note that it is not guaranteed that the result does not depend on the order of the operators in the Suzuki-Trotter formula, Eq. (7). However, applying the double commutator formula (B24) to Eq. (B3) allows one to verify that, as far as leading terms in powers of a and $(J\delta t)^2$ are concerned, this order does not influence either the classical equation of motion or the transport equation. The calculation for all three possible orderings of operators in the Suzuki-Trotter formula (7) is given below, with the result being the following semiclassical matrix Hamiltonian:

$$\hat{\mathcal{H}}_{\text{eff}}(x, p) \approx \left[\mathcal{K}(p) - \frac{\delta t^2}{24} \mathcal{K}(p) v^2(p) \right] \hat{\tau}_z + h(x) \hat{1}. \tag{B27}$$

This Hamiltonian and the associated transport equation (B18) reproduce the correct wave function up to precision $O(\delta t^4)$. Moreover, its structure is identical to that of a system without oscillations in the matrix elements, so the matrix semiclassical Hamiltonian (B27) has the same content as the following *scalar* semiclassical Hamiltonian:

$$\mathcal{H}_{\text{eff}}(x, p) \approx \mathcal{K}(p) - \frac{\delta t^2}{24} \mathcal{K}(p) v^2(p) + h(x). \tag{B28}$$

There are three features of the semiclassical matrix Hamiltonian (B30) and its scalar counterpart (B28) worth mentioning: *i*) as expected, the correction to the target Hamiltonian (B19) does not depend on the potential, *ii*) the correction is proportional to the squared group velocity $v^2(p)$, so the classical turning points defined as $\partial_p \mathcal{H}_{\text{eff}} \equiv 0$ are not shifted, and *iii*) at $p = \pm\pi/2$, one has $\mathcal{K}(p) = 0$, so the eigenvalues of the perturbed matrix Hamiltonian (B27) are degenerate, which is an important consequence of the fact that at $S'(x) = p = \pm\pi/2$ the two components $\varphi e^{ipx/a}$ and $(-1)^n \eta e^{ipx/a}$ of the full wave function (B11) are not linearly independent. Note that the points $p = \pm\pi/2$ lie within the region of applicability of the semiclassical approximation since the de Broglie wave length does not experience any discontinuity at $p = \pm\pi/2$ (due to the matrix structure of Eq. (B27), the behavior of its two eigenvalues in the vicinity of $p = \pm\pi/2$ coincides). Therefore, at $\pi/2$ the solution (B11) can switch the leading component between η and φ in order to satisfy the boundary conditions. For instance, this is important if one wishes to describe the bound state between the standard $p(x_0) = 0$ and anomalous $p(x_\pi) = \pm\pi$ turning points: close to $p = 0$, the φ component of the wave function (B11) is dominant, while close to $p = \pm\pi$ the dominant role belongs to η . There is thus a point $x_{\pi/2}$ between x_0 and x_π with $p(x_{\pi/2}) = \pi/2$ where the matching between the two solutions takes place.

a. Ordering $K_{\text{even}}, K_{\text{odd}}, P$.

Using Eqs. (B4) and (B24), we obtain the following form of the semiclassical Hamiltonian:

$$\begin{aligned} \hat{\mathcal{H}}_{\text{eff}}(x, p) &= \mathcal{K}(p) \hat{\tau}_z + h(x) \hat{1} \\ &\quad - \frac{\delta t^2}{12} \left\{ [\mathcal{K}_{\text{even}}(p), [\mathcal{K}_{\text{even}}(p), \mathcal{K}_{\text{odd}}(p)]] - \frac{1}{2} [\mathcal{K}_{\text{odd}}(p), [\mathcal{K}_{\text{odd}}(p), \mathcal{K}_{\text{even}}(p)]] \right\} \\ &\quad - \frac{\delta t^2}{12} \left\{ [\mathcal{K}(p) \hat{\tau}_z, [\mathcal{K}(p) \hat{\tau}_z, \mathcal{P}(x) \hat{1}]] - \frac{1}{2} [\mathcal{P}(x) \hat{1}, [\mathcal{P}(x) \hat{1}, \mathcal{K}(p) \hat{\tau}_z]] \right\}. \end{aligned} \quad (\text{B29})$$

We immediately observe that the last term vanishes as the matrix structure of potential energy commutes with everything, which is a manifestation of the smoothness of the potential, as explained in Subsection III A. Calculating the first term of Eq. (B29) renders

$$\hat{\mathcal{H}}_{\text{eff}}(x, p) = \mathcal{K}(p) \hat{\tau}_z + h(x) \hat{1} - \frac{\delta t^2}{24} \mathcal{K}(p) v^2(p) \hat{\tau}_z - \frac{\delta t^2}{8} \mathcal{K}^2(p) v(p) \hat{\tau}_y + O(\delta t^4). \quad (\text{B30})$$

The first two terms reproduce the original classical Hamiltonian (B19), while the second two terms represent the correction from Suzuki-Trotter evolution.

The classical equation of motion (B17) then reads

$$0 = \det \left\{ E \hat{1} - \hat{\mathcal{H}}_{\text{eff}}(x, p) \right\} = \left((E - h(x))^2 - \mathcal{K}^2(p) \right) + \frac{\delta t^2}{12} \mathcal{K}^2(p) v^2(p) + O(\delta t^4) = 0. \quad (\text{B31})$$

Note that last $O(\delta t^2)$ term of Eq. (B30) actually does not contribute to this equation of motion (B31) with precision $O(\delta t^4)$, so we can ignore it, arriving to a “reduced” effective semiclassical Hamiltonian:

$$\hat{\mathcal{H}}_{\text{eff}}(x, p) \approx \left[\mathcal{K}(p) - \frac{\delta t^2}{24} \mathcal{K}(p) v^2(p) \right] \hat{\tau}_z + h(x) \hat{1}. \quad (\text{B32})$$

The result has the same matrix structure as that of a system without oscillations in the matrix elements, Eq. (B19), so the problem is then described by the *scalar* classical Hamiltonian $\mathcal{H} + \delta\mathcal{H}$, with \mathcal{H} being the target classical Hamiltonian (19) and $\delta\mathcal{H}$ given by Eq. (35).

We now turn to the subleading term of Eq. (B24) which produces the transport equation. Essentially, we only need to compute the additional term due to the Poisson bracket, as everything else is expressed via $\hat{\mathcal{H}}_{\text{eff}}(x, p)$ and its derivatives. According to Eqs. (B4) and (B24), this extra term is given by

$$\begin{aligned} & - \frac{\delta t^2}{12} \left([\mathcal{K}_{\text{even}}(p), \{\mathcal{K}_{\text{even}}(p), \mathcal{K}_{\text{odd}}(p)\}] + \{\mathcal{K}_{\text{even}}(p), [\mathcal{K}_{\text{even}}(p), \mathcal{K}_{\text{odd}}(p)] \} \right) \\ & + \frac{\delta t^2}{24} \left([\mathcal{K}_{\text{odd}}(p), \{\mathcal{K}_{\text{odd}}(p), \mathcal{K}_{\text{even}}(p)\}] + \{\mathcal{K}_{\text{odd}}(p), [\mathcal{K}_{\text{odd}}(p), \mathcal{K}_{\text{even}}(p)] \} \right) \\ & - \frac{\delta t^2}{12} \left([\mathcal{K}(p) \hat{\tau}_z, \{\mathcal{K}(p) \hat{\tau}_z, \mathcal{P}(x) \hat{1}\}] + \{\mathcal{K}(p) \hat{\tau}_z, [\mathcal{K}(p) \hat{\tau}_z, \mathcal{P}(x) \hat{1}] \} \right) \\ & + \frac{\delta t^2}{24} \left([\mathcal{P}(x) \hat{1}, \{\mathcal{P}(x) \hat{1}, \mathcal{K}(p) \hat{\tau}_z\}] + \{\mathcal{P}(x) \hat{1}, [\mathcal{P}(x) \hat{1}, \mathcal{K}(p) \hat{\tau}_z] \} \right). \end{aligned} \quad (\text{B33})$$

The first two terms vanish because $\mathcal{K}_{\text{even(odd)}}$ does not depend on x and the resulting Poisson bracket (B23) vanishes, and the last two terms vanish because the potential term commutes with everything. As a result, the transport equation preserves the form (B18) with the effective matrix Hamiltonian given by Eq. (B30). The eigenvectors of the latter are given by

$$\left\{ \begin{array}{l} \mathcal{H}_{\text{eff}}(x, p) = E : \quad \vec{v}_0 = \varphi(x) \left\{ \begin{pmatrix} 1 \\ 0 \end{pmatrix} - \frac{i\delta t^2 \mathcal{K}(p) v(p)}{16} \begin{pmatrix} 0 \\ 1 \end{pmatrix} + O(\delta t^4) \right\}, \\ \mathcal{H}_{\text{eff}}(x, p + \pi) = E : \quad \vec{v}_0 = \eta(x) \left\{ \begin{pmatrix} 0 \\ 1 \end{pmatrix} - \frac{i\delta t^2 \mathcal{K}(p) v(p)}{16} \begin{pmatrix} 1 \\ 0 \end{pmatrix} + O(\delta t^4) \right\}, \end{array} \right. \quad (\text{B34})$$

and \vec{v}_0^\dagger is given by hermitian conjugation, so substituting these in the transport equation (B18) for both solutions actually renders the two instances of the scalar transport equation (A6) corresponding to the “reduced” effective Hamiltonian (B28) at momenta p and $p + \pi$, respectively. Finally, due to the fact that the substitution $p \mapsto p + \pi$ flips the sign of the kinetic term of Eq. (B30) and thus simply interchanges the two vectors in Eq. (B34), the two cases p and $p + \pi$ are described by a single scalar transport equation (A6) with the effective Hamiltonian (B28).

b. Ordering $K_{\text{even}}, P, K_{\text{odd}}$.

For this case, the classical Hamiltonian reads

$$\begin{aligned} \hat{\mathcal{H}}_{\text{eff}}(x, p) &= \mathcal{K}(p) \hat{\tau}_z + h(x) \hat{1} \\ &\quad - \frac{\delta t^2}{12} \left\{ \left[\hat{\mathcal{K}}_{\text{even}}(p), \left[\hat{\mathcal{K}}_{\text{even}}(p), \hat{\mathcal{P}}(x) \right] \right] - \frac{1}{2} \left[\hat{\mathcal{P}}(x), \left[\hat{\mathcal{P}}(x), \hat{\mathcal{K}}_{\text{even}}(p) \right] \right] \right\} \\ &\quad - \frac{\delta t^2}{12} \left\{ \left[\hat{\mathcal{K}}_{\text{even}}(p) + \hat{\mathcal{P}}(x), \left[\hat{\mathcal{K}}_{\text{even}}(p) + \hat{\mathcal{P}}(x), \hat{\mathcal{K}}_{\text{odd}}(p) \right] \right] - \frac{1}{2} \left[\hat{\mathcal{K}}_{\text{odd}}(p), \left[\hat{\mathcal{K}}_{\text{odd}}(p), \hat{\mathcal{K}}_{\text{even}}(p) + \hat{\mathcal{P}}(x) \right] \right] \right\}. \end{aligned} \quad (\text{B35})$$

Similarly to the previous case, the \mathcal{P} matrix commutes with everything, so the expression simplifies exactly to Eq. (B30). The Poisson bracket correction to the subleading term of the commutation formula (B24) now reads

$$\begin{aligned} &- \frac{\delta t^2}{12} \left(\left[\hat{\mathcal{K}}_{\text{even}}(p), \left\{ \hat{\mathcal{K}}_{\text{even}}(p), \hat{\mathcal{P}}(x) \right\} \right] + \left\{ \hat{\mathcal{K}}_{\text{even}}(p), \left[\hat{\mathcal{K}}_{\text{even}}(p), \hat{\mathcal{P}}(x) \right] \right\} \right) \\ &+ \frac{\delta t^2}{24} \left(\left[\hat{\mathcal{P}}(x), \left\{ \hat{\mathcal{P}}(x), \hat{\mathcal{K}}_{\text{even}}(p) \right\} \right] + \left\{ \hat{\mathcal{P}}(x), \left[\hat{\mathcal{P}}(x), \hat{\mathcal{K}}_{\text{even}}(p) \right] \right\} \right) \\ &- \frac{\delta t^2}{12} \left(\left[\hat{\mathcal{K}}_{\text{even}}(p) + \hat{\mathcal{P}}(x), \left\{ \hat{\mathcal{K}}_{\text{even}}(p) + \hat{\mathcal{P}}(x), \hat{\mathcal{K}}_{\text{odd}}(p) \right\} \right] + \left\{ \hat{\mathcal{K}}_{\text{even}}(p) + \hat{\mathcal{P}}(x), \left[\hat{\mathcal{K}}_{\text{even}}(p) + \hat{\mathcal{P}}(x), \hat{\mathcal{K}}_{\text{odd}}(p) \right] \right\} \right) \\ &+ \frac{\delta t^2}{24} \left(\left[\hat{\mathcal{K}}_{\text{odd}}(p), \left\{ \hat{\mathcal{K}}_{\text{odd}}(p), \hat{\mathcal{K}}_{\text{even}}(p) + \hat{\mathcal{P}}(x) \right\} \right] + \left\{ \hat{\mathcal{K}}_{\text{odd}}(p), \left[\hat{\mathcal{K}}_{\text{odd}}(p), \hat{\mathcal{K}}_{\text{even}}(p) + \hat{\mathcal{P}}(x) \right] \right\} \right). \end{aligned} \quad (\text{B36})$$

This time around, this correction does not vanish, the result reads:

$$+ \frac{(J\delta t)^2}{24} i\hat{\tau}_x \left[\frac{1}{2} - 3 \cos 2p \right] h'(x), \quad (\text{B37})$$

so the transport equation now differs from Eq. (B18) by this term and reads

$$\vec{v}_0^\dagger \left\{ \partial_p \hat{\mathcal{H}}_{\text{eff}} \frac{d}{dx} + \frac{1}{2} S'' \partial_p^2 \hat{\mathcal{H}}_{\text{eff}} + i \frac{\partial \hat{\mathcal{H}}_{\text{eff}}}{\partial a} + \left(+ \frac{(J\delta t)^2}{24} i\hat{\tau}_x h'(x) \left[\frac{1}{2} - 3 \cos 2p \right] \right) \right\} \vec{v}_0 = 0,$$

where $\vec{v}_0, \vec{v}_0^\dagger$ are right and left eigenvectors of $\hat{\mathcal{H}}_{\text{eff}}$ given by Eq. (B34). However, because the extra term is proportional to $(J\delta t)^2 \hat{\tau}_x$, its diagonal matrix element $\propto \vec{v}_0^\dagger (J\delta t)^2 \hat{\tau}_x \vec{v}_0 = O(\delta t^4)$, so it still can be discarded with precision $O(\delta t^4)$. The reasoning completely analogous to that of the previous Appendix Subsection B 3 a then results in the scalar transport equation (A6) with the same ‘‘reduced’’ classical Hamiltonian (B28).

c. Ordering $K_{\text{even}} + \alpha P, K_{\text{odd}} + (1 - \alpha) P$.

For this ordering, the classical Hamiltonian, according to Eqs. (B4) and (B24), reads

$$\begin{aligned} \hat{\mathcal{H}}_{\text{eff}}(x, p) &= \mathcal{K}(p) \hat{\tau}_z + h(x) \hat{1} \\ &\quad - \frac{\delta t^2}{12} \left\{ \left[\hat{\mathcal{K}}_{\text{even}} + \alpha \hat{\mathcal{P}}, \left[\hat{\mathcal{K}}_{\text{even}} + \alpha \hat{\mathcal{P}}, \hat{\mathcal{K}}_{\text{odd}} + (1 - \alpha) \hat{\mathcal{P}} \right] \right] - \frac{1}{2} \left[\hat{\mathcal{K}}_{\text{odd}} + (1 - \alpha) \hat{\mathcal{P}}, \left[\hat{\mathcal{K}}_{\text{odd}} + (1 - \alpha) \hat{\mathcal{P}}, \hat{\mathcal{K}}_{\text{even}} + \alpha \hat{\mathcal{P}} \right] \right] \right\}, \end{aligned}$$

and once again reduces precisely to Eq. (B30) as the matrix structure of $\hat{\mathcal{P}}$ commutes with all other operators. The additional contribution to the transport equation is given by

$$\begin{aligned} &- \frac{\delta t^2}{12} \left(\left[\hat{\mathcal{K}}_{\text{even}} + \alpha \hat{\mathcal{P}}, \left\{ \hat{\mathcal{K}}_{\text{even}} + \alpha \hat{\mathcal{P}}, \hat{\mathcal{K}}_{\text{odd}} + (1 - \alpha) \hat{\mathcal{P}} \right\} \right] + \left\{ \hat{\mathcal{K}}_{\text{even}} + \alpha \hat{\mathcal{P}}, \left[\hat{\mathcal{K}}_{\text{even}} + \alpha \hat{\mathcal{P}}, \hat{\mathcal{K}}_{\text{odd}} + (1 - \alpha) \hat{\mathcal{P}} \right] \right\} \right) \\ &+ \frac{1}{24} \left(\left[\hat{\mathcal{K}}_{\text{odd}} + (1 - \alpha) \hat{\mathcal{P}}, \left\{ \hat{\mathcal{K}}_{\text{odd}} + (1 - \alpha) \hat{\mathcal{P}}, \hat{\mathcal{K}}_{\text{even}} + \alpha \hat{\mathcal{P}} \right\} \right] + \left\{ \hat{\mathcal{K}}_{\text{odd}} + (1 - \alpha) \hat{\mathcal{P}}, \left[\hat{\mathcal{K}}_{\text{odd}} + (1 - \alpha) \hat{\mathcal{P}}, \hat{\mathcal{K}}_{\text{even}} + \alpha \hat{\mathcal{P}} \right] \right\} \right). \end{aligned} \quad (\text{B38})$$

For this case, this contribution is also nontrivial and reads

$$-\frac{(J\delta t)^2}{48} i\hat{\tau}_x [2 - \alpha + 3(1 + \alpha) \cos 2p] h'(x). \quad (\text{B39})$$

Repeating the reasoning of the previous Appendix Subsection B 3 b leads us to the same conclusion: with precision $O(\delta t^4)$ this case is still described by the classical Hamiltonian (B28) and the associated scalar transport equation (A6).

4. Change in the matching conditions

In the presence of matrix structure of the semiclassical Hamiltonian (B13), one has to re-examine the matching conditions. However, the matching conditions do not contain any properties of the potential except the position of turning point, which, as mentioned in comments under Eq. (B30), are not shifted by the perturbation, hence one expects no changes to the matching conditions whatsoever. In addition to that, within the matrix formalism the standard $p = 0$ and anomalous $p = \pm\pi$ turning points are treated on equal footing, as the type of the turning point defines the dominating component of the wave function (B11), so the preservation of the matching conditions from this point is also self-consistent.

To derive the matching condition, we repeat the calculation of Appendix Subsection A 2 for the Suzuki-Trotter evolution (7) with operators ordered as $K_{\text{even}}, K_{\text{odd}}, P$, with other orderings yielding the same results. By using Eq. (B4) for the problem with linear potential $h_n = \alpha an$, one obtains the following structure of the matrix elements of the effective Hamiltonian:

$$\mathcal{H}_{\text{eff}}^{nm} = \mathcal{H}^{nm} - \frac{(J\delta t)^2}{24} \frac{J}{2} \left\{ \left[\left(\frac{\alpha a}{J} \right)^2 - \frac{1}{4} + (-1)^n \frac{3}{4} \right] \delta_{n+1,m} + \left[\frac{1}{4} + (-1)^n \frac{3}{4} \right] \delta_{n+3,m} \right\} + (n \leftrightarrow m) + O(\delta t^4), \quad (\text{B40})$$

where \mathcal{H}^{nm} are the matrix elements of the target Hamiltonian (15), and the third term ($n \leftrightarrow m$) is equal to the second one with indices n, m interchanged. The solution of the corresponding stationary Shroedinger equation (A1) (with $O(\delta t^4)$ terms neglected) is still expressible in terms of integral representation (which reproduces the Bessel function solution of Eq. (A10) for $\delta t = 0$), but we will once again resort to controllable approximate solution that exploits the smoothness of the potential.

Just as with the semiclassical approximation, one first has to get rid of the oscillating terms in the stationary Schrodinger equation (A1) for $\hat{\mathcal{H}}_{\text{eff}}$, which is done by introducing the oscillating component to the solution:

$$\psi_n = \varphi(x) + (-1)^n \eta(x), \quad x = an, \quad (\text{B41})$$

with both φ, η being smooth functions of x , so one can replace the discrete differences as

$$\varphi_{n+k} + \varphi_{n-k} = 2\varphi(x) + k^2 a^2 \varphi''(x) + O(a^4), \quad \varphi_{n+k} - \varphi_{n-k} = 2ka \varphi'(x) + O(a^3), \quad (\text{B42})$$

and similarly for η , with the criteria of applicability identical to Eq. (A11). The stationary Shroedinger equation (A1) for the Hamiltonian (B40) is then described by a pair of 2nd order differential equations that can be written in the matrix form as:

$$\left(E - \left[\left\{ -J + \frac{J}{2} \hat{p}^2 + \frac{(J\delta t)^2}{24} J \hat{p}^2 \right\} \hat{\tau}_z + \frac{(J\delta t)^2}{8} J \hat{p} \hat{\tau}_y + \alpha x \hat{1} \right] + \frac{(\alpha a \delta t)^2}{24} \right) \begin{pmatrix} \varphi(x) \\ \eta(x) \end{pmatrix} = O(\hat{p}^3, \delta t^4), \quad \hat{p} := ia \frac{d}{dx}. \quad (\text{B43})$$

In this equation, we have grouped terms in such a way that the term in the square brackets of the l.h.s coincides with the expansion of the semiclassical matrix Hamiltonian (B30) around $p = 0$ up to second order, with subsequent replacement $\hat{p} \mapsto ia \frac{d}{dx}$. The last term in the l.h.s of Eq. (B43) is beyond the precision of the semiclassical expansion, as discussed in Appendix Subsection B 3.

a. Standard turning point $p = 0$

This case corresponds to $E + J = \alpha a \delta$, $\delta \in [0, 1]$, with the classical momentum p vanishing at the turning point. For $\delta t = 0$, the solution to Eq. (B43) is described by $\eta(x) = 0$ as there should be no oscillating component in the system without oscillations (such as e.g. the target Hamiltonian), and the φ component is then given by $\psi(x)$ from Eq. (A13). At nonzero δt , one can treat the term $\propto \hat{\tau}_y$ in Eq. (B43) as perturbation as finite $\eta(x)$ is induced only by this term, as seen from the second component of Eq. (B43):

$$\eta(x) = -i \left[\frac{(J\delta t)^2}{16} \hat{p} + O(a^3) \right] \varphi(x), \quad \hat{p} = ia \frac{d}{dx}, \quad (\text{B44})$$

Substituting this in the first component of Eq. (B43) then shows that the resulting contribution is beyond the precision of expansion in powers of δt , reminiscent of what happened with the classical equation of motion (B31), so the equation on φ reads

$$\left(-J + \alpha(x - a\delta) - \left\{1 + \frac{(J\delta t)^2}{12}\right\} \frac{J}{2}\hat{p}^2 + \frac{(\alpha a\delta t)^2}{24}\right) \varphi = O(\delta t^4, a^3), \quad \hat{p} = ia \frac{d}{dx}. \quad (\text{B45})$$

This equation coincides with Eq. (A12) safe for additive correction of K and δ , with the difference being small as $O(K(J\delta t)^2)$ and $O(\alpha a^2 \delta t^2)$, respectively. The matching conditions, being independent on both J and δ for this case, are thus identical to (A18).

b. Anomalous turning point $p = \pm\pi$

In this case, $E - J = \alpha a\delta$, and the solution for Eq. (B43) is described by $\varphi(x) = 0$ since the only oscillating solution is present near the anomalous turning point, while the η component is described Airy functions, with asymptotic behavior given by Eq. (A20). Just as with the previous case, the presence of the term $\propto \hat{\tau}_y$ at nonzero δt can be neglected, rendering

$$\left(-\alpha(x - a\delta) + \left\{1 + \frac{(J\delta t)^2}{12}\right\} \frac{J}{2}\hat{p}^2 + \frac{(\alpha a\delta t)^2}{24}\right) \eta(x) \approx 0, \quad \hat{p} = ia \frac{d}{dx}. \quad (\text{B46})$$

This equation is still solved by (A20) with the values of K, δ shifted by $O(K(J\delta t)^2)$ and $O(\alpha a^2 \delta t^2)$, respectively. While the matching conditions (A23) for this case do depend on δ , the shift of the latter bears additional smallness $O(a^2)$ in comparison to the effects captured by the semiclassical approximation, so we can safely discard this shift.

5. Change in the classical period of motion

In this section, we estimate the change of the classical period of motion of a given bound state due to the perturbation (35) of the semiclassical Hamiltonian, as the period enters in the subexponential prefactors in the semiclassical expressions (25) and (27). The change of the classical period of motion at a given energy E due to a perturbation is given by

$$\delta T_1(E) = \frac{\partial \delta S_{12}}{\delta E} \approx - \int_{x_1}^{x_2} \frac{dx}{v(p)} \frac{\partial}{\partial p} \left\{ \frac{\delta \mathcal{H}_{\text{eff}}(x, p)}{v(p)} \right\}, \quad (\text{B47})$$

where $x_{1,2}$ are the turning points of the unperturbed classical trajectory, $\mathcal{H}_{\text{eff}}(x, p)$ is given by Eq. (35), and the momentum p is found from the classical equation of motion (18). The integral is convergent because $v(x)$ vanishes at $x_{1,2}$ as $\sqrt{|x - x_i|}$, and the quantity $\delta \mathcal{H}_{\text{eff}}/v$ is a smooth function of momentum p with no singularities at real momenta, as can be seen from Eq. (35). We thus arrive at the following estimate for the relative change:

$$\left| \frac{\delta T_1}{T} \right| = \left| -\frac{1}{T} \int_{t_1}^{t_2} dt \left[\frac{\partial}{\partial p} \left\{ \frac{\delta \mathcal{H}_{\text{eff}}(x, p)}{v(p)} \right\} \right]_{p=p(t), x=x(t)} \right| \leq \max_x \left| \frac{\partial}{\partial p} \left\{ \frac{\delta \mathcal{H}_{\text{eff}}(x, p)}{v(p)} \right\} \right| \leq \frac{[J\delta t]^2}{24}, \quad (\text{B48})$$

where we made use of the fact that $t \equiv \int dx/v$, with $x(t), p(t)$ describing the classical trajectory. There's also a change of T due to the perturbative shift of the energy:

$$\left| \frac{\delta T_2(E)}{T} \right| = \left| \frac{T(E + \delta E) - T(E)}{T} \right| \approx \left| \frac{1}{T} \frac{\partial T}{\partial E} \delta E \right| \leq \frac{(J\delta t)^2}{24} \left| \frac{1}{T^2} \frac{\partial T}{\partial E} \right| 4n_{\text{cl}} a \quad (\text{B49})$$

where we have used estimation (39) for the energy shift δE and expression (24) for the single-particle level spacing. The quantity $T^{-2} \partial T / \partial E$ is strongly dependent on the potential profile, but it typically attains large values only if the energy E approaches the edges of the potential well beyond which the classical trajectories are not finite (or characterized by a qualitatively different shape of the allowed region). On the other hand, the estimate (B49) thus contains small parameter a , which allows one to claim that the change of the classical period of motion due to the energy shift is typically much smaller than the one due to the deformation of the semiclassical Hamiltonian.

The total relative change in the classical period of motion $\delta T_1/T + \delta T_2/T$ is thus typically a small quantity, although large values can be attained at energy that are close to local maxima of the potential (it should be mentioned that the semiclassical expressions (25) and (27) for the tunneling process cease to be applicable in the vicinity of such points, requiring accurate treatment of the potential maximum instead). However, the influence of the relative change of the classical period of motion on the tunneling rates competes with exponentially strong effect of the change in the tunneling action, Eqs. (42) and (48), with the latter being the most essential one for all practical cases.

6. Probability defect

In this subsection, we examine the total probability defect $1 - |\langle N|N_{\text{eff}}\rangle|^2$ between a given exact bound state $|N\rangle$ of a potential well and its counterpart in a perturbed system. One can estimate the overlap $\langle N|N_{\text{eff}}\rangle$ as that in the allowed region

$$\langle N|N_{\text{eff}}\rangle \approx \sum_{n \in \text{allowed}} \langle N|n\rangle \langle n|N_{\text{eff}}\rangle, \quad (\text{B50})$$

where the summation goes only over the allowed region of the either of the states, as the contribution from the difference in the position of the turning points is small, because one of the wave functions decays exponential in the corresponding. Although both wave functions are strongly oscillating functions of n , the product of the wave functions contains a slowly varying component that delivers the main contribution, so one can use semiclassical expressions to calculate the overlap. The calculation of $\langle N|N_{\text{eff}}\rangle$ is thus completely analogous to that for the normalization of the classical wave function [21, par. 48], with identical assumptions and approximations.

According to Eq. (A25), the semiclassical wave function of a bound state reads,

$$\langle n|N\rangle = \psi_N(x = an), \quad \psi_N(x) = \frac{\sqrt{C_N}}{\sqrt{v(E_N; x)}} \cos \left\{ \frac{iS(E_N, x_1; x)}{a} - \frac{\theta_1}{2} \right\}, \quad (\text{B51})$$

where $v(E; x)$ is the semiclassical velocity, $S(E_N, x_1; x)$ is the action of the classical trajectory counted from turning point x_1 , θ_1 is the corresponding reflection phase (see Appendix Subsection A 2 c), and the normalization constant is conventionally found as

$$1 \approx \sum_{n \in \text{allowed}} \langle N|n\rangle \langle n|N\rangle \approx |C_N|^2 \sum_n \frac{1/2}{v(E_N; x = an)} \approx \frac{|C_N|^2}{2a} \int_{\text{allowed}} \frac{dx}{v(E_N; x)} \equiv \frac{|C_N|^2}{4a} T(E_N), \quad (\text{B52})$$

where oscillatory part of the squared cosine has been dropped, replacement of the sum \sum_n with the integral $a^{-1} \int dx$ is legitimate because $v(E; x)$ is a smooth function of x , and the final answer expressed in terms of the classical period of motion at energy E_N . The target overlap (B50) is thus given by

$$\begin{aligned} \langle N|N_{\text{eff}}\rangle &\approx \sum_{n \in \text{allowed}} \langle N|n\rangle \langle n|N_{\text{eff}}\rangle \approx C_N^* C_{N,\text{eff}} \sum_{n \in \text{allowed}} \frac{\cos \{S_N(an)/a - \theta_1/2\}}{\sqrt{v_N(an)}} \frac{\cos \{S_{N,\text{eff}}(an)/a - \theta_1/2\}}{\sqrt{v_{N,\text{eff}}(an)}} \\ &\approx C_N^* C_{N,\text{eff}} \sum_{n \in \text{allowed}} \frac{\cos \{S_{N,\text{eff}}(an)/a - S_N(an)/a\}}{2\sqrt{v_N(an)}\sqrt{v_{N,\text{eff}}(an)}} \approx \frac{C_N^* C_{N,\text{eff}}}{a} \int_{\text{allowed}} dx \frac{\cos \{S_{N,\text{eff}}(x)/a - S_N(x)/a\}}{2\sqrt{v_N(x)}\sqrt{v_{N,\text{eff}}(x)}}, \end{aligned} \quad (\text{B53})$$

where $v_N, v_{N,\text{eff}}$ are shorthands for $v(E_N; x)$ and $v(E_N + \delta E_N; x)$, respectively, and similarly for $S_N, S_{N,\text{eff}}$. The derivation steps of the Eq. (B53) above are completely identical to those in Eq. (B52): in the product of cosines, only the slowly varying difference in classical action is left, and the sum of a slowly varying function is replaced with the integral. One can further neglect the difference between v_N and $v_{N,\text{eff}}$, C_N and $C_{N,\text{eff}}$, as the corresponding correction is small similarly to that from the difference in the positions of the turning points. One is thus left with the integral

$$\langle N|N_{\text{eff}}\rangle \approx \frac{2}{T(E_N)} \int_{\text{allowed}} \frac{dx}{v(E_N, x)} \cos \left\{ \frac{1}{a} (S_{N,\text{eff}}(x) - S_N(x)) \right\}. \quad (\text{B54})$$

The difference in actions consists of two parts:

$$S_{N,\text{eff}}(x) - S_N(x) \approx \delta S(E_N, x_1; x) + \frac{\partial S(E_N, x_1; x)}{\partial E} \delta E_N, \quad (\text{B55})$$

where the first contribution is the direct presence of perturbation, and the second contribution is due to the change in the energy level. Because S is precisely the action on the classical trajectory, Eq. (B54) can also be rewritten as

$$\langle N|N_{\text{eff}}\rangle \approx \frac{1}{T(E_N)} \int_0^T dt \cos \left\{ \frac{1}{a} \left(\delta S(E_N; t) - t \frac{\delta S(E_N; T)}{T} \right) \right\}, \quad (\text{B56})$$

where $\delta S(E_N; t) \equiv \delta S(E_N, x_1; x(t))$, with $t = \partial S(E_N, x_1; x) / \partial E$ is the time along the classical trajectory $x(t)$ measured from $x = x_1$, and we have used Eq. (38) for δE_N , with $\delta S(E_N; T) \equiv 2\delta S_{12}(E_N)$ being the total additional action along the trajectory.

In the form of Eq. (B56), it is more apparent that argument of the cosine is small, so one can expand the cosine and finally obtain

$$\delta P_N = 1 - |\langle N|N_{\text{eff}}\rangle|^2 \approx \frac{1}{T(E_N)} \int_0^T dt \left[\frac{1}{a} \left(\delta S(E_N; t) - t \frac{\delta S(E_N; T)}{T} \right) \right]^2. \quad (\text{B57})$$

This equation is applicable as long as the resulting answer is small, i.e., $\delta P_N \ll 1$, and the classically allowed region is large, i.e. $n_{\text{cl}} = (x_2 - x_1)/a \gg 1$, in which case it is guaranteed that the contribution from the bulk of the allowed region is the leading one in comparison to contributions from the boundaries of the allowed region and from the forbidden region. Compared to exact numerical diagonalization, this expression gives correct answers for $N \gtrsim 1$ (with $N = 1$ being the ground state), while overestimating the result for $N \sim 1$ by a multiple of order unity.

The value of C_N in Eq. (49) is then obtained from the exact form (35-36) of the perturbation of action, and can be estimated as

$$\begin{aligned} (J\delta t)^4 C_N &= \frac{1}{T(E_N)} \int_0^T dt \left[\frac{1}{a} \left(\delta S(E_N; t) - t \frac{\delta S(E_N; T)}{T} \right) \right]^2 \leq \max_{t \in [0, T]} \left[\frac{1}{a} \left(\delta S(E_N; t) - t \frac{\delta S(E_N; T)}{T} \right) \right]^2 \\ &\leq \left(\frac{2}{a} \delta S(E_N; T) \right)^2 = \left(\frac{2}{a} \delta E_N T \right)^2 \leq \left(\frac{(J\delta t)^2}{3} n_{\text{cl}} \right)^2, \end{aligned}$$

where at the very last step estimation (39) for δE_N was used.

7. Full effective Hamiltonian in smooth external potential

The semiclassical approximation of (B2) essentially relies on the fact that the classical momentum varies slowly with spatial coordinate, while giving little regard to the particular form of the kinetic energy. One can therefore compute kinetic energy exactly for translationally invariant system and then apply the semiclassical approximation to the total Hamiltonian. For concreteness, let's consider the Suzuki-Trotter evolution (7) with operators ordered as $\{K_{\text{even}}, K_{\text{odd}}, P\}$. We first note that for the first two kinetic operators $\mathcal{K}_{\text{even}}$ and \mathcal{K}_{odd} , with their matrix elements given by Eq. (B25), the semiclassical wave function (B11) with $S(x) = ipx$ describes the exact eigenstate upon diagonalization of the corresponding 2x2 matrix from Eq. (B26):

$$\sum_m \mathcal{K}_{\text{even(odd)}}^{nm} \begin{pmatrix} \varphi e^{ipm} \\ \eta (-1)^n e^{ipm} \end{pmatrix} = e^{ipn} \hat{\mathcal{K}}_{\text{even(odd)}}(p) \begin{pmatrix} \varphi \\ \eta \end{pmatrix}, \quad (\text{B58})$$

where the 2x2 matrix multiplication is implied on the right hand side. Consider then the Suzuki-Trotter evolution operator (7) for the pair $\{K_{\text{even}}, K_{\text{odd}}\}$, corresponding to just the kinetic part of the target Hamiltonian:

$$\mathcal{U}_{\text{kin}} =: \exp \{-i\delta t \mathcal{H}_{\text{kin}}\} = \exp \{-i\delta t \mathcal{K}_{\text{odd}}/2\} \exp \{-i\delta t \mathcal{K}_{\text{even}}\} \exp \{-i\delta t \mathcal{K}_{\text{odd}}/2\}. \quad (\text{B59})$$

Due to Eq. (B58), the action of this operator on a semiclassical wave function (B11) is also described by a 2x2 matrix:

$$\sum_m \mathcal{U}_{\text{kin}}^{nm} \begin{pmatrix} \varphi e^{ipn} \\ \eta (-1)^n e^{ipn} \end{pmatrix} = e^{ipn} \exp \{-i\delta t \hat{\mathcal{H}}_{\text{kin}}(p)\} \begin{pmatrix} \varphi \\ \eta \end{pmatrix}, \quad (\text{B60})$$

with $\hat{\mathcal{H}}_{\text{kin}}(p)$ found as

$$\begin{aligned} \hat{\mathcal{H}}_{\text{kin}}(p) &= \frac{i}{\delta t} \text{Ln} \left\{ e^{-i\delta t \hat{\mathcal{K}}_{\text{odd}}(p)/2} e^{-i\delta t \hat{\mathcal{K}}_{\text{even}}(p)} e^{-i\delta t \hat{\mathcal{K}}_{\text{odd}}(p)/2} \right\} \\ &= T(p) \frac{\sin^2 \frac{\gamma}{2} \sin 2p \hat{\tau}_y + (1 - 2 \cos^2 p \sin^2 \frac{\gamma}{2}) \hat{\tau}_z}{\sqrt{1 - (\cos p \sin \gamma)^2}}, \end{aligned} \quad (\text{B61})$$

where $\gamma = J\delta t/2$, and $\pm T(p)$ encodes the eigenvalues of $\hat{\mathcal{H}}_{\text{kin}}$:

$$T(p) = -\frac{2}{\delta t} \arcsin \{ \cos p \sin \gamma \}. \quad (\text{B62})$$

According to Eq. (7), the full Suzuki-Trotter evolution operator for the $\{K_{\text{even}}, K_{\text{odd}}, P\}$ ordering of operators is given by $\mathcal{U}_{\text{eff}} = \exp \{-i\delta t \mathcal{P}/2\} \mathcal{U}_{\text{kin}} \exp \{-i\delta t \mathcal{P}/2\}$, with \mathcal{U}_{kin} defined in Eq. B59. In the limit of smooth potential, \mathcal{U}_{eff} reduces to $\exp \{-i\delta t (\mathcal{H}_{\text{kin}} + \mathcal{P})\}$, while nonvanishing inhomogeneity of the potential leads to corrections. Given the potential term in the form $\mathcal{P}^{nm} = h(an) \delta^{mn}$ with $a \ll 1$, one can then use the semiclassical approximation (B11) for the eigenfunctions of \mathcal{U}_{eff} and obtain expansion in powers of a for the action of \mathcal{U}_{eff} on such a wave function, in complete analogy with Appendix Subsection B 2. One then expects from the results of Appendix Subsection B 3 that the result reads

$$\sum_m \mathcal{U}_{\text{eff}}^{nm} \psi_m = e^{iS(x)/a} \exp \left\{ -i\delta t \hat{\mathcal{H}}_{\text{eff}}(x, p) \right\} \vec{v} + O(a),$$

with $\hat{\mathcal{H}}_{\text{eff}}$ being the classical Hamiltonian that reads

$$\hat{\mathcal{H}}_{\text{eff}}(x, p) = \hat{\mathcal{H}}_{\text{kin}}(p) + h(x) \cdot \hat{1}, \quad (\text{B63})$$

while $O(a)$ corrections describe the transport equation (B18) corresponding to $\hat{\mathcal{H}}_{\text{eff}}$.

Another perspective on the result (B63) can be obtained by considering higher orders of expansion of the true effective Hamiltonian (8) in powers of δt . The leading order of such expansion is given by Eqs. (B2) and (B4), while higher orders contain more complicated combinations of nested commutators. Eq. (B63) then amounts to using the fact that each time \mathcal{P} gets commuted with other operators, the result is proportional to $a \ll 1$. One can thus collect all commutators that do not contain \mathcal{P} (which, in turn, corresponds to calculating \mathcal{H}_{kin}) and then neglect the commutators containing \mathcal{P} as subleading in powers of a (while also containing smallness w.r.t δt). This also explains why expanding Eq. (B63) in powers of δt (note that $\hat{\mathcal{H}}_{\text{kin}}$ explicitly depends on δt) coincides with Eq. (B30), as the latter corresponds to collecting only leading orders in powers of δt .

We now discuss the properties of the semiclassical matrix Hamiltonian of Eq. (B63). The classical equation of motion (B17) for $\hat{\mathcal{H}}_{\text{eff}}$ reads

$$\pm T(p) + E - h(x) = 0, \quad (\text{B64})$$

where $T(p)$ is given by Eq. (B62). Because $T(p + \pi) = -T(p)$, we are free to chose positive sign, in which case Eq. (B64) formally corresponds to the equation of motion (A5) for the *scalar* classical Hamiltonian $T(p) + h(x)$, thus explaining the origin of Eq. (54). In order to correctly reproduce the coefficients η, φ of the semiclassical wave function (B11), one has to use to matrix Hamiltonian (B63). The corresponding wave function is given by

$$\psi(x) = \frac{e^{iS(x)/a}}{\sqrt{v}} \left(\varphi_{p(x)} + e^{i\pi x/a} \eta_{p(x)} \right), \quad (\text{B65})$$

with $p(x) = S'(x)$ and (φ_p, η_p) being the eigenvector of the semiclassical matrix Hamiltonian (B61) corresponding to eigenvalue $+T$:

$$\begin{pmatrix} \varphi_p \\ \eta_p \end{pmatrix} = \begin{pmatrix} \cos \theta \\ -i \sin \theta \end{pmatrix}, \quad \sin 2\theta = \frac{\sin^2 \frac{\gamma}{2} \sin 2p}{\sqrt{1 - (\cos p \sin \gamma)^2}}, \quad \cos 2\theta = \frac{1 - 2 \cos^2 p \sin^2 \frac{\gamma}{2}}{\sqrt{1 - (\cos p \sin \gamma)^2}}, \quad (\text{B66})$$

and v found from the transport equation (B18). For the particular Hamiltonian of Eq. B61 the task can be solved explicitly rendering simply the group velocity

$$v = \left\langle \partial_p \hat{\mathcal{H}}_{\text{eff}} \right\rangle = \frac{\partial T}{\partial p} \cos 4\theta + \frac{1}{2} T \frac{\partial \cos 4\theta}{\partial p}. \quad (\text{B67})$$

Note that this result differs from naive group velocity $v = \partial_p T$ for $\theta \neq 0$, but the difference is present only in 4th order of $\gamma = J\delta t/2$, thus confirming our previous perturbative results.

Note that the equation of motion (59) is invariant under simultaneous substitution $E \mapsto \frac{2\pi}{\delta t} + E$, $p \mapsto \pi - p$. This is the consequence of both the Floquet periodicity and of the fact that due to Trotterization the actual period of translation in the system without potential is doubled, corresponding to the reduced Brillouin zone $[-\pi/2, \pi/2]$. In cases when the two modes corresponding to p and $\pi - p$ have energies that differ by $2\pi/\delta t$, the correct mode is chosen according to the global quantization conditions that take into account the structure of the wave function in the whole system by the matching procedure.

Finally, as expected from the analysis of Subsection III H, the kinetic term of the classical Hamiltonian (B63) does indeed have a branching point singularity at

$$1 = \sin \frac{J\delta t}{2} \cos p_c \Leftrightarrow p_c = \pm i \operatorname{arccosh} \frac{1}{\sin \frac{J\delta t}{2}} = \pm i \left[\ln \frac{4}{J\delta t} + O(\delta t^2) \right], \quad (\text{B68})$$

which coincides with the approximate value (52). In other words, this singularity is responsible for the decay rate $e^{-|p_c|(i-j)} \sim (J\delta t/4)^{|i-j|}$ of the matrix elements of the effective Hamiltonian, Eq. (29), as can be seen by discrete Fourier transform of Eq. (B60). As far as motion of the particle in the forbidden region is concerned, the presence of the singularity reflects the fact that the absolute value of the imaginary momentum $|p|$ starts to decrease with the increase of the potential barrier $h(x)$ after reaching the critical value $|p| = |p_c|$. For sufficiently large $h(x)$, the imaginary momentum reaches zero, marking the appearance of the classically allowed region inside the barrier, as explained in (III H).

Appendix C: Proposal on experimental observation of tunneling

In this Appendix, we present a detailed experimental setup to demonstrate the effects described in the main text. We consider the system discussed in Section II with $L = 50$ spins, according to the capabilities of the existing devices [1]. We will limit ourselves to the maximum depth of 10^5 two-qubit layers. Although this is ~ 60 times better than what was reported in Ref. [1], such an estimate originates from the recent advances in the coherence times [4], as well as from the possibility of post-selection of S_{total}^z , as done in Ref. [1]. One then uses the central circuit of Figure 1 and merges together the application of two-qubit gates of neighboring Trotter steps, which delivers up to $M = 5 \cdot 10^4$ Trotter steps.

The conceptual idea of the experiment is to observe tunneling in the double-well potential (see Figure 2, left). To this end, one initializes the system in a certain state localized in one of the wells and then observes the dynamics of the total number of particles in one half of the system. Due to practical limitations of existing devices, one has to carefully design the double-well potential according to the following requirements:

1. The well has to be deep enough to be amenable for the semiclassical description, i.e. accommodate many de Broglie wave length at the target energy.
2. There have to be bound states that are close to the maximum of the potential profile, so the tunnel splitting is not very small and thus resolvable within the maximum number of Trotter steps. On the other hand, the barrier has to be sufficiently long and high for the semiclassical description to be applicable.
3. Because the tunneling transparency of the barrier strongly depends on energy, one wishes to minimize the trivial effect of the energy shift of the bound states inside the well due to Trotterization. From Eqs. (35-38) it then follows that one should choose initial states with average momenta close to $\pi/2$, i.e. with energies close to J from the bottom of the well.
4. To maximize the visibility of the Rabi oscillations, one has to maximize the overlap of the initial state with the target bound state. As it will be demonstrated below, the precision of preparation is not essential, i.e. even 10% error in the amplitude of the wave function at each site renders good visibility of the oscillations. One can thus use the semiclassical approximation (17) for the wave function in the well. Such a state can be created by flipping one spin at the end of the system and evolving it with a sequence of n_{cl} purely two-qubit gates, where n_{cl} is the number of sites in the classically allowed region.
5. The potential should be smooth enough, so the semiclassical treatment is applicable away from the classical turning points, i.e., the criterion (21) should be satisfied.

Based on these requirements, we employ the following profile of the potential:

$$h_n = P \frac{f(n, \delta n)}{f(n_0, \delta n)} + \alpha \left(\frac{n - (L+1)/2}{L} \right), \quad n_0 = \lfloor (L+1)/2 \rfloor, \\ f(n, \delta n) = \exp \left\{ -\frac{1}{2} \left(\frac{n - \delta n - (L+1)/2}{w} \right)^4 - \frac{L/2}{\sqrt{(n-1)(L-n)}} \right\}. \quad (\text{C1})$$

Examples of this potential profile for various parameters are shown on Figures C1 and C4. The potential (C1) includes two terms: the first one governs the principal profile, while the second term enables one to tune accidental resonance in asymmetric potentials. The parameters P, w in Eq. (C1) control the height and the width of the barrier. The second term in the exponent of Eq. (C1) is needed to force $h_n \rightarrow 0$ close to the ends of the system. Tuning δn in Eq. (C1) away from zero breaks the mirror symmetry of the

potential, so the two wells are of different spatial size. One then manually tunes α away from zero to create accidental resonance between the localized levels in the two wells. The resulting eigenlevels for various choices of the parameters are also shown on Figs. C1 and C4.

For simplicity, we choose the initial state to be the superposition of left and right states that maximizes the population in the left half of the system (for instance, in case of symmetric potential the superposition is equally weighted with properly chosen signs). To imitate the inaccuracies of the state preparation, we further add 10% multiplicative noise to the amplitude of the wave function independently on each site as $\psi_i \mapsto \psi_i (1 + \epsilon_i)$, $\epsilon_i \in [-0.1, 0.1]$, after which the state is normalized.

The wave function is then evolved according to the central circuit of Figure 1 during $M = 60000$ Trotter steps. The value of the total number of particles in the left half of the system,

$$\mathcal{N}_{\text{left}}(t) = \sum_{i=1}^{L/2} |\langle i | \psi(t) \rangle|^2, \quad (\text{C2})$$

is recorded every $\delta M = 250$ trotter steps. The Fourier transform $n_\omega = \frac{\delta M}{M} \sum_t \mathcal{N}_{\text{left}}(t) e^{i\omega t}$ of the resulting time series is calculated for $\omega_n = \frac{2\pi}{\delta t \delta M} \frac{n-1}{M/\delta M - 1}$, $n \in \{0, M/\delta M - 1\}$. Due to the presence of the Rabi oscillations of the form (70), one observes a sharp peak in $|n_\omega|^2$ at the Rabi frequency. The density plots of the result as a function of both ω and δt are shown on Figs. C2 and C5. Given the Fourier transform n_ω , one then extracts the observed period of Rabi oscillations as $T_{\text{Rabi}} = 2\pi/\omega_{\text{max}}$, where $\omega_{\text{max}} = \text{argmax}_\omega |n_\omega|$ is the angular frequency with the maximum magnitude of the Fourier harmonic. The resulting dependencies of T_{Rabi} on the Trotter step δt are shown on Figs. 6, C3, and C5 for various values of the parameters. The particular choices of the latter are to demonstrate the effects discussed in the main text, as explained below.

1. Semiclassical description

One can describe the observed dynamics analytically. One starts with determining the semiclassical position of the eigenenergies by solving (numerically) the following quantization condition:

$$S_{\text{cl}}(E) := \int_0^{x_t(E)} p(E; x) dx = \pi \left(n - \frac{1}{4} \right), \quad n \in \mathbb{N}, \quad (\text{C3})$$

where p is found from the equations of motion for the semiclassical Hamiltonian 54 of the Suzuki-Trotter approximation at given δt , and $x_t(E)$ is the position of the turning point corresponding to $p(E; x_t) = 0$. The unusual phase factor in the r.h.s of Eq. (C3) in comparison to (22) is due to open boundary conditions $\psi_{n=0} = \psi_{n=L+1} = 0$ for the potential (C1). The classical period of motion in the well is then given by

$$\frac{T_{\text{cl}}}{2} = \frac{\partial S_{\text{cl}}}{\partial E} = \int_0^{x_t(E)} \frac{dx}{v(E; x)}, \quad \frac{1}{v(E; x)} = \frac{\partial p}{\partial E}. \quad (\text{C4})$$

Note that v is different from the group velocity (57) entering the normalization of the wave function. Because the states in two wells are in resonance, they experience finite tunnel splitting, and the corresponding period of Rabi oscillations is given by

$$T_{\text{Rabi}}(E) = 2\pi T_{\text{cl}}(E) e^{+S_b}, \quad S_b = \int_{x_t(E)}^{L+1-x_t(E)} \text{Im} p(E; x) dx. \quad (\text{C5})$$

The analysis can be easily generalized for asymmetric wells. In what follows, all integrals are evaluated numerically, and Eq. (C3) is also solved numerically.

2. Demonstration of tunneling and its enhancement

We start by demonstrating the enhancement of tunneling in case of symmetric potential with $P = 1.25$, $w = 8$, $\delta n = 0$, $\alpha = 0$. In this case, the 10th pair of energy levels is situated at energy $E_{10} \approx -J + 1.156J$ (the first term is trivially connected to the energy of a particle with zero momentum), which fulfills all the requirements listed above. Figure C1 shows the corresponding

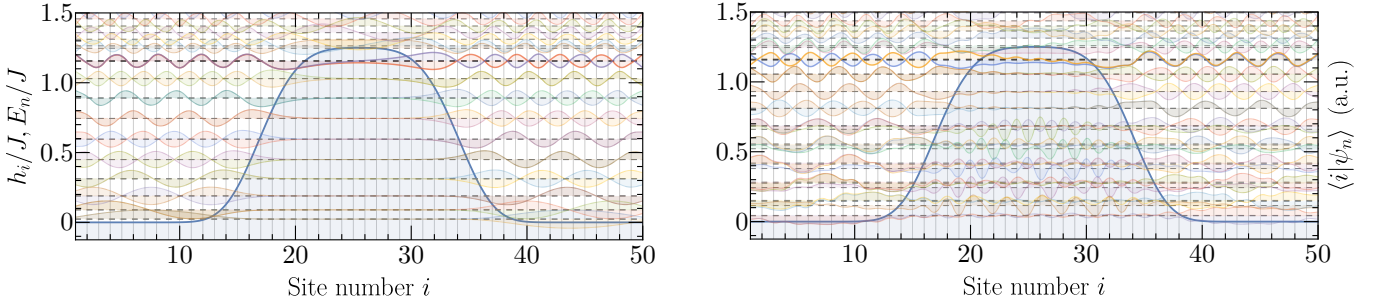


Figure C1. Visualization for the eigensystem for the potential profile (C1) with $P = 1.25J$, $\omega = 8$, $\delta n = 0$, $\alpha = 0$ (left) and its Suzuki-Trotter approximation with $J\delta t/\pi = 0.795$ (right). Energies E_n of the highlighted pair of eigenlevels are close to $1.156J$ (left) and $1.159J$ (right). Level splitting η of the highlighted pair of eigenlevels is $1.102 \times 10^{-3} J$ (left) and $4.82 \times 10^{-3} J$ (right). Note the strong distortion of the wave functions at low energies on the right plot. The energies of all eigenlevels are shifted by J to facilitate comparison with the potential profile.

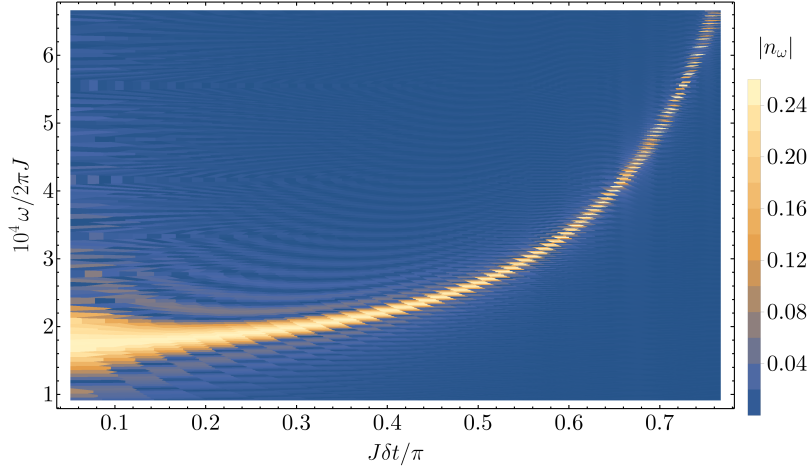


Figure C2. Density map of the absolute value of the Fourier harmonic $|n_\omega|$ of the occupation number in the left well, Eq. (C2), as a function of the angular frequency ω and Trotter step δt . The parameters of the unperturbed system are the same as those for Figure C1. The position ω_{\max} of the maximum amplitude $|n_\omega|$ for each δt corresponds to a point $T_{\text{Rabi}} = 2\pi/\omega_{\max}$ on Figure 6 of the main text.

eigenpair and its counterpart for large Trotter step $J\delta t/\pi \approx 0.795$. Two details are worth pointing out: *i*) the energy shift due to Suzuki-Trotter distortion is nearly absent due to the correct choice of the energy level, but *ii*) the eigenstates at low energies are strongly distorted by the Suzuki-Trotter approximation, as described in Subsection III H. One then applies the protocol described above to probe the period of the Rabi oscillations.

The density map of the occupation number harmonic $|n_\omega|$ as a function of angular frequency ω and Trotter step δt is shown on Figure C2. The corresponding dependence of the Rabi oscillation period T_{Rabi} on δt are shown on Figure 6 of the main text. The latter also contains the theoretical curve corresponding to the semiclassical approximation for T_{Rabi} : Eq. (C5) is evaluated for the energy E from the quantization condition (C3) for each δt , thus taking into account the energy shift. Crucially, the period of Rabi oscillations does decrease in agreement with the semiclassical prediction, even despite the lack of energy shift of the corresponding eigenpair, as can be verified both by semiclassical approximation and by exact diagonalization.

3. The effect of the energy shift

In this subsection, we demonstrate the two important effects due to the shift of the bound state energies: additional enhancement of tunneling and resonance detuning. To observe the former, we consider the symmetric version of potential (C1) with $P = 1.14J$, $\omega = 15$, $\delta n = 0$, $\alpha = 0$. The 7th eigenpair is located at $E \approx -J + 1.087J$, and thus experiences a noticeable shift due to Trotterization. The resulting period of Rabi oscillations as a function of the Trotter step is shown on Figure C3 along with the corresponding semiclassical predictions. To illustrate the presence of the energy shift, the dashed red curve on Figure C3 shows the semiclassical period of Rabi oscillation at the energy of the unperturbed eigenpair $E \approx -J + 1.087J$, as opposed to the actual energy of the eigenpair, which is itself a function of the Trotter step via the quantization condition (C3). In contrast to

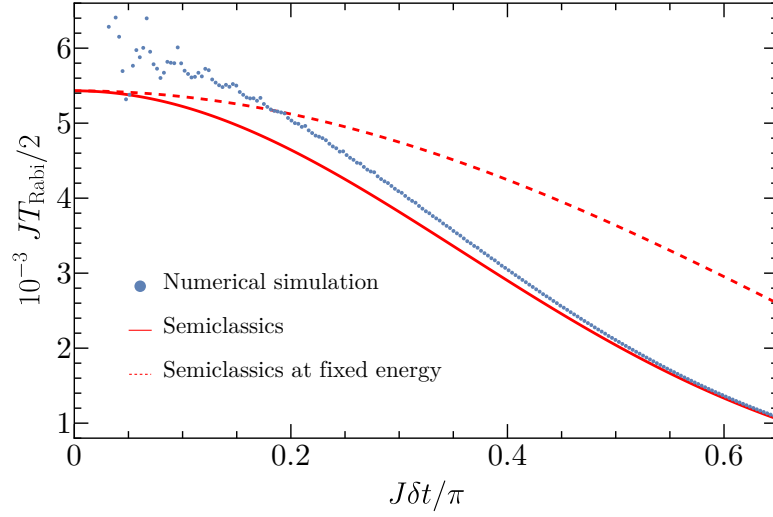


Figure C3. Dependence of the Rabi oscillation period T_{Rabi} on the Trotter step δt . The evolution is performed according to potential (C1) with the following parameters: $P = 1.14$, $w = 15$, $\delta n = 0$, $\alpha = 0$ (symmetric potential), the initial state is based on the 7th eigenpair. Red curves correspond to semiclassical description of the Rabi oscillations. *Dashed line*: the semiclassical period (C5) calculated at the energy of the eigenpair for $\delta t = 0$. *Solid line*: semiclassical period (C4) is calculated at the energy found from the correct quantization condition (C3) for each δt . In contrast to Figure 6, the two approaches yield manifestly different result due to the perturbation-induced energy shift. The remaining discrepancy between the solid line and direct simulation is due to corrections beyond the semiclassical description (the potential is not sufficiently smooth).

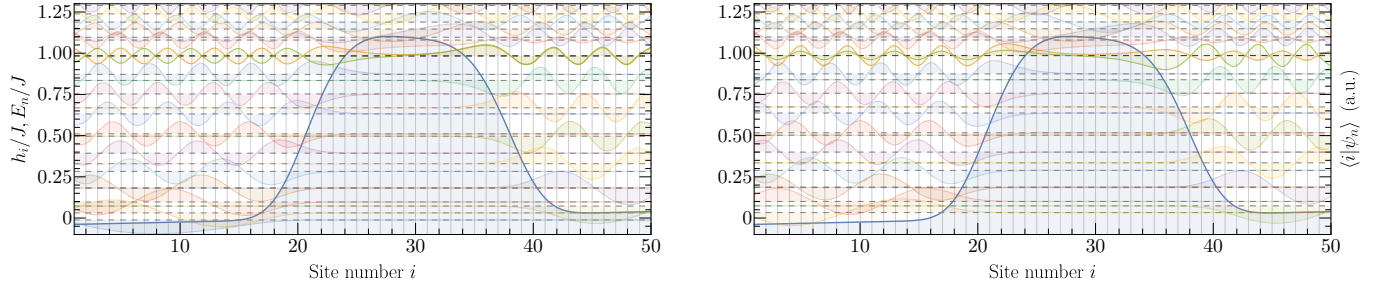


Figure C4. Visualization for the eigensystem for the potential profile C1 with $P = 1.05$, $w = 8$, $\delta n = 4$ and $\alpha \approx 0.0394$ determined with high precision from maximizing the Rabi period for the 9th pair of eigenstates (highlighted). *Left*: $J\delta t = 0$. *Right*: $J\delta t/\pi \approx 0.223$. In contrast to Figure C1, the value of $J\delta t$ on the right plot is not large enough to cause noticeable distortion of the low-energy eigenfunctions. However, due to the asymmetry of the potential, the hybridization between the two eigenstates is destroyed, causing them to occupy predominantly only one of the two wells.

Figure 6 of the main text, the difference due to this energy shift is well pronounced, indicating the practical importance of this effect.

We then turn to the effect of resonance detuning, which is present in asymmetric potentials. To this end, we set $P = 1.05J$, $w = 8$, $\delta n = 4$, and $\alpha \approx 0.0394$ is then found from maximizing the period of Rabi oscillation for the 9th pair of states. The resulting eigensystem and its Suzuki-Trotter approximation are shown on Figure C4. In full agreement with Subsection III D of the main text, one can clearly observe that the Suzuki-Trotter approximation introduces shifts in the bound state energies that are different between the two wells. As a result, the hybridization of the eigenpair is destroyed, so each state is mostly present in only one of the two wells.

The density map of $|n_\omega|$ is shown on Figure C5. Notably, the oscillation period decreases with δt considerably faster than in the case of symmetric resonance due to finite detuning (c.f. Figure 6):

$$T(\delta t) = \frac{T(0)}{\sqrt{1 + (\delta E T(0)/2\pi)^2}}, \quad \delta E = \beta J (J\delta t)^2, \quad (\text{C6})$$

where $T(0)$ is the period of oscillations in the target system (i.e., for $J\delta t = 0$), and δE is the perturbation induced energy shift, quadratic in δt in accordance with Subsection III C. Moreover, according to Eq. (70), the magnitude of the Rabi oscillations also

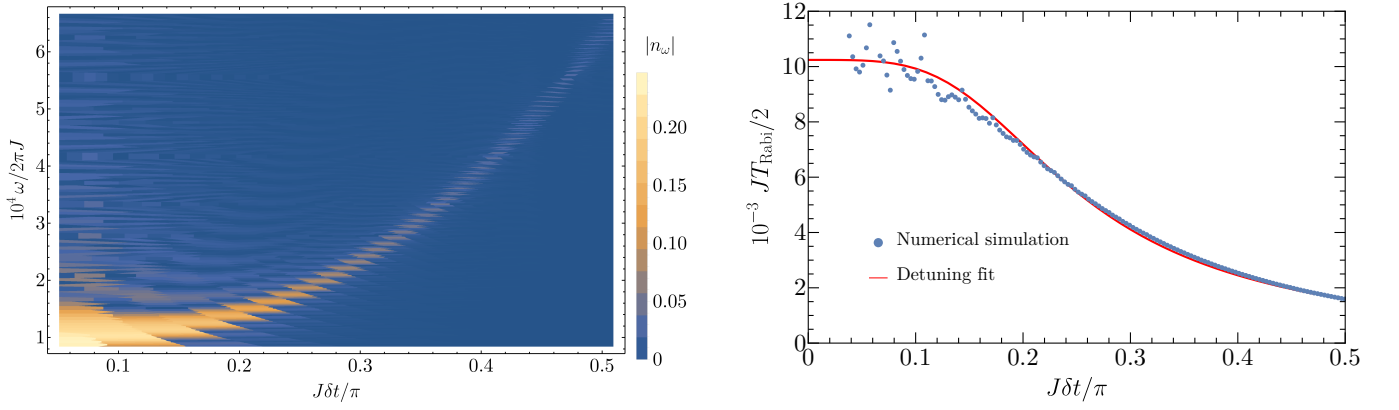


Figure C5. *Left*: Density map of the absolute value of the Fourier harmonic $|n_\omega|$ of the occupation number in the left well (C2) as a function of angular frequency ω and Trotter step δt . The evolution is performed for the same parameters as those for Figure C4. The initial state is based on the 9th eigenpair (highlighted on Figure C4). In contrast to Figure C2, the visibility of the resonance sharply decreases with δt due to detuning, according to Eq. (C7). *Right*: dependence of the Rabi oscillation period T_{Rabi} on the Trotter step δt for the same set of parameters. The blue dots are extracted from the data on the left figure, and the red line corresponds to Eq. (C6), with $T(0)$ extracted from exact diagonalization at $\delta t = 0$, and $\beta \approx 1.58 \times 10^{-3}$ obtained from fitting to the numerical data. Both $T(0)$ and β are consistent with the semiclassical description of Subsection C1.

decreases due to detuning, which reflects itself in reduced visibility of the maximum Fourier harmonic $|n_{\omega, \text{max}}|$ of the occupation number:

$$|n_{\omega, \text{max}}| \approx n_0 \left[\frac{T(\delta t)}{T(0)} \right]^2, \quad (\text{C7})$$

where n_0 is the magnitude at $J\delta t = 0$, and $T(\delta t)$ is found from Eq. (C6).

4. The effect of finite gate precision

Lastly, we estimate the required gate precision, by which we understand the tolerance to random shifts in phases of one- and two-qubit gates that are constant during each realization of the experiment, as opposed to time-dependent error that induces decoherence and thus requires more careful study. As it follows from Subsection III D, the main effect of the gate error is that it causes uncontrolled energy shifts of the bound states in each well, thus detuning the resonance. Below we consider uncorrelated disorder in the single-qubit gates as an example. The latter translates to potential disorder in the model and thus produces a random energy shift in the position of the energy level E_N of the bound state. The dispersion of this quantity can be estimated perturbatively:

$$\langle \delta E^2 \rangle = \delta V^2 \sum_i \psi_N^4(i) \sim \delta V^2 \frac{1}{n_{\text{cl}}}, \quad (\text{C8})$$

where in the last equality we have estimated the inverse participation ratio $\sum_i \psi_N^4(i)$ of the bound state inside the well as inverse number of sites in the allowed region. The measured expectation value of the total occupation number in the left well is given by averaging of the quantum expectation value (70) over distribution of the detuning ϵ , whose dispersion σ is given by Eq. (C8):

$$\begin{aligned} \bar{n}(t) &= \overline{\left(\frac{\epsilon^2/4}{\eta^2 + \epsilon^2/4} \right) + \left\{ 1 - \left(\frac{\epsilon^2/4}{\eta^2 + \epsilon^2/4} \right) \right\} \cos^2 \sqrt{\eta^2 + \epsilon^2/4t}} \\ &= \begin{cases} 1 + \tau^2 + \frac{1}{3}\tau^4 \left(1 + \frac{\sigma^2}{4} \right), & \tau \ll 1, \\ F(\sigma) + \frac{1}{2} \text{Re} \left\{ \sqrt{\frac{4-2\sigma^2 i\tau}{\pi\sigma^2}} \exp \left\{ 2i\tau + \frac{(4-2\sigma^2 i\tau)^2}{8\sigma^2} \right\} K_{\frac{1}{4}} \left(\frac{(4-2\sigma^2 i\tau)^2}{8\sigma^2} \right) [1 + O(\sigma^2)] \right\}, & \sigma^2\tau \ll 1, \\ F(\sigma) - \frac{\sin 2\tau}{\sqrt{2\tau}} [1 + O(\frac{1}{\tau})], & \sigma^2\tau \gg 1, \end{cases} \quad (\text{C9}) \end{aligned}$$

$$F(\sigma) = 1 - \sqrt{\frac{\pi}{2\sigma^2}} e^{\frac{2}{\sigma^2}} \text{erfc} \left(\frac{\sqrt{2}}{\sigma} \right) = \frac{1}{2} + \frac{\sigma^2}{8} + O(\sigma^4) \quad (\sigma \ll 1), \quad (\text{C10})$$

where $\sigma^2 = \langle \delta E^2 \rangle / \eta^2$, $\tau = \eta t$, $K_n(z)$ stands for the modified Bessel function of the 2nd kind of order n , and we have assumed Gaussian distribution of ϵ to compute the asymptotic expressions.

As it clearly both from Eq. (C9) and from the uncertainty principle, if the standard deviation $\sqrt{\langle \delta E^2 \rangle}$ is smaller than the target tunnel splitting $\eta = 2\pi/T$, the tunneling effect will still be visible. This yields the following restriction on the typical error in the phase of the single-qubit gates:

$$\sqrt{\langle \delta \phi^2 \rangle} = \sqrt{\langle \delta V^2 \rangle} \delta t \lesssim \eta \delta t \sqrt{n_{\text{cl}}} \sim \sqrt{20} \times 10^{-3} J \delta t. \quad (\text{C11})$$

where the last estimation uses the parameters proposed in this Appendix. Similar perturbative estimations can be made for the two-qubit gates, in which case one can also cast the result (C11) in a bound on the relative gate precision $\sqrt{\langle \delta \phi^2 \rangle} / J \delta t \sim \sqrt{20} \times 10^{-3} \sim 5 \times 10^{-3}$. For existing devices, condition (C11) is fulfilled even for the smallest value of $J \delta t = 0.2$ used in the simulations presented above, as the currently existing calibration procedure [1] allows one to achieve precision of order $1 \cdot 10^{-4}$.